Sizing and Operation of Multi-Energy Hydrogen-Based Microgrids

Bei Li

THÈSE DE DOCTORAT DE L'ÉTABLISSEMENT UNIVERSITÉ BOURGOGNE FRANCHE-COMTÉ

PRÉPARÉE À L'UNIVERSITÉ DE TECHNOLOGIE DE BELFORT-MONTBÉLIARD

École doctorale n°37

Sciences Pour l'Ingénieur et Microtechniques

Doctorat de Génie Électrique

par

BEI LI

Sizing and Operation of Multi-Energy Hydrogen-Based Microgrids

Thèse présentée et soutenue à Belfort, le 24 septembre 2018

Composition du Jury :

IDOUMGHAR LHASSANE	Professeur à l'Université de Haute Alsace	Président
ROBOAM XAVIER	Directeur de Recherche CNRS à l'Université de Toulouse	Rapporteur
PIERFEDERICI SERGE	Professeur à l'Université de Lorraine	Rapporteur
PRODAN IONELA	Maître de Conférences à Grenoble INP	Examinatrice
MIRAOUI ABDELLATIF	Professeur à l'Université de Technologie de Belfort-Montbéliard	Directeur de thèse
ROCHE ROBIN	Maître de Conférences à l'Université de Technologie de Belfort-Montbéliard	Co-encadrant
PAIRE DAMIEN	Maître de Conférences à l'Université de Technologie de Belfort-Montbéliard	Co-encadrant

SPIM

école doctorale **sciences pour l'ingénieur et microtechniques**

UBFC UNIVERSITÉ BOURGOGNE FRANCHE-COMTÉ

Université Bourgogne Franche-Comté
32, avenue de l'Observatoire
25000 Besanon, France

ABSTRACT

With the development of distributed, renewable energy sources, microgrids can be expected to play an important role in future power systems, not only to reduce emissions and maximize local energy use, but also to improve system resilience. Due to the intermittence and uncertainty of renewable sources (such as photovoltaics or wind turbines), energy storage systems should also be integrated. However, determining their size and how to operate them remains challenging, especially as the adopted control strategy impacts sizing results, and for systems considering multiple, interdependent forms of energy. This thesis therefore contributes to solving the sizing and operation problems of full-electric and multi-energy (electricity, gas, heat, cooling and/or hydrogen) microgrids integrating storage systems.

First, based on the characteristics of different components, a mathematical model of a microgrid is built. Then, the operation problem is formulated as a mixed integer linear problem (MILP), based on an objective function (minimize the operation cost) and different constraints (maximum power, startup/shutdown times, state-of-charge limits, etc.). Next, a co-optimization structure is presented to solve the sizing problem using a genetic algorithm. This specific structure enables to search for sizing values based on the operation results, which enables determining the best sizing for the selected operation strategy.

Using the above method, four specific problems are then studied. The first one focuses on sizing a full-electric islanded microgrid combining battery and hydrogen storage systems for short and long-term storage, respectively. Results for two types of operation strategies are compared: the MILP approach and a rule-based strategy. A one-hour one-year rolling horizon simulation is used to check the validity of the sizing results.

Second, a multi-energy islanded microgrid with different types of loads is studied. Specifically, the influence of three factors on sizing results is analyzed: the operation strategy, the accuracy of load and renewable generation forecasts, and the degradation of energy storage systems.

Third, the work focuses on a grid-connected microgrid attached to a gas, electricity and heat hybrid network. Specifically, the resilience of the network is considered in order to maximize resistance to contingency events. Betweenness centrality is used to find the worst case under contingency events and analyze their impact on sizing results. Two test systems of different sizes are used with the proposed method and a study of its sensitivity to various parameters is carried out.

Fourth, a structure with multiple grid-connected multi-energy-supply microgrids is considered, and an algorithm for determining electricity prices is developed. This price is used for energy exchanges between microgrids and load service entities interacting with the utility. The proposed co-optimization method is deployed to search for the best price that maximizes benefits to all players. Simulations on a large system show that the obtained price returns better results than a basic time-of-use price and helps reduce the operation

cost of the whole system. To reduce the computation time, a neural network is presented to estimate the operation of the whole system and enable obtaining results faster with a limited impact on performance. At last, a sizing algorithm for grid-connected multi-energy supply microgrids operating under different prices is presented.

The obtained results on these different applications show the usefulness of the proposed method, which is a promising contribution toward the creation of advanced design tools for such microgrids.

Keywords: microgrid, hydrogen, optimization, sizing, multi-energy, price.

RÉSUMÉ

Avec le développement de la production décentralisée d'électricité à partir de sources renouvelables, il est fort probable que les micro-réseaux joueront un rôle central dans les réseaux du futur, non seulement pour réduire les émissions de gaz à effet de serre et maximiser l'utilisation d'énergie produite localement, mais également pour améliorer la résilience du système global. Du fait de l'intermittence et de l'incertitude sur la production renouvelable (par exemple, photovoltaïque ou éolien), des systèmes de stockage de l'énergie doivent être intégrés. Cependant, déterminer leur dimensionnement et comment les contrôler pose plusieurs défis, en particulier parce que le dimensionnement optimal dépend de la stratégie de gestion utilisée, ou encore lorsque différents types d'énergie sont utilisés. Cette thèse contribue à résoudre les problèmes de dimensionnement et de gestion de micro-réseaux électriques et multi-énergies (électricité, gaz, chaleur, froid et/ou hydrogène) intégrant du stockage.

Tout d'abord, à l'aide des caractéristiques des différents composants, un modèle mathématique de micro-réseau est développé. Le problème de sa gestion est ensuite formulé comme un problème de programmation linéaire (MILP), utilisant une fonction objectif (minimiser le coût de fonctionnement) et différentes contraintes (puissance maximum, durée de démarrage/arrêt, limites d'état de charge, etc.). Ensuite, une structure permettant une co-optimisation est présentée pour résoudre le problème du dimensionnement à l'aide d'un algorithme génétique. Cette structure permet de explorer l'espace des valeurs de dimensionnement en fonction des résultats de la stratégie de gestion, ce qui permet de tendre vers le meilleur dimensionnement possible pour la stratégie sélectionnée.

A l'aide de la méthode ci-dessus, quatre problèmes spécifiques sont étudiés. Le premier s'intéresse au dimensionnement d'un micro-réseau îloté entièrement électrique, combinant stockage par batteries et hydrogène-énergie pour du stockage à court et long terme, respectivement. Les résultats pour deux stratégies de gestion sont comparés : l'approche proposée (MILP) et une stratégie basée sur des règles. Une simulation à horizon glissant d'une heure sur un an est ensuite utilisée pour vérifier la validité du dimensionnement obtenu.

Un second problème s'intéresse un à micro-réseau multi-énergies îloté avec différents types de charges. L'influence de trois facteurs sur les résultats du dimensionnement est en particulier étudiée : la stratégie de gestion, la précision des prévisions de consommation et de production renouvelable, ainsi que la dégradation des moyens de stockage.

Une troisième partie de la thèse traite du dimensionnement d'un micro-réseau connecté aux réseaux de gaz, électricité et chaleur. La résilience du réseau est étudiée de façon à maximiser la résistance à une panne ou un défaut. La notion de centralité intermédiaire est utilisée pour déterminer le cas le plus défavorable pour une contingence et analyser son impact sur le dimensionnement. Deux systèmes de test de tailles différentes sont utilisés pour valider l'application de la méthode proposée et sa sensibilité à différents

paramètres.

Enfin, une quatrième application s'intéresse à un ensemble de micro-réseaux multi-énergies connectés entre eux et à un réseau principal. L'algorithme proposé est alors appliqué à la détermination du prix utilisé pour les échanges d'énergie entre les micro-réseaux et des fournisseurs de service en interaction avec le réseau principal. L'algorithme détermine alors le prix qui maximise les bénéfices pour l'ensemble des participants. Des simulations sur un réseau montrent que le prix obtenu retourne de meilleurs résultats qu'une tarification classique de type heures creuses-heures pleines et permet de réduire le coût global de fonctionnement. Pour réduire le temps de calcul, un réseau de neurones est proposé pour accélérer la modélisation de la gestion du système et permet d'obtenir un gain de temps tout en ayant un impact limtié sur la performance. Enfin, un algorithme de dimensionnement pour les micro-réseaux multi-énergies connectés au réseau à différents prix est présenté.

Les résultats obtenus sur ces différentes applications montrent l'utilité de la méthode proposée, qui constitue une contribution prometteuse pour la création d'outils de conception avancée de tels micro-réseaux.

Mots-clés: micro-réseau, hydrogène, optimisation, dimensionnement, multi-énergies, prix.

ACKNOWLEDGEMENTS

The thesis is prepared at the FEMTO-ST laboratory and the FCLAB research federation.

This work was supported by many researchers, collegues and friends.

Firstly, I would like to thank my advisor, Dr. Robin Roche, who gave me research guidance and helped me revise the papers. Without his help, I would not have finished this work, and published papers in journals. Dr. Roche can always put forward valuable advices, which enlightened me on the research project. Dr. Roche always fed me back his review comments in time, and encouraged me to go forward. Thanks Dr. Robin Roche for his guidance, support, valuable advices, and encouragements.

Secondly, I would like to thank my supervisor Prof. Abdellatif Miraoui, who gave me this PhD position. Thanks to Dr. Damien Paire for helping me revise papers and this thesis. Also thanks to Prof. Fei Gao for his support and help.

Then, I would like to thank my colleague Dr. Berk Celik, who gave me encouragement and provided valuable advices on market problem. Thanks to my friends Mr. Hailong Wu, Mr. Hanqing Wang, Mr. Rui Ma, Mr. Chen Liu, Mr. Huan Li, and Ms. Suyao Kong for their help and support.

Then, I would like to thank the China Scholarship Council (CSC), which funded me to study and live in France. With the funding, I could concentrate on my research project, and could also travel around Europe to explore a new world.

At last, I would like to thank my parents and relatives for supporting and encouraging me to go forward.

Belfort, 20 July, 2018.

CONTENTS

NOMENCLATURE

Acronyms

ABSO	artificial bee swarm optimization
ACO	ant colony optimization
BSS	battery storage systems
CCHP	combined cooling heat and power
CHP	combined heat and power
DG	distributed generation
DR	demand response
EA	evolutionary algorithms
EH	energy hub
EMS	energy management systems
ESS	energy storage system
FC	fuel cell
FCL	following the cooling load
FEL	following the electric load
FTL	following the thermal load
GA	genetic algorithm
HSS	hydrogen storage systems
ISO	independent system operator
LF	load following
LOH	level-of-hydrogen
LSE	load service entity
MES	multi-energy-supply
MG	microgrid
MILP	mixed integer linear programming

MINLP mixed integer nonlinear problem

MIP mixed integer problem

MRM maximum rectangle method

NN neural network

PSO particle swarm optimization

PV photovoltaic

RBS rule-based strategies

RES renewable energy sources

SOC state-of-charge

TOU time of use price

UC unit commitment

UG utility grid

WT wind turbine

I

CONTEXT AND OBJECTIVES

1

INTRODUCTION

1.1/ INTRODUCTION

Power systems are increasingly suffering from damage caused by natural disasters (e.g., hurricanes, storms, floods, earthquakes), which often result in blackouts and power interruptions [1]. In traditional centralized power supply systems, no alternative power source can be used if the main distribution network is damaged by a natural disaster, which makes traditional power systems fragile. Through distributed generation (DG), loads can be powered by local resources, and reduce the dependence on the rest of the system and improve overall power system resilience. Local DG and loads can be combined to build a microgrid (MG), with multiple benefits such as the ability to enhance resistance to natural disasters [1, 2].

We should however notice that, for local DG, diesel gensets are conventional sources and have some drawbacks such as the emissions resulting from their operation, as well as dependence on fuel supply [1, 2]. Generation from renewable energy sources (RES) can also be considered to form renewable energy-based MGs. Due to the intermittence and uncertainty on energy output (such as for photovoltaics and wind turbines), energy storage systems should also be integrated into MG systems.

There are different types of energy storage technologies, such as batteries, supercapacitors, compressed air energy storage systems (CAES), flywheels, and hydrogen storage systems (fuel cell + tanks + electrolyzer) [3]. For renewable energy-based MG, the selected storage should have the ability to operate over short and long periods, up to a year or longer, to limit unwanted and inefficient generation curtailment and load shedding. The energy and power density (Wh/kg and W/kg) of the storage system should also be high to facilitate installation. Storage dynamics should also be able to handle the variability of RES. Hydrogen storage systems have a high energy density, but the cycle efficiency is low due to low electrolyzer and fuel cell efficiency. Batteries, on the other hand, have a medium energy density and a higher efficiency. The energy density of capacitors/supercapacitors and flywheels are among the lowest, below 30 Wh/kg, but their power density is high, which makes them suitable for applications with fast responses to handle the uncertainty of RES [3]. A power and energy density comparison of fuel cells, batteries and capacitors can be seen in Fig. 1.1 [4].

In this dissertation, a form of hybrid storage is considered: the hydrogen storage system (HSS, combining the fuel cell, the electrolyzer and the hydrogen tanks) is used as the long term storage system (e.g., for seasonal trends), and the battery storage system is

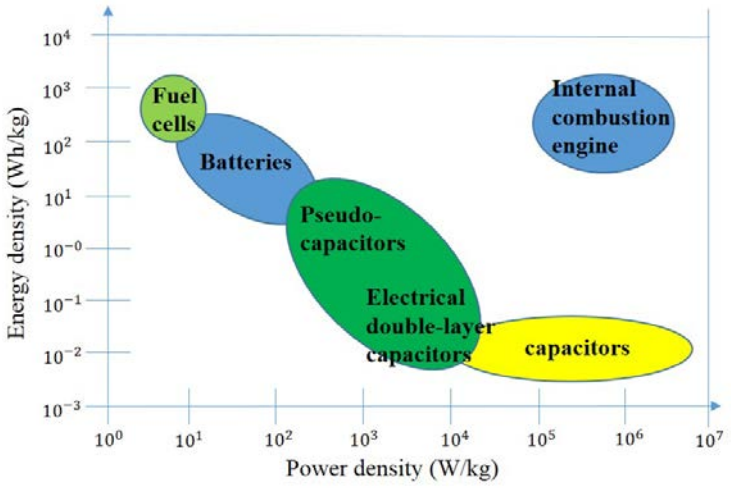

Figure 1.1: Power and energy density comparison of fuel cell, battery and capacitor [4].

used as the short term storage system (e.g., for day/night cycles). The HSS has several advantages, such as a high storage capacity, and a high energy per unit of mass [5]. They are therefore expected to play an important role in future energy storage systems [6]. The battery system is inappropriate for long-term storage, due to its low energy density and nonnegligible self-discharge rate [7]. This hydrogen storage-based MG structure can be seen in Fig. 1.2.

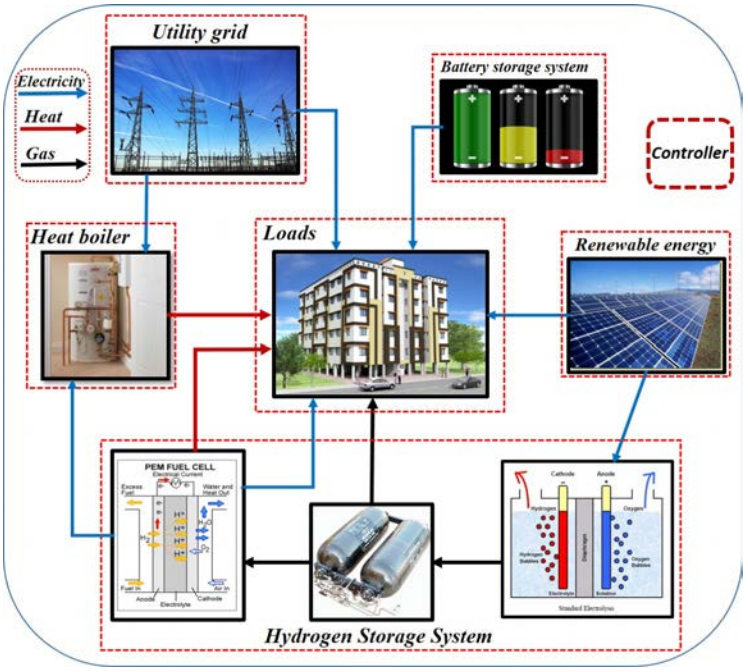

Figure 1.2: Microgrid structure.

The electrolyzer is powered by renewable energy, and produces hydrogen which can be stored in hydrogen tanks. There are three main types of electrolyzers: solid oxide electrolysis cells (SOECs), polymer electrolyte membrane cells (PEM), and alkaline electrolysis cells (AECs). “SOECs operate at high temperatures, typically around 800^{o}C. PEM elec-

trolysis cells typically operate below 100^{o}C and are becoming increasingly available commercially. AECs optimally operate at high concentrations of electrolyte (KOH or potassium carbonate) and at high temperatures, often near 200^{o}C" [8]. A comparison of the different electrolyzer types can be found in [8, 9]. In this dissertation, an alkaline electrolyzer is used to convert the renewable energy output to hydrogen.

Hydrogen can then be supplied to a fuel cell to produce electricity and heat. There are five main types of fuel cells: proton exchange membrane fuel cells (PEMFC), alkaline fuel cells (AFC), phosphoric acid fuel cells (PAFC), molten carbonate fuel cells (MCFC), and solid oxide fuel cells (SOFC). PEMFCs operate below 120^{o}C, and use a proton-conducting polymer membrane containing the electrolyte solution that separates the anode and cathode sides [10]. AFCs, for which "the space between the two electrodes is filled with a concentrated solution of KOH or NaOH which serves as an electrolyte", operate below 100^{o}C [10]. PAFCs operate between 150^{o}C and 200^{o}C. "In these cells phosphoric acid is used as a non-conductive electrolyte to pass positive hydrogen ions from the anode to the cathode" [10]. MCFCs require a high operating temperature, typically 650-700^{o}C. "MCFCs use lithium potassium carbonate salt as an electrolyte, and this salt liquefies at high temperatures, allowing for the movement of charge within the cell" [10]. Finally, SOFCs require high operating temperatures (800–1000^{o}C) and can be run on a variety of fuels including natural gas. "SOFCs use a solid material, most commonly a ceramic material called yttria-stabilized zirconia (YSZ), as the electrolyte" [10]. A comparison of different fuel cell can be found in [10, 11]. In this dissertation, a PEMFC is used to produce electricity and heat.

By enabling high penetration levels of RES, hydrogen-based MGs can be expected to play an important role in future smart grids, not only to friendly integrate RES (based on the energy storage system to reduce the intermittence influence of renewable energy sources on the utility grid and the demands), but also to resist to natural disasters (islanded operation ability under disasters). Moreover, integrating electricity supply with other forms of energy, such as gas or heat, can help further improve resilience as well as emissions reduction.

In this thesis, we focus on the planning (sizing) and operation of hydrogen storage-based and multi-energy microgrids.

First, when building a microgrid, one needs to decide the capacity of each component. Because renewable energy resources are nondispatchable sources, a reasonable capacity of energy storage systems is needed. We need to consider load-supply power balance to minimize the load shedding and curtailment of RES, and we also need to consider the investment costs of the whole system to avoid wasting money. It can be seen from Fig. 1.3 that, on the one hand, if we invest lots of money to install enough capacity of renewable energy resources and energy storage systems, the whole system certainly can operate well and achieve minimal load shedding, but the economic viability of the microgrid is bad. On the other hand, if we do not invest in enough capacity of renewable energy resources and energy storage systems to primarily satisfy the economic goal, then the microgrid may not operate well, with unacceptable load shedding. How to decide the capacity of each component in a microgrid to achieve a cost-effective solution is therefore a problem.

Second, for the load demands, there are not only the electricity demands, but also several other types of energy demands at the same time. For example, when people use gas to cook, they also need electricity to serve electronic devices, and heat energy to warm up the room. A multi-energy-supply microgrid is then needed, which can be seen in Fig. 1.2.

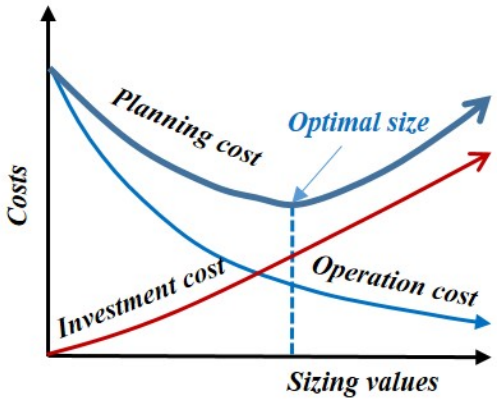

Figure 1.3: Sizing values vs. Costs.

For such a microgrid, more components are needed, with for example, heating devices to cover heat demands, and cooling devices to cover cooling demands. How to decide the capacity of each component in the microgrid to achieve a cost-effective solution is therefore another, more complex problem. Additionally, for the energy storage system, long term running and frequent charging-discharging cause degradation over time. So, how the degradation of energy storage system will influence the sizing results is also a problem.

Third, a multi-energy-supply microgrid can connect to the electricity/heat/gas utility grids. For this case, we need to consider the operation of the utility grid, because the microgrid can import energy from the utility grid, which will influence the energy flow of the whole system. So how to decide the capacity of each component in such a microgrid when considering the utility grid is a also problem. In fact, for a large-node utility grid, the impact of contingency events (such as the destruction of the power lines) must be considered. When the utility grid is severely damaged under natural disasters, the islanded MG can still operate to supply the load demands using the local renewable energy and the storage systems. If the utility grid is partially destroyed, the MG power imports from the utility grid are limited, due to damage on transmission lines or pipelines. This means that the impact of contingency events will influence the MG power imports from the utility grid, and then influence the power flow inside the MG. At last, the sizing results of the components are different.

Finally, when large amounts of multi-energy-supply microgrids are interconnected to the utility grid, how to operate this system well is another complex problem. Because of the privacy concerns of each microgrid, centralized control (requiring to collect all information from all microgrids) is not practical. If the number of microgrids is in the hundreds, centralized control will also be impossible. So, how to operate a large numbers of multi-energy-supply microgrids interconnected with utility grid is a challenging problem.

1.2/ Objectives of the Dissertation

In this thesis, we therefore focus on microgrid sizing and operation problems. We explore this problem from four perspectives:

1. Sizing of a full-electric hydrogen storage-based islanded microgrid.
2. Sizing of a multi-energy-supply islanded microgrid considering the degradation of energy storage systems.
3. Sizing of multi-energy-supply microgrids considering the gas/electricity/heat utility grid.
4. Sizing and price decision algorithm for multiple grid-connected multi-energy-supply microgrids.

In short, we first research about the sizing problem of a full-electric hydrogen-based islanded MG. Then, we expand the load demands to several types (electricity/heat/cooling/hydrogen), and research about the sizing problem of such a multi-energy-supply islanded microgrid. After that, we interconnect the microgrid into the utility grid, and research about the sizing problem of the grid-connected microgrid. Then, for the grid-connected microgrid, the price must be considered, and we research about the price decision algorithm for multiple grid-connected multi-energy-supply microgrids. Also, the sizing algorithm for grid-connected MES MGs based on the different prices is presented.

Based on the above specific aspects, the detailed objectives of the dissertation can be listed as the following:

- **Develop a strategy to control the operation of a microgrid**.
- **Develop a co-optimization-based sizing method**.
- **Present a rolling-horizon optimization method to check the sizing results**.
- **Integrate the degradation of energy storage systems in the sizing method**.
- **Consider the impact of contingency events on the sizing results of a microgrid**.
- **Develop a price decision approach for multiple grid-connected microgrids**.
- **Develop a sizing algorithm for grid-connected MES MGs based on the different prices**.

1.3/ OUTLINE OF THE DISSERTATION

The rest of this dissertation is structured as follows. Chapter 2 is contains a state-of-the-art review. The sizing and operation problem of hydrogen-based microgrids is introduced from four aspects: the model of the hydrogen-based microgrid, the operation strategy of the microgrid, the sizing method of the microgrid and the price decision algorithm for a grid-connected microgrid.

Chapter 3 presents the microgrid model. Two types of hydrogen-based microgrids are modeled: the full-electric microgrid and the multi-energy supply microgrid.

Chapter 4 **presents the sizing of a full-electric hydrogen storage system based islanded microgrid.** In this islanded microgrid, two storage systems are considered

(battery storage system and hydrogen storage system). A combined sizing and energy management methodology, formulated as a leader-follower problem, is presented. The leader problem focuses on sizing and aims at selecting the optimal size for the microgrid components. It is solved using a genetic algorithm (GA). The follower problem, i.e., the energy management issue, is formulated as a unit commitment problem and is solved with a mixed integer linear program (MILP). Uncertainties are considered using a form of robust optimization method. Several scenarios are modeled and compared in simulations to show the effectiveness of the proposed method, especially compared to a simple rule-based strategy.

Chapter 5 **presents the sizing of a multi-energy-supply islanded microgrid considering the degradation of energy storage system.** A stand-alone microgrid considering electric power, cooling/heating and hydrogen consumption is built. A unit commitment algorithm, formulated as a MILP problem, is used to determine the best operation strategy for the system. A GA is used to search for the best size of each component. The influence of three factors (operation strategy, accuracy of load and renewable generation forecasts, and degradation of fuel cell, electrolyzer and battery) on sizing results is discussed. A 1-h rolling horizon simulation is used to check the validity of the sizing results. A robust optimization method is also used to handle the uncertainties and evaluate their impact on results.

Chapter 6 **presents the sizing of multi-energy-supply microgrids considering gas/electric/heat utility grid.** We focus on a gas/electricity/heat hybrid network. A hydrogen storage system is used as the main electricity storage system. MILP is used to determine the optimal operation of the multi-energy hybrid system, where the goal is to minimize shed load. A GA is used to search for the best size of each component, with the goal to minimize the investment costs. In order to resist to contingency events, betweenness centrality (describing the relative importance of each node in a graph) is then used to find the worst case under contingency events. This worst case scenario is used to research about the influence of contingencies on the sizing results. At last, two cases (modified 13-node network and IEEE 30+Gas20+Heat14-nodes system) are tested using the proposed sizing method. The results show that the renewable energy location, investment cost of components, and the structure of the whole system influence the sizing values of each component.

Chapter 7 **presents the sizing and price decision algorithm for multiple grid-connected multi-energy-supply microgrids.** Local generation, energy storage systems, and renewable energy sources can form load service entities (LSE), which can provide ancillary services to the utility grid and consumers. On the other hand, the microgrids can also sell energy to load service entities/utility grid to obtain profits. But how the load service entities can decide the selling electricity price to multiple microgrids, and how the microgrids can decide the selling electricity price to load service entities are problems. In this chapter, we present a guidance price decision method for multiple microgrids considering demand response. MILP is used to control the operation of each microgrid, and also used to operate the load service entities. GA is used to search for the best price for each microgrid and the load service entities. The simulation results show that the new searched price works better than a time-of-use (TOU) price, which can reduce the operation cost of the whole system. Also with higher penetration of renewable energy in MGs, the energy bought from the utility grid is reduced. At last, a large system is tested, in which 4 LSEs, 16 MGs and the IEEE 30-node network are considered. The simulation results show the feasibility of the presented pricing method. After then, in order to

reduce the GA searching time, a neural network (NN) model is presented to estimate the operation of the whole system. Based on the NN model, the prices are obtained, and the results show that the searching prices based on the NN model are better than with the TOU price. After that, we present the sizing algorithm for grid-connected MES MGs based on the different prices.

Finally, chapter 8 concludes on the thesis, by summarizing the main contributions and highlighting possible future research areas.

2

RELATED WORKS

In this chapter, related works about the sizing and operation problem of microgrids are reviewed. Three specific aspects are considered: 1) hydrogen-based microgrid; 2) operation strategy of microgrid; 3) sizing method of microgrid. At last, when we consider the grid-connected microgrid, the prices are often considered, then the related work about the price decision approach in multiple multi-energy supply microgrids are reviewed.

2.1/ HYDROGEN-BASED MICROGRID

In order to limit global warming and reduce fossil fuel consumption, renewable energy sources such as photovoltaic panels (PV) and wind turbines (WT) are more and more commonly used to generate electricity. The integration of such intermittent sources is a challenge for grid operators, as the balance between generation and demand must be met in real-time. This is especially a concern for small power systems such as microgrids, that can operate islanded, i.e., not connected to the main grid. Microgrids typically include distributed generation and storage [12, 13], and are increasingly found in remote areas [14, 15] or where power system resilience is a crucial concern [1, 16].

To enable RES integration, energy storage systems are considered as a key solution, as they enable storing excess generation for later use [17]. Battery storage systems (BSS) are typically used for short-term storage [18], but seem inappropriate for long-term storage [7]. Hydrogen storage systems (HSS) have a high energy density [3], and are used for long-term storage, such as seasonal storage. HSSs combine an electrolyzer to produce hydrogen from electricity, a hydrogen storage tank and a fuel cell (FC) to produce electricity from hydrogen.

Works about **hydrogen-based full-electric microgrid** have been presented in the literature. For example, [19] discusses FC systems, while [20] researches about the control strategy of PV/FC hybrid systems. In [21], a Matlab/Simulink model is built to simulate a grid-connected PV/FC hybrid system. [22] also builds a simulation model of another PV/FC/ultacapacitors stand-alone microgrid.

On the other hand, when there are different types of load demands, such as electricity, heat, cooling or hydrogen, “combined cooling heat and power systems” are typically used to form multi-energy-supply microgrids. Different devices can be chosen to build a multi-energy-supply microgrid. The main component is the prime mover (the combined heat and power plant). For a traditional system, there are several types of prime movers, such as internal combustion engine, combustion turbine, steam turbine, micro-turbine, stirling

engine, etc. A comparison of these prime movers can be seen in [23].

Fuel cells are a promising technology for efficient and sustainable energy conversion [24], and are expected to play an important role in future distributed energy generation [6]. Xe adopt the fuel cell as the equivalent of a “prime mover” that produces electricity and heat. The fuel cell consumes hydrogen, which is emissions-free when it is generated from renewable energy and water electrolysis.

Thus, a **hydrogen-based multi-energy-supply microgrid** can be built. Some works about fuel cell based multi-energy-supply microgrid have been presented. For example, [25] investigates the feasibility of combining an SOFC and a gas turbine system for marine applications. The efficiency of the configuration with double-effect absorption chiller can achieve 43.2% compared to 12% for the conventional system. In [26], an SOFC with a capacity of 215 kW is combined with a recovery cycle and is used to meet the load demand in a hotel. The results show that based on fuel lower heating value, a maximum efficiency of 83% for simultaneous energy generation and heat recovery cycle can be achieved.

According to industry analysts Delta-ee, fuel cell CHP units represent 64% of the CHP unit sale market, which doubles the results from 2011. It is becoming the most common technology employed in micro-CHP systems [23].

The above papers show that hydrogen-based microgrids are expected to play an important role in future smart grids. The structure of such hydrogen-based microgrid can be seen in Fig.1.2. In the following section, the operation strategy of hydrogen-based microgrids is introduced.

2.2/ OPERATION STRATEGY OF MICROGRID

The operation strategy of an MG system needs to be considered from two aspects: time scale and solution method.

Based on the selected time scale, two strategies can be considered: day-ahead scheduling and short term dispatching. A day-ahead scheduler provides unit commitment solutions aiming to find cost-effective combinations of generating units output, while a short term dispatcher returns the economic dispatch aiming to minimize the operation cost of the committed assets based on short term forecasts.

In [27], authors review the energy management of a microgrid, and point out that based on the time scale, two scheduling strategies (unit commitment and economic dispatch) are used together. In [28], a multi-timescale MG scheduling and dispatching strategy is developed for the coupled multi-type energy supply in an MG. In day-ahead scheduling, the objective function is to minimize the operation cost, and the objective of real-time dispatching is to make the real-time actual electricity power exchange between the MG and to make the main grid follow its day-ahead schedules as close as possible. In [29], authors present a two-stage coordinated control approach for CCHP microgrid energy management. The first stage is a rolling-horizon economic dispatch. The second stage is a real-time adjustment stage, which adjusts the controllable sources to make the real-time energy exchanged with the main grid and the state of the battery follow its economic dispatch as closely as possible.

In our sizing problem, our goal is to decide the sizing value of each component in the MG

system. So we not only need to consider the long-term planning (e.g. one year), namely to make the MG system cost-effective, but we also need to consider the short-term operation (e.g. 1 hour) to make the MG system operate normally, as illustrated in Fig. 2.1. If the selected time scale is small (such as 1 minute), the short-term operation will be more precise, but the long-term planning will cause lots of computation burden. On the other hand, if the selected time scale is large (such as 1 day), the short-term operation check will be not precise, but the long-term planning will cause a small computation burden. This relationship can be seen in Fig. 2.2.

Figure 2.1: Sizing and operation.

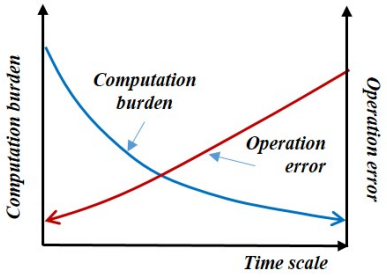

Figure 2.2: Computation burden, operation error vs. time scale.

Based on the above analysis, considering the tradeoff between accuracy and the computation burden, hourly profiles are adopted in the operation strategy [30].

In the following subsections, we mainly introduce the solution method of the operation problem. We classify this from two specific aspects: 1) the operation of full-electric microgrid; 2) the operation of multi-energy supply microgrid.

2.2.1/ OPERATION OF FULL-ELECTRIC MICROGRID

In this section, we review related works about the operation problem of full-electric microgrids.

A simple operation strategy is often selected to operate the full-electric microgrid, namely, the load following (LF) strategy: when there is surplus power, the excess energy is stored in the ESS, and when there is a shortage of power, the ESS discharges, or controllable generators (diesel gensets or FC) are turned on. Economic criteria are not considered in most cases.

For example, [31, 32] compare several EA for the optimal sizing of a hybrid MG system, where the objective function is the total annual cost, and the operation strategy is the LF strategy. Other papers use various metaheuristics to search for the sizing values for different MG cases, and the operation principle is also LF. [33] uses ant colony optimization (ACO) to determine the size values of a PV/wind hybrid system, where the objective funtion is the sum of the total capital cost and total maintenance cost. In [34], artificial bee swarm optimization (ABSO) is used to solve the sizing problem of PV/WT/FC hybrid system considering the loss of power supply probability (LPSP). [35] studies the performance of different particle swarm optimization (PSO) algorithm variants to determine the size results of a hybrid (PV/wind/Batt) system.

Some papers use more advanced strategies based on rules (rule-based strategies (RBS)) to control energy flows. For example, in [36], the operation mode of the islanded MG is determined by the SOC of the battery storage. Three operation modes are set based on different rules to achieve the goals, such as maximize the utilization of the RES units, or ensure the reliability and longevity of the battery storage. In [37], the energy flow is controlled depending on the charge and discharge states, different rules are built based on the preset parameters. In [38], authors set knowledge-based rules to control the operation of a diesel generator for an isolated MG with diesel-wind-ESS resources. The objective of this rule-based strategy is to minimize the diesel generation by minimizing the power wasted through the dump load for every hour.

The main advantage of using an RBS is that it can optimize the system performance without requiring an optimization function or tools, thus reducing computational complexity [38]. However, the limits of RBS are quickly reached when more than a few components are included in the system, as the number of required rules significantly increases. Moreover, these strategies cannot provide optimal results regarding how the state-of-charge of storage units is controlled over time.

More advanced energy management systems (EMS) that primarily focus on economic dispatch with EA, are also presented in the literature. [39] proposes a bilevel optimization energy management approach of multiple microgrids. Economic dispatch is solved in each microgrid, and then a secondary-level optimization is used to seek the minimum operation cost for the set of microgrids. Multiperiod ABCO [40], multi-layer ACO [41] are also used for economic dispatch applications. The objective of the economic dispatch problem is to minimize the total production cost while satisfying generation resources constraints.

EA-based optimization relies on stochastic search, which can give a satisfatory solution with a reasonable computation time, but it does not guarantee obtaining an optimal solution.

An improved method for energy management that can take into account multiple objectives and constraints is thus required. Model-predictive control (MPC) offers a solution, and is commonly used in power systems in the form of unit commitment (UC). UC enables scheduling the use of multiple generation units over a given time horizon [42], for example over a day. It can also be extended to consider storage units and other devices. For example, in [7], authors present a UC optimization method to economically schedule BSS and HSS. [43] studies the thermal power plant UC problem integrated with a large scale ESS. In [44], an integrated framework for a stand-alone microgrid with objectives of increasing stability and reliability and reducing costs is described. The UC method is used to determine generators outputs for the next day. [45] presents a two-stage planning

and design method for microgrids. GA is used to solve the optimal design problem and a MILP algorithm enables determining the optimal operation strategy.In [46], a mixed integer nonlinear programming (MINLP) approach for day-ahead scheduling of a combined heat and power plant is proposed. Another MINLP-based EMS algorithm is presented in [47]. [48] describes an approach for security-constrained UC with integrated ESS and wind turbines.

Overall, the above research papers show that the UC method is commonly used and adequate for scheduling the use of microgrid components, including energy storage units. The advantage and disadvantage of UC optimization-based EMS can be concluded as follows:

- **Advantages:**
  1. compared to EA algorithms, UC optimization can simply consider varieties of constraints, e.g., binary variable constraints (ON/OFF state of battery, etc.), continuous variable constraints (ouput power of fuel cell, etc.), logical constraints (charging and discharging can not occur at the same time, etc.), and so on;
  2. compared to RBS strategy, UC optimization can simply set the operation priority of each component by adjusting parameters in the objective function, and can also consider the economic criteria and different constraints as in 1).
- **Disadvantages:**
  1. require an optimization function or tools;
  2. the computation complexity and time burden is increasing as the number of variables increases;
  3. especially, when there are nonlinear constraints or variables, the UC problem causes lots of computation burden.

A UC algorithm does however rely on forecast data to compute schedules. As forecasting errors are inevitable, the scheduling algorithm must consider these errors. In the case studied in this paper, errors on PV output and load impact schedules as well as sizing results. Two main approaches to consider forcasting uncertainty are found in the literature: the scenario-based method [49, 50, 51] and robust optimization [52, 53, 54, 55]. [49] presents a stochastic method based on cloud theory to handle uncertainty, and uses a krill herd algorithm to solve the optimization problem. [50] describes a stochastic optimization for microgrid energy and reserve scheduling. Wind and PV generation fluctuations for each hour are represented by 5 interval discrete probability distribution functions. A scenario tree technique is then used to combine different states of wind and PV fluctuations. [51] presents a scenario-based robust energy management method. Taguchi's orthogonal array testing method is used to provide possible testing scenarios, and determine the worst-case scenario. At last, the Monte Carlo method is used to verify the robustness of the approach. In [52], uncertainty is quantified in terms of prediction intervals by a non-dominated sorting genetic algorithm (NSGA-II) trained by a neural network. Robust optimization is then used to seek the optimal solution to the problem. [53] uses robust optimization-based scheduling for multiple microgrids considering uncertainty. The problem is transformed into a min-max robust problem, and is then solved using linear duality theory and the Karush-Kuhn-Tucker (KKT) optimality conditions. [55] presents a robust

EMS for microgrids. Authors use a fuzzy prediction interval model to obtain the uncertainty boundary of wind output, and then the upper and lower boundaries of wind energy are interpreted as the best and worst-case operating conditions.

In the above papers, scenario-based methods usually require generating many scenarios, which can take a lot of time to simulate. On the other hand, robust methods are used to find the worst case, which requires less computation time although results are more conservative. As a consequence, in this thesis, a robust optimization method is selected to find the worst case and best case based on the forecasting error.

In this section, different operation strategies are presented for full-electric MG, including LF-EMS, RBS-EMS, EA-EMS, and UC-EMS. In the following section, the operation strategy for CCHP MG is presented.

2.2.2/ Operation of multi-energy supply microgrid

Regarding the solution method (i.e., decision-making), the operation strategies of a CCHP system can be also divided into two main types: rule-based strategies and optimization-based strategies.

In a multi-energy system, several loads must be satisfied. This means that some priority rules must be set, leading to traditional rule-based strategies: following the electric load (FEL), following the thermal load (FTL) or following the cooling load (FCL). In [56], authors review different optimization operation strategies, including basic operation strategies and hybrid operation strategies. [57] presents a novel optimal operational strategy for a CCHP system based on two typical operating modes: FEL and FTL. An integrated performance criterion which considers primary energy consumption, carbon dioxide emissions and operational cost, is used to decide which operating mode is chosen. In [58], authors compare five strategies: electrical-equivalent load following, continuous operation, peak shaving, and base load. In [59], five operation strategies are compared: FCL, FTL, FEL, maximum power output, and waste heat allocation proportion. [60] presents a multi-agent-based demand-side energy management system for autonomous polygeneration microgrids. With three types of demands (electricity, hydrogen, potable water). The goals are to have no potable water and hydrogen shortages, and to prevent the battery from deep discharging. The activation of each agent is based on rules. These rule-based operation strategies are however difficult to use for complex systems, where a large number of rules are needed, especially in multiple energy system.

Due to the drawbacks of rule-based strategies, optimization methods are also commonly used. A first category includes heuristic optimization methods, which are adequate to solve non-linear and non-convex problems. [61] proposes a time-varying acceleration coefficient particle swarm optimization (PSO) algorithm to solve the non-linear and non-convex CHP economic dispatch problem. The objective is to minimize the total heat and power production cost. [62] presents an artificial immune system algorithm for solving the CHP economic dispatch problem. The objective is to minimize the total fuel cost. [63] proposes a bacterial foraging-based fuzzy satisfactory optimization algorithm to solve the multi-objective energy management problem for a CHP-based microgrid. The objectives are to minimize the total operating cost and the emissions. [64] introduces a multi-objective PSO economic dispatch optimization method for a system that incorporates CHP and wind power units. [65] proposes a multi-objective optimization model which aims to maximize the energy-saving ratio and minimize the energy costs of a micro-

CCHP system. [66] presents a scenario-based scheduling method for a fuel cell-based CHP microgrid, which aims at maximizing the expected profit. A modified firefly algorithm is used to solve the problem.

As discussed in section 2.2.1, “EA-based optimization relies on stochastic search, which can give a satisfatory solution with a reasonable computation time, but it does not guarantee obtaining an optimal solution”.

The second category corresponds to mixed integer programming optimization (MIP), which uses deterministic methods. [67] explores opportunities for increasing the flexibility of CHP units using electrical boilers and heat storage tanks for better integration of wind power. A linear model is proposed for the centralized dispatch of integrated energy systems. [68] presents an MILP optimization model for combined cooling, heat and power system operation. The objective is to minimize the total operation and maintenance costs. [69] presents the optimization of a CCHP system using MILP to determine the preliminary design of such systems with thermal storage. The objective function is to minimize the total annual cost. The effect of legal constraints in the design and operation of CCHP systems is highlighted in this study. In [70], the objective of the operation strategy is to maximize the gross operational margin and net present value, and the problem is formulated as an MIP model. In [71], the optimal control problem is formulated as an MINLP, and is solved using discrete dynamic programming. In [45], an MILP algorithm is used to solve the optimal dispatch problem, and the objective function is to minimize the operation cost. In [72], an operation strategy is formulated as an MILP problem aiming to maximize greenhouse gas emissions reductions.

UC optimization, formulated as an MILP problem, can be solved using a linear-programming based branch-and-bound algorithm [73], which is appropriate to solve energy management problems in CCHP systems. The optimal sheduling set points are determined based on current and future conditions, which can guarantee obtaining the global optimal results.

In a CCHP system, a rule-based operation strategy is difficult to use, because a large number of rules would need to be built to satisfy the power flow and system constraints. In EA operation strategies, premature convergence and reasonable computation times need to be considered. In this thesis, we adopt the UC method to control the operation of the CCHP microgrid system. The optimization problem is formulated as an MILP problem, and several constraints are used to describe different operation strategies.

2.3/ SIZING METHOD OF MICROGRID

The above section 2.2 introduced the operation strategy for different types of MGs. As shown in Fig. 2.1, after we know the operation strategy of the MGs, then we can find a method to size the MGs. For the sizing problem, the goal is to achieve cost-effectiveness, namely, minimize the total costs (including investment, maintenance, operation and penalty costs) of the system, and at same time, satisfy different constraints (e.g. technical criteria, logical constraints etc.).

In this section, sizing methods of microgrids are introduced. We also introduce this problem from three aspects:

1. the sizing of a full-electric microgrid;

2. sizing of a multi-energy supply microgrid;

3. sizing of a multi-energy supply microgrid considering utility grids.

2.3.1/ SIZING OF FULL-ELECTRIC MICROGRID

The optimal sizing problem is a non-convex and non-linear combinatorial optimization problem [32], and for the solution of this problem, various optimization methods have been presented in [74].

Firstly, there are large numbers of simulation tools to solve the combination sizing problem. In [75], authors review 68 computer tools which can be used for analyzing RES integration, but the results show that there is no tool that can address all aspects of hybrid microgrid systems.

The conventional method is the trial-and-error method: firstly, list all combinations of the sizing values; after that, deploy these combinations in the simulation model to calculate the annual total cost of the system; at last, the solution with the lowest annual total cost contains the optimum sizing values. This method will be impossible to deploy, because the combination of sizing values will be large when there are several sizing variables, which leads to lots of computation time.

At last, the most appropriate method to solve the combination sizing problem is the evolutionary algorithm (EA) [32, 74].

For example, [31, 32] compare several EAs for the optimal sizing of a hybrid system, where the objective function is the total annual cost. Other papers use various metaheuristics, such as [33] which uses ACO to get size values of a PV/wind hybrid system. In [34], ABSO is used to solve the sizing problem of a PV/WT/FC hybrid system considering loss of power supply probability. Simulated annealing and tabu search (TS) are used in [14]. [35] studies the performance of different PSO algorithm variants to determine the size results of a hybrid (PV/wind/battery) system.

In section 2.2.1, the operation strategy of the full-electric MG has been presented. Then with the EA method, the sizing problem considering energy management of a full-electric MG can be solved. This co-optimization algorithm considering the combinations of sizing and energy management is shown in Fig. 2.1.

Several papers have considered such co-optimization algorithms. For example, in [36], the operation mode of the islanded MG is determined by the SOC of the battery storage. Three operation modes are set based on different rules. The GA method is used to solve the sizing optimization problem with multiple objectives including the minimization of lifecycle cost, the maximization of renewable energy source penetration and the minimization of pollutant emissions. [76] presents a co-optimization method to size standalone microgrids with two GA: one for the sizing, and another one for the scheduling. In [77], authors present a co-optimization method for microgrid planning in electrical power systems. The leader problem optimizes the planning decisions for the microgrids and the main grid, and, with the proposed plan, the short-term and economic operation subproblems are solved to check whether constraints are met or not. In [78], authors also present a microgrid planning model. The problem is decomposed into an investment master problem and an operation subproblem. The two problems are linked via the benders decomposition method. Finally, in [79], the authors present a bi-level program for the

sizing of islanded microgrids with an integrated compressed air energy storage (CAES). The upper level problem is solved using GA, and the lower level problem is solved using the MILP technique.

2.3.2/ SIZING OF MULTI-ENERGY SUPPLY MICROGRID

The above section presented the sizing method of the full-electric MG, and the co-optimization method is often adopted. In this section, the sizing method of multi-energy supply MG is presented.

The traditional sizing method for CCHP systems is the maximum rectangle method (MRM) which uses the hourly load curve and finds the rectangle area under this curve [80], [81]. But this method cannot represent the dynamic, changing performance of the system.

Co-optimization methods are also adopted to search for the optimal sizing values in CCHP MGs. Based on different sizing methods and different operation strategies, the co-optimization methods can be classified as the following types:

a) The first type uses sizing values chosen from a set of discrete values, and the operation strategy is based on rules. For example, [58] presents a method to design a trigeneration plant. Operation strategies are based on rules. The objective of this trigeneration planning model is to minimize the energy production and investment costs over the planning horizon, achieving maximum investment returns. The sizing value of each component is selected from a set of discrete values. [59] researches about the operation and configuration optimization of a CCHP system. Firstly, it chooses different configurations of sizing values, then chooses an operation strategy (FCL, FTL, FEL, and maximum power output) and waste heat allocation proportion. At last, the daily costs are compared, and the optimal system configuration is obtained.

b) The second type of co-optimization method has sizing values chosen from a set of discrete values, and the operation strategy is based on an optimization method. For example, [82] presents an optimal sizing method for cogeneration systems in two steps: first the capacity of each equipment is selected from a set of discrete values, then the optimal operation problem is solved using MINLP based on the above sizing values. [83] presents a generic deterministic linear programming model (which aims to minimize expected annual cost of the system) to determine the optimal size of a micro-CHP unit. [70] presents an optimal design method for a hospital complex. The objective of the operation strategy is to maximize the gross operational margin and net present value. It is formulated as an MIP model.

c) The third type of methods uses sizing values chosen using an evolutionary algorithm, and the operation strategy is based on rules. For example, in [84], authors adopt MRM to determine the lower and higher limits for the total nominal power of the prime mover. GA is used to search for the optimal sizing value of each component. Four operation strategies based on rules are compared. The objective function is named relative annual benefit, and includes investment and maintenance costs of equipment, buying and selling electricity, as well as operational and environmental costs. [85] presents an optimization-based sizing method for CCHP. GA is used to search for the best sizing values, and the objective function is to minimize the total fossil energy consumption. Two operation strategies (improved strategy and base FEL strategy) are compared, and the

primary energy saving ratio is employed to evaluate the strategy. [86] describes a thermodynamic performance analysis to optimize the configurations of a hybrid CCHP system incorporating solar energy and natural gas. GA is used to search for the best configuration, and the operation strategy is based on rules. The objective function is to maximize the annual primary energy savings and the annual total cost savings.

d) The fourth type of methods relies on sizing values chosen using an evolutionary algorithm, and an operation strategy based on optimization. For example, [71] presents a multi-objective model based optimization approach for the optimal sizing of all components. GA and non-linear mesh adaptive direct search method are used to decide the sizing values. The objectives are the capital expenditure, the levelized cost of energy, and emissions. The optimal control problem is formulated as an MINLP, and is solved using discrete dynamic programming. In [79], authors present a bilevel program for islanded MGs with compressed air energy storage. The upper level problem is solved using GA, and the lower level problem is solved using the MILP technique. [45] presents a two-stage optimal planning and design method for a CCHP microgrid system. On the first stage, a multi-objective GA based on NSGA-II is applied to solve the optimal design problem. The objective function is to minimize the total net present cost and carbon dioxide emissions. On the second stage, an MILP algorithm is used to solve the optimal dispatch problem, where the objective function is to minimize the operation cost.

In addition to the above main types, a few other co-optimization methods can be mentioned. For example, in [72], the authors provide an analysis that shows that CHP systems should be sized and operated to reduce greenhouse gas emissions. A controlled random search method is used to search for optimal sizing values, and the operation strategy is formulated as an MILP problem aiming to maximize greenhouse gas emissions reductions. In [77], authors present a co-optimization method for microgrid planning in electrical power systems. The leader problem optimizes the planning decisions for the MG and the main grid. Then, with the proposed plan, the short-term and economic operation subproblems are solved to check constraints violations. In [78], authors present an MG planning model. This problem is decomposed into an investment master problem and an operation subproblem. The two problems are linked via the benders decomposition method. In [87], a multi-objective MINLP model is formulated for the simultaneous system synthesis, technology selection, unit sizing, and operation optimization of a large-scale CCHP system. The objective function is to minimize the total annual cost and the annual global CO_2 emissions. The augmented constraint method is applied to determine the Pareto frontier of the design configuration.

The reviewed co-optimization methods are summarized in Table 2.1.

From the above review, we can conclude that the sizing problem is a hybrid optimization problem. Based on a given operation strategy, different sizing combinations are generated to run the strategy. In this thesis, we therefore research about the optimal sizing problem using the co-optimization method. Namely, GA is used to search for the sizing values, and UC optimization is used to derive the operation strategy.

2.3.3/ SIZING OF MULTI-ENERGY SUPPLY MICROGRID CONSIDERING UTILITY GRIDS

The above works are about the islanded microgrids, or when the utility grid is considered as an infinite power source. In this section, we consider a more realistic utility grid, and

Table 2.1: Selected papers on co-optimization methods.

Refs.	Sizing method	Operation strategy
[82]	discrete values	MINLP
[83]	discrete values	LP
[58, 59]	discrete values	rule-based
[84, 85, 86]	GA	rule-based
[70]	discrete values	MIP
[71]	GA/NOMAD	MINLP
[79]	GA	MILP
[87]	augmented ε-constraint	MINLP
[45]	NSGA-II	MILP
[72]	controlled random search	MILP

research about the sizing of grid-connected multi-energy supply MGs. When MGs are connected into the utility grid, the import power from the utility grids should be considered, which will influence the power flow inside the MG, and result in different sizing values. The export power to MGs will also influence the power flow in utility grid, then the operation state of the utility grid should be checked to ensure the security operation.

In the electricity supply system, many works have been presented about the optimal sizing and siting of distributed generation (DG). [88] reviews classical and heuristic approaches for optimal sizing and placement of DG units in distribution networks. In [89], DG allocation problems are reviewed from the viewpoint of the used optimization algorithms, objectives, decision variables, DG type, applied constraints, and kind of uncertainty models. Papers show that metaheuristic-based approaches are effective in solving the DG allocation problem and are the most common approaches for solving this problem, but these approaches may converge into false local optima rather than the global optimum.

In [90], authors propose an independent system operator (ISO) model for coordinating transmission expansion planning with competitive generation capacity planning in electricity markets. The security-constrained planning problem consists of three problems: transmission capacity planning (maximizing the investment profits), security assessment (minimizing real power mismatch at each bus) and optimal operation (maximizing the revealed surplus based on submitted bids for generation, demand, and incremental transmission). At last, a modified IEEE 30-bus system is used to evaluate the method. [77] presents an algorithm for microgrid planning as an alternative to the co-optimization of generation and transmission expansion planning in electric power systems. The problem is decomposed into a planning problem and an annual reliability sub problem. When the annual reliability limits are violated, the planning decisions will be revised using proper feasibility cuts. The method is tested on a modified IEEE 118-bus system. In [78], authors present a microgrid planning model. This problem is decomposed into an investment master problem and an operation subproblem. These problems are linked via the benders decomposition method. [91] describes an approach to address the microgrid expansion planning problem. The master problem is to maximize the profit of individual investors, the second layer problem is to check the reliability criteria, and the third layer problem is to minimize the operation cost. The proposed method is examined on a four-bus test system. [92] presents an electric expansion planning approach, which includes three options for network expansion as generating units (i.e., wind, solar, and diesel), ESSs, and lines. The problem is described as a two-level MILNP problem, the first level

is to minimize the planning cost, and the second level is to minimize the operation cost. Both problems are solved by a hybrid meta-heuristic optimization technique which collects the benefits of particle swarm optimization (PSO), cultural algorithm, and co-evolutionary algorithms at the same time.

The above papers use the co-optimization methods to solve the microgrid planning problem. The co-optimization method decomposes the planning problem into a master problem and a subproblem which can consider two time scales: long term planning and short term operation. The master problem aims to search for the planning results, and the subproblem is to evaluate the correctness of the operation problem.

Some works about the sizing problem of multi-energy microgrids have also been published, as shown in section 2.3.2. Also the sizing problem of multi-energy microgrids considering utility grid are presented. For example, in [93], authors present an MILP model for the optimal design of DG systems coupled with heating, cooling, and power distribution networks, aiming to minimize the annual overall cost. [94] presents a multi-objective optimization approach based on GA for CHP system within microgrid system. The two objectives are to minimize the total cost and the total gas emissions from the main grid, boiler and DG units. The operation strategies are “following electrical load” and “following thermal load”.

Works about the co-planning of natural gas and power electric systems are also researched. For example, in [95], an integrated electricity and natural gas transportation system planning algorithm is proposed for enhancing the power grid resilience in extreme conditions. The first stage problem is to minimize the investment and the operation costs for the integrated electricity and natural gas, the second stage problem is to minimize load curtailment after the occurrence of the most severe event. The test results on the IEEE-RTS1979 point out that the integrated planning of electricity and natural gas can improve the power system resilience. [96] proposes a long-term co-optimization planning model which incorporates the natural gas infrastructure planning in power system planning. The investment problem is formulated to optimally determine appropriate candidates for generating units, transmission lines, and natural gas pipelines. The second subproblem is the power system feasibility and optimality (minimizing the load curtailment). The third subproblem is the natural gas transportation feasibility (minimizing the nodal natural gas load imbalance). At last, the power system reliability is evaluated. [97] proposes an integrated expansion planning framework for gas and power systems. The model aims to maximize the benefit/cost ratio by calculating benefits in operation reduction, carbon emissions reduction and reliability improvement against augmentation investment costs. [98] presents a long-term, multiarea, and multistage model for supply/interconnections expansion planning of an integrated electricity and natural gas system. The proposed model is formulated as an optimization problem, which minimizes the investment and operation costs to determine the optimal location, technologies, and installation times of any new facility for power generation, power interconnections, and the complete natural gas chain value (supply/transmission/storage) as well as the optimal dispatch of existing and new facilities over a long range planning horizon.

The co-planning method can consider the characteristics of the power system and the natural gas system at the same time, which includes the interactions between both systems on supply and demand sides, and help achieve higher market efficiency in the cost benefit analysis [97].

However research works about the sizing problem of gas/electricity/heat hybrid systems

have not been given a lot of attention so far. [30] researched about the sizing problem of an electricity/heat system, and showed that a single-node aggregate approach (namely, ignore the interconnection structure inside the microgrid) cannot capture the internal energy transfers and the limitations of the electrical/thermal networks.

2.4/ PRICE DECISION ALGORITHM FOR GRID-CONNECTED MICROGRIDS

When the MGs are connected into the utility grid, the prices must be considered. MGs can buy energy from the utility grid, and also can sell energy to utility grid. So how to decide the selling prices of utility grid, and selling prices of MGs are essential problems.

Then in this section, we review related works about the price decision method for MGs. The price decision approaches can be classified into two main categories: 1) game theory approaches; 2) bilevel approaches.

2.4.1/ GAME THEORY APPROACH

In this subsection, we introduce price decision using the game theory approach. One function of the price is to guide the consumers to arrange their demands with the help of demand response (DR). Based on game theory, there exists an optimal price which can make both the supplier and demander maximize profits. So how is game theory used to obtain the best price?

FOR PRICE-BASED DR

[99] presents a Stackelberg game-based demand response model between one utility company and multiple users, aiming at flattening the aggregated load in the system. The utility company acts as the leader, updates the price based on the marginal cost, and the users play as the followers, and update the load demand based on the received price. At last, the Stackelberg equilibrium is reached. [100] develops a model to optimize individual storage device control in response to prices. Optimization is achieved as a function of cost savings versus customer comfort. Two models, Cournot and supply function equilibrium are used to describe the market competition and determine the market clearing price.

[101] presents an energy management scheme for a smart community consisting of a large number of residential units (RUs) and a shared facility controller (SFC) using a non-cooperative Stackelberg game. Firstly, RUs change their own energy consumption based on the selling price to SFC, then the SFC optimizes its cost function, until the cost of SFC is lower than the purchasing from utility grid, the optimal selling price is then obtained. [102] presents a dispatch and bidding strategy for multiple virtual power plants (VPP). Firstly, linear programming is used to dispatch the output of each VPP to minimize the operation cost, then GA is used to decide the bidding price of each VPP, aiming at minimizing the variance of profit of per kWh.

[103] develops an integrated DR program for multiple energy carriers fed into an energy hub in a smart grid. The IDR program is formulated for the electricity and natural gas

networks. The interaction among the hubs is modeled as an ordinal potential game with a unique Nash equilibrium. Electricity and gas utility companies update the electric and gas prices to maximize the potential function until the stopping criterion is reached, at last, the Nash equilibrium is obtained. Results show that when the gas price is high, customers prefer to shift their loads. However, when the gas price is low, they convert gas to electricity using the micro turbines to reduce the peak demand on the supplier side.

[104] proposes a DR algorithm for customers in a smart grid to reduce the peak load of the system. The problem is formulated as two games to maximize the utility companies profit and customers payoff. Electricity suppliers update the bids based on the load demands, then calculate the market clearing price; customers receive the market clearing price, and update the load profile. This process is repeated until the stopping criterion for the algorithm is met. Simulation results show that the algorithm increases the customers payoff and reduces the peak load by shifting the load demand to off-peak periods. The utility companies' profits are also increased by participating in the DR game.

FOR INCENTIVE-BASED DR

[105] proposes a novel type of DR program. This scheme is referred as coupon incentive-based demand response (CIDR). When a wholesale price spike is expected, the load service entities (LSEs) offer coupon incentives to retail customers, and then consumers respond to the coupon incentives and submit their binding demand reduction offers to the LSEs. If the LSEs profit no longer increases (or equivalently the LSE financial loss no longer decreases) from the previous iteration, the convergence criterion stops; otherwise, LSEs increase the coupon price by a price step. Results show that CIDR can effectively induce inherent demand flexibility and reduce system-wide operational cost while maintaining a basic flat rate structure on the retail level.

[106] proposes a bidding approach for LSEs with coupon demand response considering wind power uncertainty and customers behavior patterns toward different coupon prices. The forecasted wind power production is expressed as a set of probabilistic scenarios. A practical probabilistic model of demand reduction under different coupon prices is established based on a residential energy consumption survey. The simulation steps can be concluded as:

1. the LSE offers a coupon price to its customers;
2. the customers provide the range of corresponding demand reduction to the LSE;
3. the LSE calculates its expected net revenue through bidding this revised demand in the ISO electricity market;
4. steps 1)-3) are repeated with different coupon prices.

[107] proposes a novel incentive-based demand response model. It includes three hierarchical levels of a grid operator, multiple service providers, and corresponding customers. A two-loop Stackelberg game is proposed to capture interactions among different actors spanning from the generators, grid operator, service providers, to end consumers.

Based on the above researches, we can see that, for the game theory model, the following steps are often adopted. The leader proposes a price, then followers adjust their load

profiles using DR strategies according to the price. After that, the leader updates a new price, then followers adjust their load profiles again. This process is repeated until a stopping criterion is satisfied. The game theory model proves that there is a best strategy for both the leader and the followers, namely, the Nash equilibrium.

2.4.2/ BILEVEL APPROACH

The above section discusses about the price decision based on game theory. In this subsection, the bilevel approach is introduced.

Because the price is the link between the upper-level problem (the LSE operation is the upper-level problem) and the lower-level problem (the MGs operation is the lower-level problem), this means that price is often the decision variable in the upper-level problem, and is treated as a parameter in the lower-level problem. Then how to solve this problem?

Two specific problems are presented here to introduce the bilevel approach: the market problem and the scheduling problem.

FOR THE TRADING MARKET PROBLEM

[108] presents a real-time market concept architecture for EcoGrid EU. In it, small-scale DERs and small end-consumers can actively participate in a new real-time electricity market by responding to 5-min. real-time electricity prices. The TSO uses a single-period optimization model for the deployment of up and down regulating power and determination of real-time price. The objective function of the problem aims to minimize the regulating power cost while taking into account the prosumer response (demand and DERs) to real-time price signals.

[109] proposes a hierarchical market structure for the smart grid paradigm which is composed of a wholesale electricity market (WEM) and a distribution network electricity market. A new load aggregator is used as the middle agent to participate in the distribution network and the WEMs competing with microgrids and generation companies. The bidding strategy chosen by each market participant is procured using bi-level problem with the upper-level problem representing the market participant's payoff maximization and the lower-level problem minimizing the operation cost of the network.

[110] presents an optimal pricing design for DR integration in the distribution network. An LSE is used to serve two types of loads, namely inflexible and flexible loads. The interaction between the LSE and the customers is formulated as a bilevel optimization problem where the LSE is the leader and DR aggregators are the followers. The goal of the LSE is to maximize the profit; while the goal of the DR aggregators is to maximize the payoff function. The bilevel problem is transferred to an MILP formulation and solved by a branch and bound algorithm.

[111] presents a bilevel problem to decide the dynamic price for the retailer, whose goal is to maximize the profits. The consumers shift their demands based on the dynamic price given by the retailer. The goal is a utility function trading-off the cost of electricity procurement and the discomfort for deviating from the reference temperature band. The problem is reformulated as a single-level MILP.

FOR THE OPERATION SCHEDULING PROBLEM

[112] presents a trading strategy of a proactive distribution company (PDISCO) engaged in the transmission-level (TL) markets. The problem is formulated as a bilevel model. The lower-level problems include the TL day-ahead market and scenario-based real-time markets, aiming to maximize social welfare and minimize operation cost. The upper-level problem is to maximize the PDISCO's profit across these markets. The PDISCO's offering/bidding day-ahead price and real-time price are upper-level problem's decision variables, but treated as parameters in the lower-level problems. An equivalent primal-dual approach is used to reformulate this bilevel model.

[113] presents a decentralized power dispatch model for the coordinated operation of multiple MGs and a distribution system. The problem is formulated as a stochastic bi-level problem with the distribution network operator (DNO) in the upper level and MGs in the lower level. In the bi-level model structure, the first level problem is to minimize the DNO's costs, while the second level problem is to minimize the costs of all MGs. At last, the problem is transformed into a stochastic mathematical program with complementarity constraints (MPCC).

[114] presents a bilevel structure to solve the scheduling of multiple microgrids. A distribution network operator aims to minimize the operation costs, and each MG aims to maximize profits based on a demand response program. MGs can exchange energy with each other. This multiple follower bilevel problem is transferred to single level problem based on KKT conditions.

[115] proposes an autonomous optimization model of an active distribution system with multiple MGs. The distribution network (DN) aims to minimize the generation cost of the units and the interaction cost with the MGs, while each MG aims to minimize the total cost. Due to the exchanged power flow between the DN and MGs, the economic dispatching model of the DN and MGs are coupled with each other. Then in this paper, the authors decouple the model based on analytical target cascading theory, namely, a Lagrange penalty function is proposed to add to the objective function of the DN and MGs. This enables the DN and MGs to autonomously solve their dispatching optimization problem.

The bilevel problem is often converted to a single level MILP problem using the equivalent primal-dual approach. But this method is complex to solve.

We can also note that research works about the price decision of multiple multi-energy-supply MGs have not been given a lot of attention so far, especially, about the relationship between the bidding price, renewable energy penetration and demand response. In this thesis, our goal is to find the best price for both LSE and MGs that can minimize the operation costs of MGs and maximize the profits of the LSE. We combine GA and MILP to decide the prices. MILP is used to control the operation of LSE and MGs. GA is used to update the price.

2.5/ CONCLUSION

In this chapter, we reviewed related works about the sizing and operation problem of microgrids. Three specific aspects were reviewed: the operation strategy of full electric microgrids and multi-energy supply microgrids; the sizing method of full electric microgrids,

multi-energy supply microgrids and grid-connected microgrids; and the price decision approach for grid-connected multiple multi-energy-supply microgrids.

We found that although a large number of papers have been presented to solve the microgrid sizing problem, there are still some problems that need to be solved. These problems can be concluded as:

1. How to size and operate hydrogen-based microgrids (combining hydrogen storage and battery storage);
2. How to size and operate multi-energy supply microgrids (considering electricity/heating/cooling/hydrogen demands);
3. How to size and operate multi-energy supply microgrid considering the electricity/gas/heat utility grid;
4. How to decide the prices for grid-connected multiple multi-energy-supply microgrids.

In the following chapters, the solutions to the above problems will be discussed and explained in details.

II

CONTRIBUTION

3

MICROGRID MODELING

In this thesis, we research about the sizing and operation of microgrids. Firstly, we need to build the model of the microgrid system. Two types of microgrids are modeled in this section:

1. A full-electric microgrid, where five components are contained: PV panels, a battery storage system, a hydrogen storage system (including an electrolyzer, hydrogen tanks and a fuel cell).
2. A multi-energy supply microgrid, where nine components are contained: PV panels, a solar heating system, a battery storage system, a hydrogen storage system, a heat boiler, an air conditioner, an absorption heat chiller, a heat storage system, and electricity, heat, cooling and hydrogen loads.

In the following sections, the mathematical model of each component is introduced.

3.1/ SOLAR GENERATION COMPONENTS

The output of the PV generator can be calculated from [79, 116]:

$$P_{PV} = N_{PV} \cdot f_{PV} \cdot P_{STC} \cdot \frac{G_A}{G_{STC}} \cdot (1 - (T_C - T_{STC}) \cdot C_T) \tag{3.1}$$

where N_{PV} is the number of PV panels, f_{PV} the conversion efficiency, P_{STC} the PV array power under standard test conditions (STC), G_A the global solar radiation on the PV array, G_{STC} the solar radiation under STC, T_C the temperature of the PV cells, T_{STC} the STC temperature (298 K), and C_T the PV temperature coefficient.

For the solar heating system, the output is computed with [117]:

$$Q_{sh} = N_{sh} \cdot \eta_{sh} \cdot G_A \tag{3.2}$$

where N_{sh} is the area of the heating system, and η_{sh} its efficiency.

3.2/ FUEL CELL MODEL

A fuel cell (FC) can produce electricity from hydrogen (H_2), which can be drawn from hydrogen tanks. In this thesis, we use the voltage electrical model presented in [118] to

describe the characteristic of FC:

$$V_{fc} = (E_{OC} - r_{fc} \cdot i_{fc} - A \cdot ln(i_{fc}) - m \cdot e^{n \cdot i_{fc}}) \cdot N_{fc} \tag{3.3}$$

where V_{fc} is the FC voltage, E_{OC} is the open-circuit voltage of one cell, i_{fc} is the current density in one cell, N_{fc} is the number of cells, and n, r_{fc}, A, and m are empirical coefficients.

As an PEM FC generates electricity and heat at the same time, the produced heat can be calculated as in [119]:

$$Q_{fc} = N_{fc} \cdot (1.48 - \frac{V_{fc}}{N_{fc}}) \cdot I_{fc} \tag{3.4}$$

Then the hydrogen consumed by the FC is computed using:

$$\dot{n}_{H2}^{con} = \frac{N_{fc} I_{fc}}{2FU} \tag{3.5}$$

where F is the Faraday constant, and U is the utilization efficiency of hydrogen in the FC.

From the above equations, we can derive that $P_{fc} = f(\dot{n}_{H2}^{con})$, where $f(.)$ is a nonlinear function. In order to reduce the calculation time and obtain a linear model, we use linear regression to simplify this function, without significant loss of model accuracy in the normal operation zones:

$$\dot{n}_{H2}^{con} = k_{fc} \cdot P_{fc} \tag{3.6}$$

where k_{fc} is a constant.

In the following, we give an example of PEM FC model based on the above analysis. The main parameters of the PEM FC model is shown in Tab. 3.1.

Table 3.1: PEM FC parameters.

Fuel cell [19, 21, 118, 76]	
A	0.03
r_{fc}	2.45×10^{-4}
m	2.11×10^{-5}
n	0.008

The voltage and current characteristic curve of one fuel cell can be seen in Fig. 3.1.

The voltage and power characteristic curve of one fuel cell stack can be seen in Fig.3.2.

The relationship between output power and consumed hydrogen of one fuel cell stack can be seen in Fig.3.3.

The FC operates as the main power source, which means that it will run for a large number of hours, and over time, its performance will decrease. The degradation of the fuel cell must thus be considered [120, 121]. Here, we consider a steady-state lifetime FC model, where the output current is a constant value, which reduces the degradation of fuel cell. As the FC operates as a long term storage system, cycling loads (load changes, start-stop, idling, and high power) will be the main load demands, which will accelerate the degradation of the fuel cell [122]. But in this first planning stage, the future operation states of the fuel cell are unknown, which means that the accelerated factors of degradation are unknown. In other words, the future operation states can only be

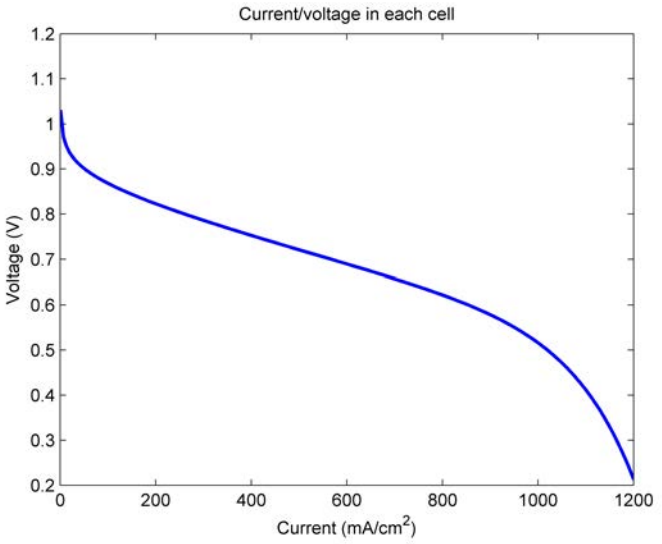

Figure 3.1: Voltage/current characteristic of a fuel cell.

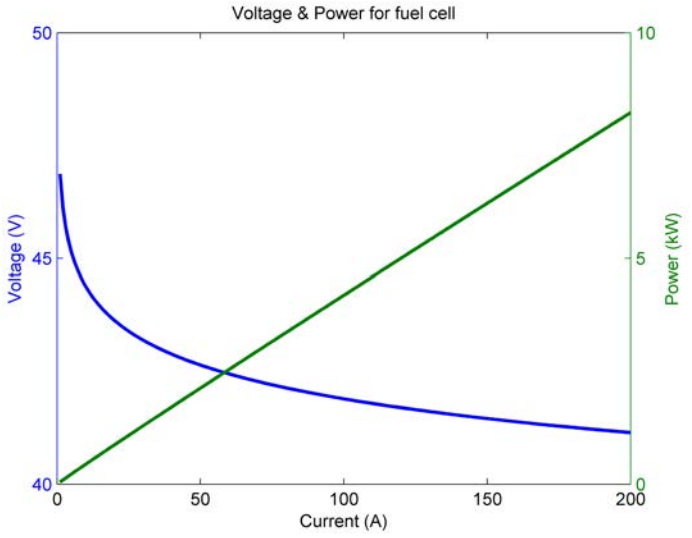

Figure 3.2: Voltage and power characteristic of a fuel cell stack.

estimated. The steady state lifetime model is therefore adopted, where it is assumed that the FC will operate at a constant output.

The degradation of the fuel cell causes a voltage drop, which can be modeled as:

$$\Delta V_{fc} = k_{vd} \cdot t_{day} \tag{3.7}$$

where ΔV_{fc} is the voltage drop of fuel cell, t_{day} is the operation duration, k_{vd} is a constant value.

The degradation of the fuel cell mainly influences the resistance r_{fc} [120]. This means that resistance r_{fc} increases as the fuel cell keeps operating. This can be written as:

$$r_{fc}(t_{day}) = k_{rfc} \cdot k_{vd} \cdot t_{day} \tag{3.8}$$

where $r_{fc}(t_{day})$ is the resistance at time t_{day}, and k_{rfc} is a constant coefficient.

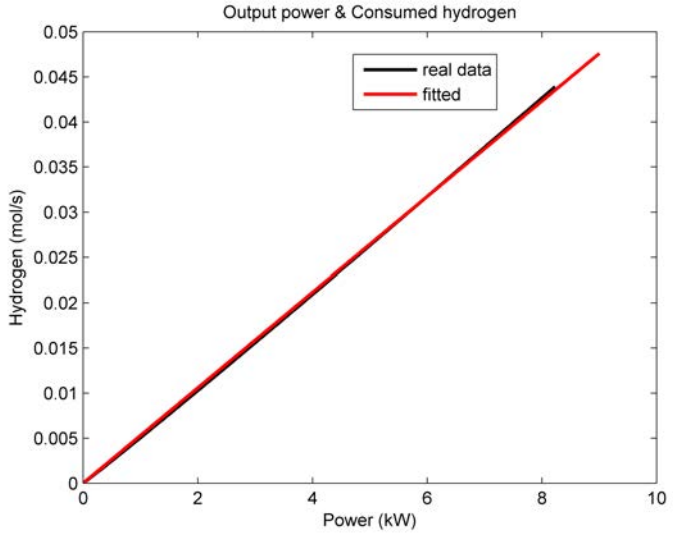

Figure 3.3: Relationship between output power and consumed hydrogen.

The degradation model of the fuel cell can then be written as:

$$V_{fc} = (E_{OC} - r_{fc}(t_{day}) \cdot i_{fc} - a \cdot ln(i_{fc}) - m \cdot e^{n_0 \cdot i_{fc}}) \cdot N_{fc} \tag{3.9}$$

With the above degradation model, Fig. 3.4 can be obtained, which shows the voltage/current characteristic of the fuel cell after different operation durations.

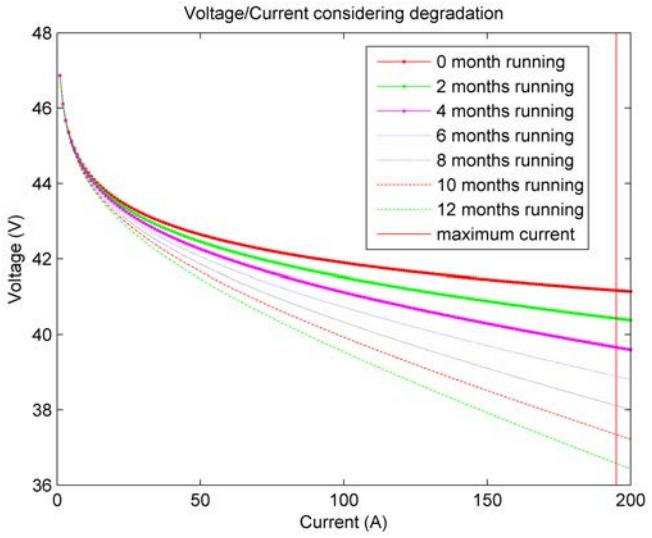

Figure 3.4: Voltage/current characteristic of a fuel cell after different operation durations.

From Fig. 3.4, the relationship between output power and consumed hydrogen considering the degradation model can be obtained:

$$\dot{n}_{H2}^{con} = k_{fc}(t_{day}) \cdot P_{fc} \tag{3.10}$$

where $k_{fc}(t_{day})$ is the coefficient value in time t_{day}, derived from current and voltage curves, as shown in Fig. 3.4.

On the other hand, the degradation of the fuel cell also decreases the maximum output power. As a fuel cell has a maximum output current, with different voltage/current curves, the maximum output power is also different. This can be represented as:

$$P_{fc}^{max}(t_{day}) = P_{ini}^{max} - k_{fcm} \cdot t_{day} \tag{3.11}$$

where $P_{fc}^{max}(t_{day})$ is the maximum output power at time t_{day}, P_{ini}^{max} is the initial maximum output power, and k_{fcm} is the coefficient.

3.3/ ELECTROLYZER MODEL

An electrolyzer can produce hydrogen from electricity, and this hydrogen is then usually stored in tanks. The characteristic of an electrolyzer can be described as follows [123, 124]:

$$\begin{aligned} V_{el} &= N_{el} \cdot V_{rev} + (r_1 + r_2 \cdot T) \cdot \frac{I_{el}}{A_{el}} \\ &+ (s_1 + s_2 \cdot T + s_3 \cdot T^2) \cdot log(1 + (t_1 + \frac{t_2}{T} + \frac{t_3}{T^2}) \cdot \frac{I_{el}}{A_{el}}) \end{aligned} \tag{3.12}$$

where V_{el} is the voltage of the electrolyzer, N_{el} the number of cells, V_{rev} the reversible cell potential, T the temperature and $I_{el}/A_{el}(A/m^2)$ the current density. r_1, r_2, s_1, s_2 , s_3, t_1, t_2, and t_3 are empirical coefficients.

As for the FC, the theoretical production rate of hydrogen in a cell is given by:

$$\dot{n}_{H2}^{pro} = \eta_F \frac{N_{el} I_{el}}{2F} \tag{3.13}$$

Based on Faraday's efficiency, we can obtain the relation between the real production rate of hydrogen and the theoretical one, using:

$$\eta_F = \frac{(I_{el}/A_{el})^2}{f_1 + (I_{el}/A_{el})^2} f_2 \tag{3.14}$$

where f_1 and f_2 are coefficients.

As for the FC, we also linearize the model to obtain:

$$\dot{n}_{H2}^{pro} = k_{el} \cdot P_{el} \tag{3.15}$$

where k_{el} is a constant.

In the following, we give an example of an alkaline electrolyser model. The main parameters of the electrolyzer are shown in Tab. 3.2.

The voltage and power characteristic curve of one electrolyzer stack can be seen in Fig.3.5. The relationship between input power and produced hydrogen of one electrolyzer stack can be seen in Fig.3.6.

Contrary to the FC, the degradation of the electrolyzer will cause the cell voltage to increase [125, 9], which can be represented as:

$$\Delta V_{el} = k_{vi} \cdot t_{day} \tag{3.16}$$

Table 3.2: Alkaline electrolyzer parameters.

Electrolyzer [123, 124, 76]	
r_1	0.0015
r_2	-6.019 $\times$ 10^{-6}
s_1	2.427
s_2	-0.0307
s_3	3.9 $\times$ 10^{-4}
t_1	0.214
t_2	-9.87
t_3	119.1
f_1	150
f_2	0.99

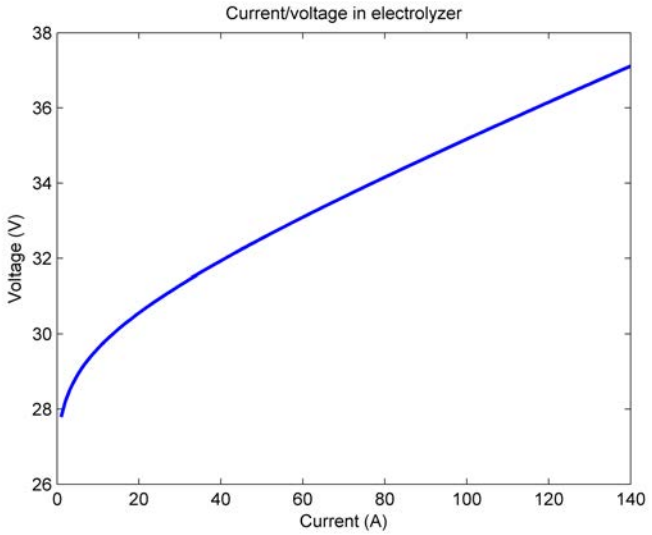

Figure 3.5: Voltage and current characteristic of one electrolyzer stack.

where ΔV_{el} is voltage increase of the electrolyzer, t_{day} is the operation time, and k_{vi} is a constant value.

Electrolyzer degradation mainly influences the resistance r_1 in equation (3.12) [9]. This means that resistance r_1 will change as the electrolyzer continues operating. This can be written as:

$$r_1(t_{day}) = k_{rele} \cdot k_{vi} \cdot t_{day} \tag{3.17}$$

where $r_1(t_{day})$ is the resistance at time t_{day}, and k_{rele} is a coefficient.

The degradation model of the electrolyzer can then be written as:

$$\begin{aligned} V_{el} &= N_{el} \cdot V_{rev} + (r_1(t_{day}) + r_2 \cdot T) \cdot \frac{I_{el}}{A_{el}} \\ &+ (s_1 + s_2 \cdot T + s_3 \cdot T^2) \cdot log\left(1 + \left(t_1 + \frac{t_2}{T} + \frac{t_3}{T^2}\right) \cdot \frac{I_{el}}{A_{el}}\right) \end{aligned} \tag{3.18}$$

With the above degradation model, Fig. 3.7 can be obtained, which shows the voltage/current characteristic of the electrolyzer after different operation durations.

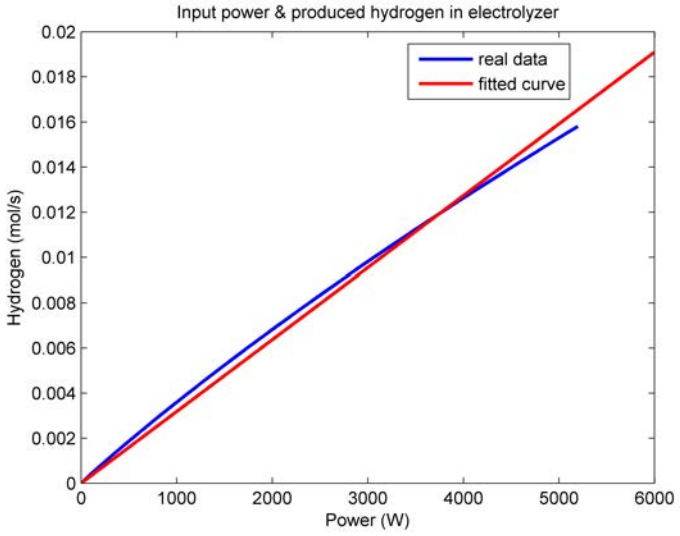

Figure 3.6: Relationship between input power and produced hydrogen.

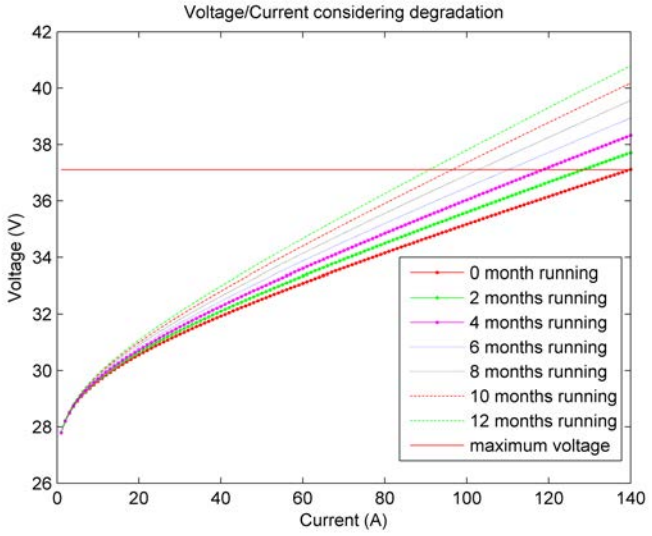

Figure 3.7: Voltage/current characteristic of an electrolyzer after different operation durations.

From Fig. 3.7, the relationship between input power and produced hydrogen with the degradation model can be obtained:

$$\dot{n}_{H2}^{pro} = k_{el}(t_{day}) \cdot P_{el} \tag{3.19}$$

where $k_{el}(t_{day})$ is the coefficient value at time t_{day}.

On the other hand, the degradation of the electrolyzer also increases the maximum input power. As the electrolyzer has a maximum input voltage, this means that with different voltage/current curves, the maximum input power will be different. This can be represented as:

$$P_{ele}^{max}(t_{day}) = P_{inie}^{max} - k_{elem} \cdot t_{day} \tag{3.20}$$

where $P_{ele}^{max}(t_{day})$ is the maximum input power in time t_{day}, P_{inie}^{max} is the initial maximum input

power, and k_{elem} is the coefficient.

3.4/ HYDROGEN TANK MODEL

A hydrogen tank is used to store the hydrogen produced by the electrolyzer, as well as to supply hydrogen to the fuel cell. We use the level of hydrogen (LOH) to represent the state of the hydrogen tank:

$$LOH(t) = LOH(t - \Delta t) + \dot{n}_{H2}^{pro} \cdot \Delta t - \dot{n}_{H2}^{con} \cdot \Delta t - L_{H_2}(t) \tag{3.21}$$

where $L_{H_2}(t)$ is the hydrogen load demand. Then, with the law of perfect gases ($PV = nRT$), the volume of the H_2 tanks can be calculated.

3.5/ BATTERY

We use the state-of-charge (SOC) to represent the state of the battery as follows:

$$SOC(t) = SOC(t - \Delta t) + \frac{\eta_{ch} \cdot P_{ch}(t) \cdot \Delta t}{C_{ba}} - \frac{\eta_{dis} \cdot P_{dis}(t) \cdot \Delta t}{C_{ba}} \tag{3.22}$$

where η_{ch}, η_{dis} are the charging and discharging efficiency, $P_{ch}(t)$ is the charging power, $P_{dis}(t)$ is the discharging power, Δt is the interval time, and C_{ba} is the capacity of the battery.

For the battery, we use the same linear degradation model as for the fuel cell. Calendar and cycling age [126] are the two main factors that cause the degradation of the battery. Four models are used to fit the state-of-health (here, the ratio of the current usable capacity to the initial or nominal capacity) of the battery [126]. In addition, the degradation of the battery is also caused by the cycling operation. For example, [127] shows the degradation of the capacity with the number of cycles. Therefore, a linear model is used to describe the degradation of the battery.

As in the first planning stage, the future operation of battery is uknown, so it is assumed that the degradation of the battery is linear. Based on the linear model, the remaining capacity of the battery in each day can be calculated:

$$C_{ba}(cycles) = C_{ini} - \frac{C_{ini} - C_{last}}{Cycles_{max}} \cdot cycles \tag{3.23}$$

3.6/ THERMAL COMPONENTS

The above sections describe the electric components, in order to serve the heat/cooling load demands, the thermal components are needed. The thermal components use electric energy to produce heat, such as the heat boiler; or use the electric energy to produce

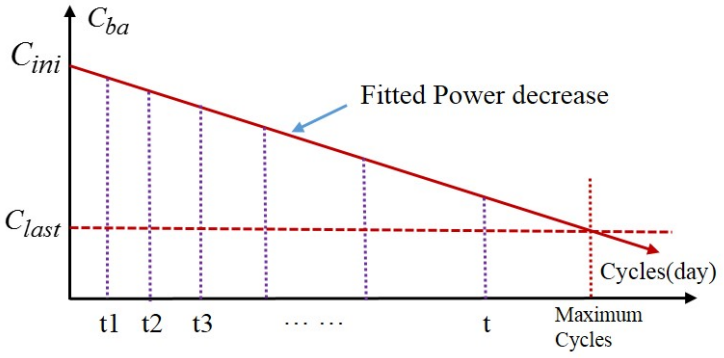

Figure 3.8: Remaining capacity of battery vs. number of cycles.

cooling, such as the air conditioner; or use the heat energy to produce cooling, such as the absorption heat chiller. In this section, different thermal components are modeled.

We use simple models for the thermal components. A heat boiler uses electricity to produce heat, as follows:

$$Q_{hb} = \eta_{hb} \cdot P_{hb} \tag{3.24}$$

where P_{hb} is the input power, η_{hb} the efficiency, and Q_{hb} the output heat.

An air conditioner is used to cool air [128]:

$$C_{ac} = \eta_{ac} \cdot P_{ac} \tag{3.25}$$

where P_{ac} is the input power, η_{ac} the efficiency, and C_{ac} the cooling output power.

Similarly, the absorption heat chiller uses heat to produce cooling, so the relation is [128]:

$$C_{ahc} = \eta_{ahc} \cdot Q_{ahc} \tag{3.26}$$

where Q_{ahc} is the input heat, η_{ahc} the efficiency, and C_{ahc} the output cooling power.

Finally, the state of the heat storage system is represented by the amount of heat stored [63]:

$$HS(t) = HS(t - \Delta t) + \eta_{hs}^{ch} \cdot Q_{hs}^{ch}(t) \cdot \Delta t - \frac{Q_{hs}^{dis}(t)}{\eta_{hs}^{dis}} \cdot \Delta t \tag{3.27}$$

where $HS(t)$ is the stored heat at time Δt. $Q_{hs}^{ch}(t)$ and $Q_{hs}^{dis}(t)$ are the charge and discharge heating power at time t. η_{hs}^{ch} and η_{hs}^{dis} are the charge and discharge efficiency, respectively.

3.7/ CONCLUSION

In this chapter, different components are modeled, to form the microgrid systems. A PEM fuel cell and an alkline electrolyzer are used as the long term storage system, and the characteristics of the PEMFC and alkline electrolyzer are presented. The relationship between output power and consumed hydrogen in the fuel cell is calculated, also the relationship between input power and produced hydrogen in the electrolyzer is formulated. Then the linear degradation model of the fuel cell, the electrolyzer and the battery are developed. At last, thermal components are modeled. For the following chapters, different cases will be presented and discussed.

4

SIZING OF A FULL-ELECTRIC ISLANDED MICROGRID

This chapter is based on the author's published paper: Li Bei, Robin Roche, and Abdellatif Miraoui. "Microgrid sizing with combined evolutionary algorithm and MILP unit commitment." Applied energy 188 (2017): 547-562.

In this chapter, we focus on the optimal sizing of microgrids where PV panels are used as the primary energy source, and BSS and HSS are used as storage units (Fig. 4.1).

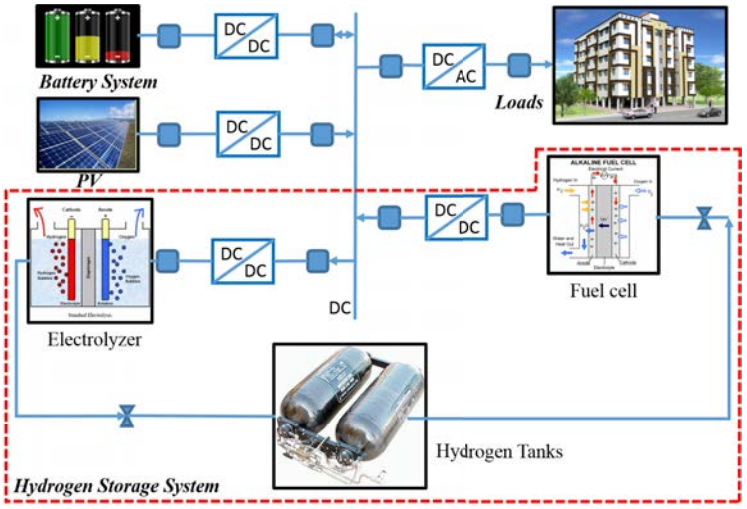

Figure 4.1: Microgrid architecture.

Finding the optimal size for each of these components, i.e., finding the capacity or rated power for each component that ensures adequate supply at minimum cost, is a challenge because the sizing result is affected not only by the architecture of the system, but also by the adopted energy management strategy [129]. Depending on how components such as storage units are used, the necessary capacity may change significantly, which in turn impacts the size of other components as well as overall costs. Another aspect to consider is the impact of uncertainty on PV output and load. Forecasting errors change the input data profiles and lead to sub optimal scheduling results, which in turn influences sizing results. To address these challenges, this chapter presents a leader-follower co-optimization method to size islanded microgrids, which also considers uncertainty on input data.

This chapter introduces a general method to size a stand-alone microgrid considering technical and economic criteria, with a combination of EA and UC optimization. A genetic algorithm is used to compute the sizing of the components to minimize the total annual cost (capital, maintenance and operation) of the system. Each candidate solution (set of components sizes) is evaluated with a MILP UC algorithm. The designed bi-level optimization framework is shown in Fig. 4.2.

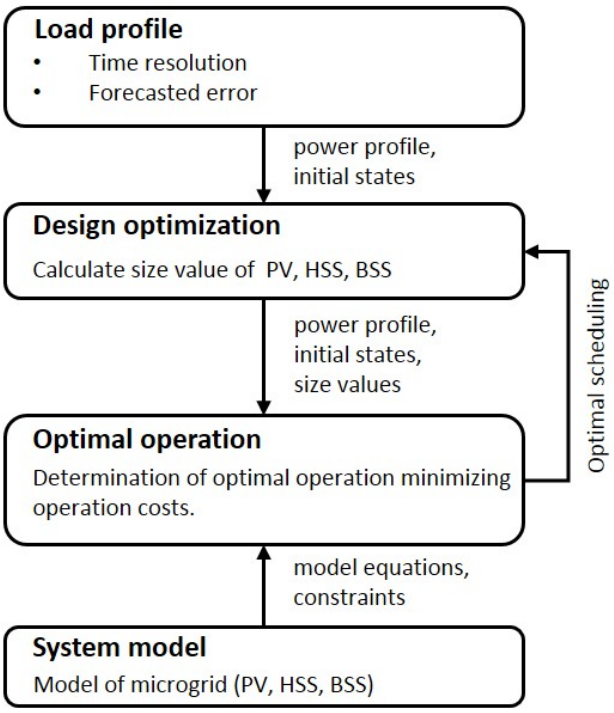

Figure 4.2: Bi-level optimization framework.

The rest of this chapter is structured as follows. Section 4.1 describes the UC strategy and Section 4.2 the EA-based sizing problem formulation. Finally, Section 4.3 presents the simulation results while Section 4.4 concludes the chapter.

4.1/ SCHEDULING STRATEGY

As the results of the sizing process depend on how the different components are used (i.e., what is their output), an appropriate control strategy is required. Contrary to classical components, ESS introduce a temporal link between time steps and scheduling algorithms have to consider this link to ensure that the SOC remains within allowed bounds. This constraint is necessary to ensure that the results of the sizing are adequate, and components oversizing is avoided. As a consequence, it is necessary to predict the evolution of the entire system, including PV generation, which is the primary source of energy for the microgrid.

This section uses a form of MPC to plan the operation of the system in advance, using forecasts. Due to the presence of mixed logical and integer variables, the problem is expressed as an MILP problem.

4.1.1/ COST FUNCTION

In order to achieve economically efficient operation, the utilization cost of the BSS and the HSS need to be quantified and minimized over a given time horizon [7, 76, 130]. For the BSS, aging is a major concern that limits the lifetime of the device. As a consequence, the investment cost and the degradation of the BSS have to be taken into account in the operation cost. For the BSS, when it discharges/charges more power, then the degradation of the BSS is more, in other words, the utilization cost is larger. Then, the utilization cost for charge and discharge are then implemented as follows [130]:

$$B_{cost}^{ch}(t) = \frac{C_{bat}^{inv} \cdot P_{ch}(t) \cdot \eta_{ch}}{2 \cdot N_{cycles}} \tag{4.1}$$

$$B_{cost}^{disch}(t) = \frac{C_{bat}^{inv} \cdot P_{disch}(t) \cdot \eta_{dis}}{2 \cdot N_{cycles}} \tag{4.2}$$

where C_{bat}^{inv} is the investment cost for the BSS, and N_{cycles} the number of cycles over its lifetime.

For the HSS, the O&M and the startup costs must also be considered. The utilization cost of the electrolyzer and the FC can be computed as follows [130]:

$$H_{cost}^{ele}(t) = \left(\frac{C_{ele}^{inv}}{N_{hours}^{ele}} + C_{ele}^{o\&m} \right) \cdot \delta_{ele}(t) + C_{ele}^{start} \cdot \Delta\delta_{ele}(t) \tag{4.3}$$

$$H_{cost}^{fc}(t) = \left(\frac{C_{fc}^{inv}}{N_{hours}^{fc}} + C_{fc}^{o\&m} \right) \cdot \delta_{fc}(t) + C_{fc}^{start} \cdot \Delta\delta_{fc}(t) \tag{4.4}$$

where C_{ele}^{inv} and C_{fc}^{inv} are the investment costs for the electrolyzer and the FC. $C_{ele}^{o\&m}$ and $C_{fc}^{o\&m}$ are the operation and maintenance costs of both components. Similarly, C_{ele}^{start} and C_{fc}^{start} are their startup cost. N_{hours} represents the number of hours of operation of the HSS over its lifetime. $\delta_{ele}(t)$ and $\delta_{fc}(t)$ describe their state (i.e., 1 for on, 0 for off). Finally, $\Delta\delta_i$ represents whether the unit is starting or not, and is defined as:

$$\Delta\delta_i(t) = \max\{\delta_i(t) - \delta_i(t-1), 0\}, i = \{ele, fc\} \tag{4.5}$$

Based on the previous cost functions, the total operation cost function for the entire microgrid, over a time horizon of T_{hor} steps, can be built:

$$C_{\text{op}} = \sum_{t=1}^{T_{hor}} \left(B_{cost}^{ch}(t) + B_{cost}^{dis}(t) + H_{cost}^{ele}(t) + H_{cost}^{fc}(t) + \alpha \cdot P_{LS}(t) + \beta \cdot P_{curt}(t) \right) \tag{4.6}$$

where $P_{LS}(t)$ is the shed load, $P_{curt}(t)$ is the curtailed PV output, and α and β are the corresponding penalty values. Load shedding (LS) and PV curtailment (PVC) are two means of flexibility to ensure a balance between generation and demand. However, their use has to be minimized due to their impact on customer comfort and system efficiency, respectively. The values of penalty coefficients α and β are thus chosen to discourage the use of LS and PVC. A form of demand response could however also be used [131, 132], but is kept for future work.

4.1.2/ CONSTRAINTS

The operation of the various components is subject to several constraints, as is the islanded operation of the system. In the following equations, $i = \{ele, fc\}$ and $j = \{ele, fc, ch, disch\}$. First, all component outputs have to be between their minimum and maximum values:

$$P_j^{min} \leq P_j(t) \leq P_j^{\max} \tag{4.7}$$

In order to consider the status of each device (on or off), the above equation becomes:

$$\begin{aligned} \delta_j(t) \cdot P_j^{min} \leq & Z_j(t) \leq \delta_j(t) \cdot P_j^{\max} \\ & Z_j(t) = \delta_j(t) \cdot P_j(t) \end{aligned} \tag{4.8}$$

where $Z_j(t)$ represents actual outputs of component j at time t.

Due to linearity constraints, this equation can then in turn be transformed into the following two inequalities:

$$\begin{aligned} Z_j(t) &\leq P_j(t) - (1 - \delta_j(t)) \cdot P_j^{min} \\ Z_j(t) &\geq P_j(t) - (1 - \delta_j(t)) \cdot P_j^{\max} \end{aligned} \tag{4.9}$$

Another constraint is that the electrolyzer and the FC should not be working at the same time, as this would mean charging and discharging at the same time. The HSS is thus either charging or discharging:

$$\delta_{ele}(t) + \delta_{fc}(t) \leq 1 \tag{4.10}$$

A similar constraint is used for the BSS:

$$\delta_{ch}(t) + \delta_{disch}(t) \leq 1 \tag{4.11}$$

The SOC and LOH constraints also have to be verified:

$$SOC_{min} \leq SOC(t) \leq SOC_{max} \tag{4.12}$$

$$LOH_{H_2}^{min} \leq LOH_{H_2}(t) \leq LOH_{H_2}^{\max} \tag{4.13}$$

Then, equation (4.5) can be rewritten as:

$$\Delta\delta_i(t) = \delta_i(t) \cdot (1 - \delta_i(t-1)), i = \{ele, fc\} \tag{4.14}$$

From [133], the above nonlinear equation can be transformed into the following linear constraints:

$$-\delta_i(t) + \Delta\delta_i(t) \leq 0 \tag{4.15}$$

$$-(1 - \delta_i(t-1)) + \Delta\delta_i(t) \leq 0 \tag{4.16}$$

$$\delta_i(t) + (1 - \delta_i(t-1)) - \Delta\delta_i(t) \leq 1 \tag{4.17}$$

Finally, as the system is islanded, the balance between generation and demand has to be met at all time steps, so:

$$P_{PV}(t) - P_{curt}(t) - (P_{load}(t) - P_{LS}(t)) = Z_{ele}(t) - Z_{fc}(t) + Z_{ch}(t) - Z_{dis}(t) \tag{4.18}$$

4.1.3/ PROBLEM FORMULATION

Using the above cost function and constraints, the microgrid UC problem can be summarized as follows, where $\widetilde{S}$ is the set of variables:

$$\min_{\widetilde{S}}\{C_{\text{op}}\} \quad \text{s.t.} \quad (3.22), (3.15), (3.6), (3.21), (4.7) - (4.18) \tag{4.19}$$

4.2/ SIZING ALGORITHM

The scheduling strategy presented in the previous section requires several input variables. Some of these variables correspond to the maximum rating or capacity of each component, which are the results of the sizing algorithm. Other inputs are parameters set by the user, such as the initial SOC and LOH values, and the penalty coefficients α and β. The impact of these parameters on results will be discussed in Section 4.3.

4.2.1/ LEADER-FOLLOWER STRUCTURE

The sizing problem aims at finding the optimal size of the PV, BSS, electrolyzer and FC components to achieve the most cost-effective solution over a given time period. Let $N_{PV} \in \mathbf{N_{PV}}$, $C_{bat} \in \mathbf{C_{bat}}$, $V_{H_2}^{\max} \in \mathbf{V_{H_2}}$, $P_{el}^{\max} \in \mathbf{P_{el}}$, $P_{fc}^{\max} \in \mathbf{P_{fc}}$. Set $\mathbf{U}$ represent the whole set of sizing variables, namely, $\mathbf{U} = \mathbf{N_{PV}} \cup \mathbf{C_{bat}} \cup \mathbf{V_{H_2}} \cup \mathbf{P_{el}} \cup \mathbf{P_{fc}}$, and $U \in \mathbf{U}$.

The problem can be formulated as a leader-follower problem [134]. The leader problem (the sizing problem) is as follows:

$$\min_{U \in \mathbf{U}}\{F(\mathbf{U})\} \tag{4.20}$$

where $F(.)$ is a function representing the total cost of the system over the simulation duration.

The follower problem (the scheduling problem), is defined as:

$$\min_{U^*, \widetilde{S}}\{C_{\text{op}}\} \quad \text{s.t.} \quad (3.22), (3.15), (3.6), (3.21), (4.7) - (4.18) \tag{4.21}$$

where U^* is the set of sizing values obtained from the leader.

In other words, the leader first returns a candidate set of values for N_{PV}, C_{bat}, $V_{H_2}^{\max}$, $P_{el}^{\max}$, and $P_{fc}^{\max}$. Then the follower uses these values to calculate the total operation cost using the algorithm described in Section 4.1. Based on this cost information, the leader adjusts the sizing values until an optimal value that minimizes the overall cost is found.

4.2.2/ LEADER PROBLEM OBJECTIVE FUNCTION

To obtain a valid estimate of the actual cost of the system, operation cost is insufficient as capital and maintenance costs must also be considered [32, 31, 76]. In order to convert the initial capital cost to an annual capital cost, the capital recovery factor (CRF) is used [32]:

$$CRF = \frac{r(1+r)^{n_{inv}}}{(1+r)^{n_{inv}} - 1} \tag{4.22}$$

where r is the real interest rate and n_{inv} is the expected life span of the microgrid.

The total capital cost corresponds to the cost of buying the equipment, given by:

$$C_{\text{cap}} = CRF \cdot (N_{PV} \cdot C_{PV}^{inv} + P_{fc}^{\max} \cdot C_{fc}^{inv} + P_{el}^{\max} \cdot C_{ele}^{inv} + V_{H_2} \cdot C_{tank}^{inv} + C_{bat} \cdot C_{bat}^{inv}) \tag{4.23}$$

where C^{inv} variables represent the costs of the PV, FC, electrolyzer, hydrogen tanks and battery components.

Similarly, the annual maintenance cost is given by:

$$C_{\text{mnt}} = N_{PV} \cdot C_{PV}^{mnt} + V_{H_2} \cdot C_{tank}^{mnt} + C_{bat} \cdot C_{bat}^{mnt} \tag{4.24}$$

where C^{mnt} variables represent the annual maintenance costs of the PV, hydrogen tanks and battery components. As the O&M cost of the FC and the electrolyzer are considered in the operation strategy equations (4.3) to (4.4), they are not included in the annual cost.

The fitness function of the leader problem is thus the total cost function $F(.)$ given by:

$$F = C_{\text{cap}} + C_{\text{op}} + C_{\text{mnt}} \tag{4.25}$$

Finally, the overall sizing problem can be formulated as:

$$\begin{aligned} &\min_{U \in \mathbf{U}} \{C_{\text{cap}} + \min_{U^*, \bar{S}} \{C_{\text{op}}\} + C_{\text{mnt}}\} \\ &s.t. \quad (3.22), (3.15), (3.6), (3.21), (4.7) - (4.18) \end{aligned} \tag{4.26}$$

4.2.3/ Simulation process

In order to obtain the optimal sizing for the system, an MILP-based scheduling algorithm and an EA-based sizing algorithm are combined.

A GA [37, 135] is used to solve the leader problem. GA are based on the natural selection process similar to biological evolution. Operators such as selection, crossover and mutation enable generating candidate solutions. The decision variables of the GA are rounded to the nearest higher value, namely sizing values, and are then used in the MILP algorithm.

The simulation process is shown in Fig. 4.3

1. A population of N candidate solutions for the GA is randomly initialized.
2. Each of these solutions is then used with the follower problem. The UC MILP optimization is run. If the solution is infeasible (namely, the MILP problem can not be solved), a new candidate solution is generated.
3. The GA fitness function value is then computed to determine the total cost of each candidate solution.
4. The process continues until any stopping criterion is met. An adaptive method is selected for this. Firstly, if the fitness function values for two consecutive steps are the same, then counter Num is incremented. If Num exceeds a given maximum value, the simulation stops as the fitness function is not improving anymore. The second criterion is on the number of iterations, for which a maximum number is set.

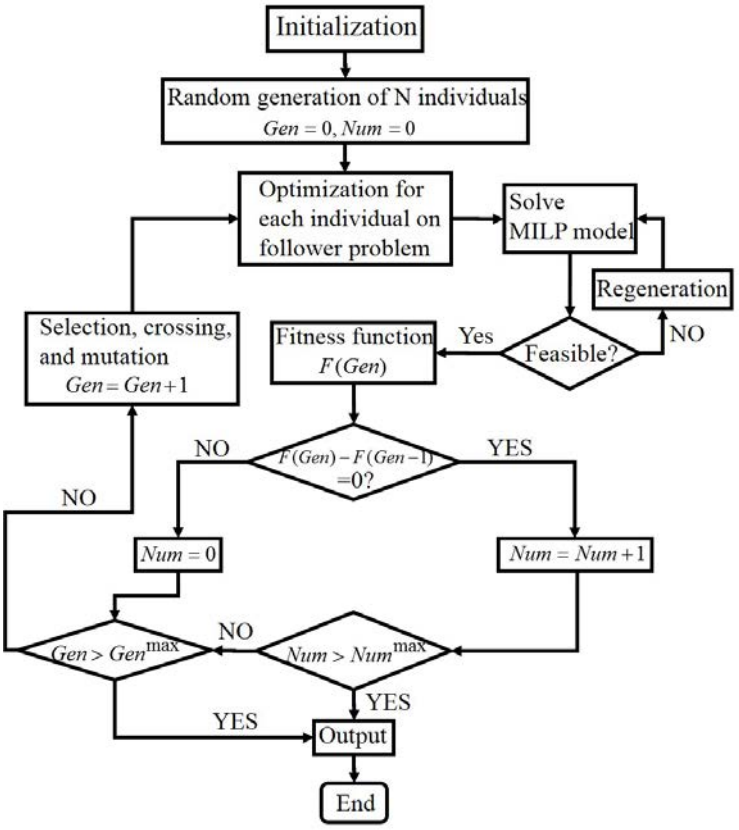

Figure 4.3: Optimization process outline.

4.3/ SIMULATION RESULTS

In order to validate the sizing methodology, we run several simulation cases. Different operation strategies are compared to research about the influence of operation strategies on the sizing values. Also different initial states (such as SOC, LOH) are deployed in the operation strategy to evaluate their influence on the sizing results.

4.3.1/ SIMULATION SETUP

Simulations are performed using Matlab R2014a and Gurobi 6.5.1, running on a desktop computer with an Intel Xeon 3.1 GHz processor, 16 GB RAM, and Microsoft Windows 7. Input data profiles for solar radiation and load (Fig. 4.4) are obtained and adapted from a research building (FCLAB) located on the UTBM campus in Belfort, France. In order to analyze the sensitivity of sizing results to load levels, we use two load profiles. As shown in Fig. 4.4, load profile 2 is 50% larger than load profile 1. Component parameters used in the simulations are given in Table 4.1.

In order to keep simulation time to reasonable durations, weekly average data is used for the input data. The approximate duration for each run is then of approximately 30 minutes. Although resolutions of 1 hour or more could be used, simulation durations would increase significantly and could not be performed on a regular computer within reasonable time.

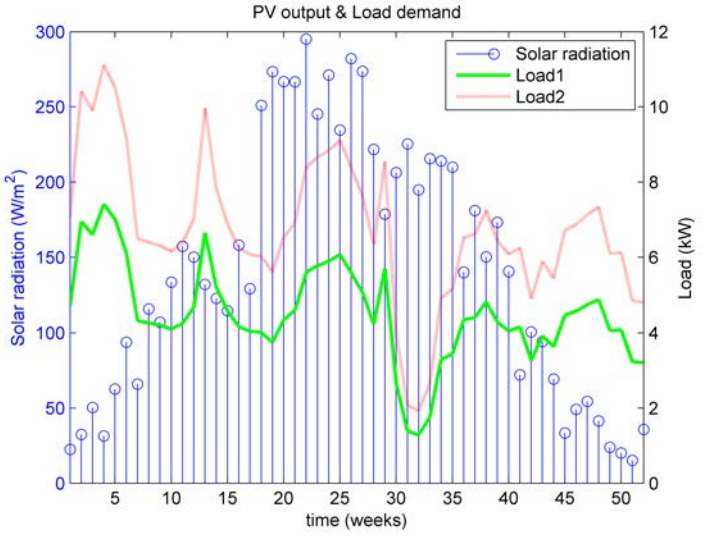

Figure 4.4: Weekly average solar radiation and load profiles.

4.3.2/ CASES OVERVIEW

To evaluate the impact of initial conditions and parameters, five cases are compared. Each case assumes different values for SOC_{ini}, LOH_{ini} [1], α and β, and one of the two load profiles. Case assumptions are summarized in Table 4.2. Cases 1A and 1B, and Cases 2A and 2B are designed to compare the influence of different initial states for SOC and LOH on the sizing results. Case 2 is also used to analyze the influence of different load levels on the sizing of the HSS and the BSS. Case 3 is designed to analyze the influence of the penalty values (α and β) on sizing results, with values ranging from 10^1 to 10^5. Results are summarized in Table 4.3.

4.3.3/ RESULTS FOR CASE 1

For Case 1A, the sizing results return 52 PV panels, a 6 kW FC, a 7 kW electrolyzer, tanks with a capacity of 7178 Nm^3, and 189 kWh of batteries, for a total cost of €201,970. Here, unit Nm^3 corresponds to the volume under standard conditions (1 bar, 0°C). Based on the ideal gas law, we can estimate the volume for a higher pressure and temperature. For example, under 700 bar/15°C, the above volume would amount to 10.82 m^3 [2]. Convergence results of the GA are shown in Fig. 4.5, and indicate that 200 generations seem sufficient. Similar convergence results are obtained for other cases. Here, it should notice that different runs of GA return different results, unless each run of GA converges to optimal results. Then, in our case, we run the GA algorithm for several times, and choose the smallest one. Tab. 4.4 shows the simulation results of GA for case 1A within 5 times running.

Fig. 4.6 shows the scheduling results. The HSS is more frequently used than the BSS, as the HSS is cheaper to use when the power gap between PV output and load demand

[1] Unit is $N.m^3$.

[2] This calculation is based on the ideal gas law $PV = nRT$. Actually, we should notice that under high pressure P, the ideal gas law does not apply well.

Table 4.1: Component and simulation parameters.

Fuel cell [19, 21, 118, 76]	
A	0.03
r_{fc}	2.45×10^{-4}
m	2.11×10^{-5}
n	0.008
C_{fc}^{inv}	4,000 €/kW
$C_{fc}^{o\&m}$	0.2 €/h
Life cycles	30,000h
P_{fc}^{min}	1kW
Electrolyzer [123, 124, 76]	
r_1	0.0015
r_2	-6.019×10^{-6}
s_1	2.427
s_2	-0.0307
s_3	3.9×10^{-4}
t_1	0.214
t_2	-9.87
t_3	119.1
f_1	150
f_2	0.99
C_{ele}^{inv}	3,200 €/kW
$C_{fc}^{o\&m}$	0.2 €/h
Life cycles	30,000h
P_{ele}^{min}	1kW
Battery [76]	
C_{bat}^{inv}	470 €/kWh
C_{bat}^{mnt}	1 €/kW.year
$N_{bat,cyc}$	2,000
SOC_{min}	0.5
SOC_{max}	0.9
Hydrogen tanks [76]	
C_{tank}^{inv}	150 €/Nm^3
C_{tank}^{mnt}	10 €/Nm^3.year
$V_{H_2}^{min}$	1Nm^3
PV panels[76]	
C_{PV}^{inv}	7,400 €/kW
C_{PV}^{mnt}	6 €/kW.year
CRF [76]	
n_{inv}	20 years
r	0.05

is large. Fig. 4.7 shows the change in hydrogen level in the tanks. As in winter the PV output is insufficient, the HSS discharges mostly to supply the load, but in summer, PV output is large enough to enable the HSS to recharge and store hydrogen. Due to the large penalty values (10^5) for LS and PVC, these two options are almost not used.

Fig. 4.7 also shows the SOC profile of the BSS, that is used as an auxiliary storage system

Table 4.2: Simulation cases assumptions.

Cases	1A	1B	2A	2B	3
SOC_{ini}	0.5	0.9	0.5	0.9	0.5
LOH_{ini}	5000	3000	8000	7000	5000
α	10^5	10^5	10^5	10^5	10^3
β	10^5	10^5	10^5	10^5	10^3
Load profile	1	1	2	2	1

Table 4.3: Sizing results.

Case	Load	SOC_i	LOH_i	Total Cost [€]	C_{op} [€]	C_{cap} [€]	N_{PV}	$P_{fc}^{\max}$ [kW]	$P_{el}^{\max}$ [kW]	V_{H_2} [N.m^3]	C_{bat} [kWh]
1A	1	0.5	5000	201970	1697.8	127980	52	6	7	7178	189
1B	1	0.9	3000	160070	1663.2	105070	52	6	7	5283	179
2A	2	0.5	8000	219410	1725.1	137210	50	11	6	8000	158
2B	2	0.9	7000	200290	1674.5	128090	54	10	7	7000	190
3	1	0.5	5000	205160	4562.2	125120	52	7	7	7515	2
RBS	1	0.5	5000	276560	151.9	174640	57	7	8	10100	407

Table 4.4: 5 times running of GA for case 1A.

Objective function	N_{PV}	$P_{fc}^{\max}$ [kW]	$P_{el}^{\max}$ [kW]	V_{H_2} [N.m^3]	C_{bat} [kWh]
214,290	52	9	14	7598	203
218,850	51	11	9	7578	373
206,950	51	14	7	7234	244
201,970	**52**	**6**	**7**	**7178**	**189**
232,940	54	20	22	7970	293

to ensure the balance between generation and demand, while avoiding load shedding and PV curtailment.

For Case 1B, the initial SOC is larger and the initial LOH lower. The capacity of the hydrogen tank decreases to 5283 Nm^3, while the battery capacity decreases to 179 kWh. Consequently, the total cost also decreases to €160,070€. The scheduling results for Case 1B are similar to the ones obtained for Case 1A, and are thus not shown. Fig. 4.8 shows the LOH and SOC levels. As the initial SOC is larger than for 1A, the total required capacity is lower. For the LOH, the profile is almost the same as in Case 1A. For the SOC, in Case 1A, the initial state is the minimum SOC, so the BSS cannot discharge at the beginning, but for Case 1B, the initial state is the maximum SOC and the BSS can then discharge.

4.3.4/ Results for Case 2

For Cases 2A and 2B, the second load profile with a 50% higher demand is used. For Case 2A, the sizing results return 50 PV panels, a 11 kW FC, a 6 kW electrolyzer, tanks with a capacity of 8000 Nm^3, and 158 kWh of batteries, for a total cost of €219,410. Fig. 4.9 shows the scheduling results, and Fig. 4.10 the LOH and SOC profiles. The HSS is sufficient to provide energy to the load, especially at the beginning, so the needed battery capacity is lower. However, in Case 2B, the HSS is insufficient to meet the load, so more PV panels and battery energy are needed. We can also see that the rating of

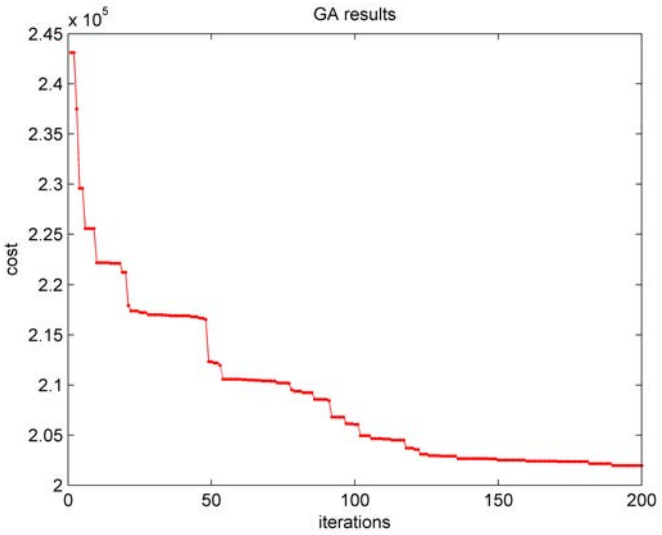

Figure 4.5: GA searching results for Case 1A.

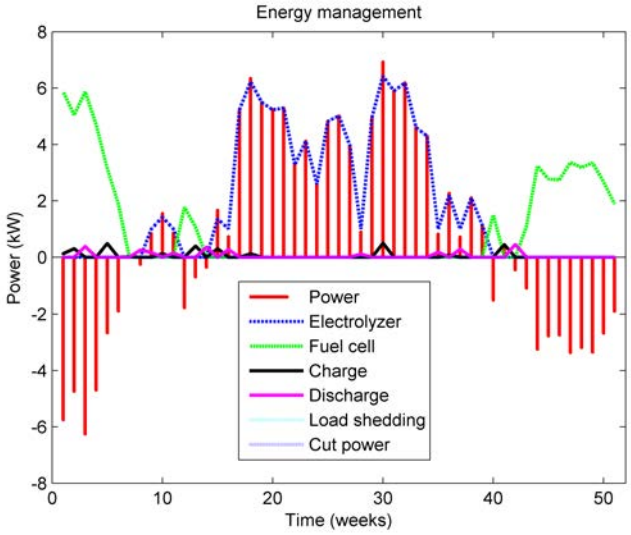

Figure 4.6: Scheduling results for Case 1A. The curve labelled “Power” corresponds to the PV output minus the load.

the FC is larger than in Case 1. As more energy is needed, it becomes cheaper to use the FC than the battery, hence the higher FC rating.

For Case 2B, the sizing results return 54 PV panels, a 10 kW FC, a 7 kW electrolyzer, tanks with a capacity of 7000 Nm^3, and 190 kWh of batteries, for a total cost of €200,290. As the load is higher than that of Case 1, more storage, in the form of BSS and HSS is needed. As the cost of the energy initially contained in the storage units is not accounted for, the algorithm increases the size of the storage units rather than increasing the number of PV panels. The obtained scheduling results are close to the ones shown in Fig. 4.9. Fig. 4.11 shows the LOH and SOC profiles. Due to slight differences in the scheduling results, the SOC curve is difference from the one in Case 2A. However, the curves for LOH is similar, as the HSS operates as a longer term storage unit.

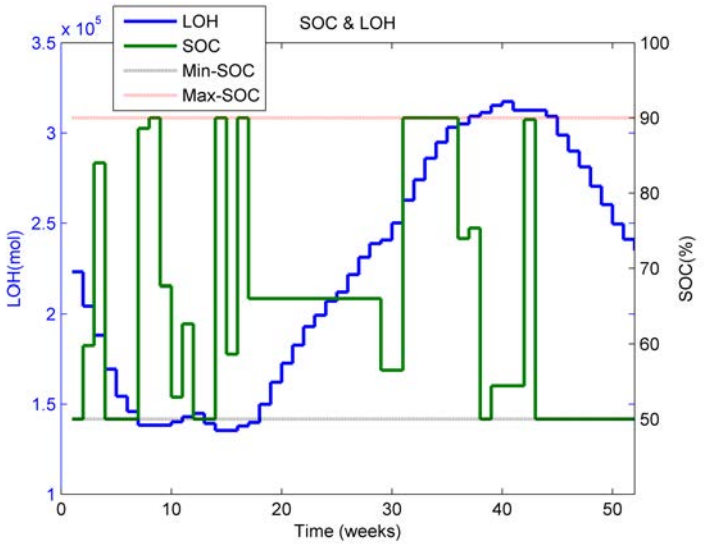

Figure 4.7: LOH and SOC for Case 1A.

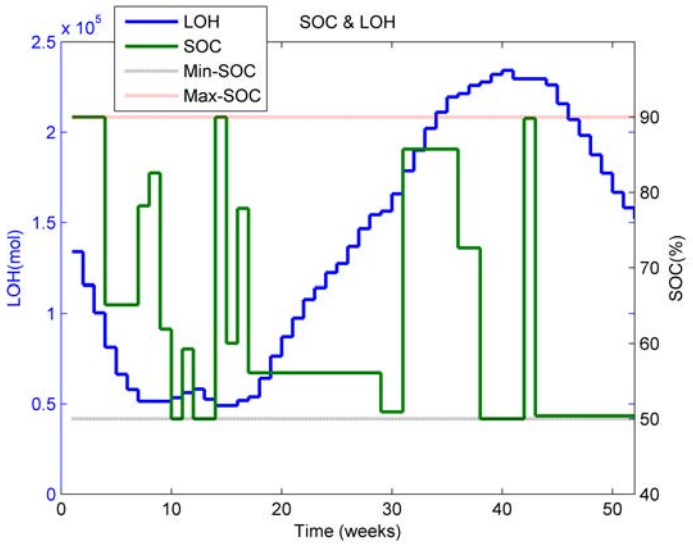

Figure 4.8: LOH and SOC for Case 1B.

4.3.5/ RESULTS FOR CASE 3

In this case, as the penalty values are lower (10^3 instead of 10^5), more energy is shed or curtailed. As a consequence, the sizing results return 52 PV panels, a 7 kW FC, a 7 kW electrolyzer, tanks with a capacity of 7515 Nm^3, and 2 kWh of batteries, for a total cost of €205,160. Detailed LS, PVC, LOH and SOC profiles are shown in Fig. 4.15.

The size of the battery is significantly smaller than in other cases. This can be explained by the lower values of the penalties for LS and PVC, which make these two options more competitive compared to using the BSS. In order to futher evaluate the influence of the different penalty values, we simulate different combinations of α and β with Case 1A. The results are shown in Table4.5 and Figs. 4.12 and 4.13, and indicate that the smaller the values of α and β, the larger the magnitude of LS and PVC, respectively.

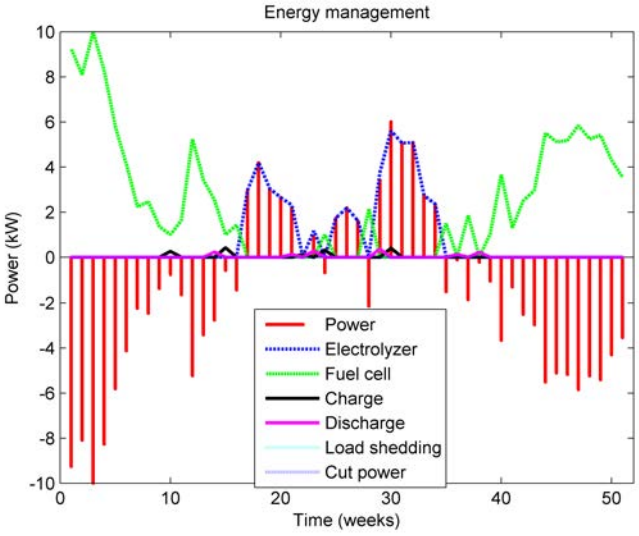

Figure 4.9: Scheduling results for Case 2A. The curve labelled “Power” corresponds to the PV output minus the load.

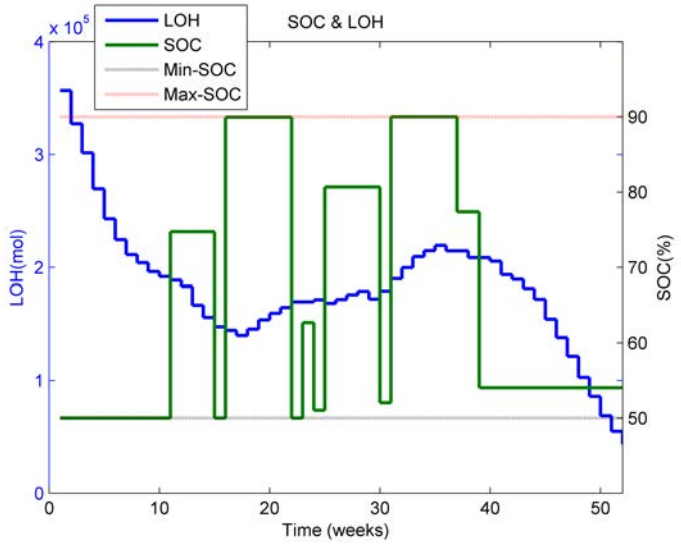

Figure 4.10: LOH and SOC for Case 2A.

Scheduling results are shown in Fig. 4.14, where we observe that limited LS and PVC occur, although for Cases 1 and 2 the BSS was used to supply the load (due to its cheaper cost). As expected, the algorithm chooses the most economical way to operate the system.

4.3.6/ Discussion of Cases 1 to 3

From the summary of results shown in Table 4.3, it can be observed that the sizing results and the total cost are impacted by the use of different input data and initial states. A comparison of the breakdown of costs for all cases is shown in Fig. 4.16. Results indicate that the capital costs are the highest, while O&M costs remain relatively small.

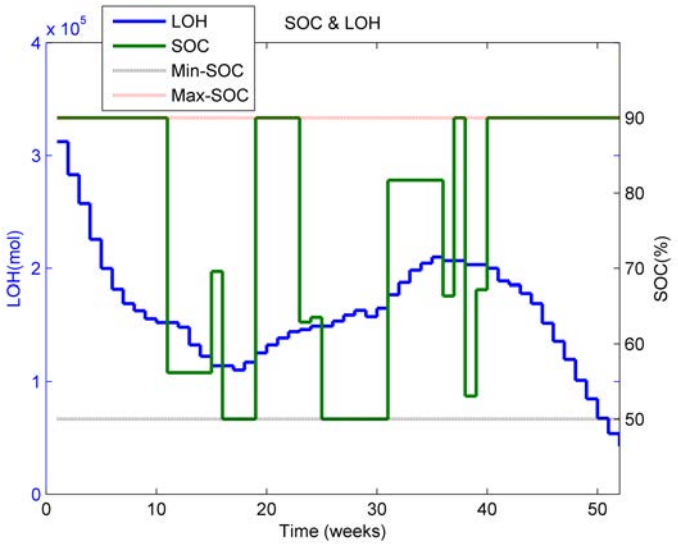

Figure 4.11: LOH and SOC for Case 2B.

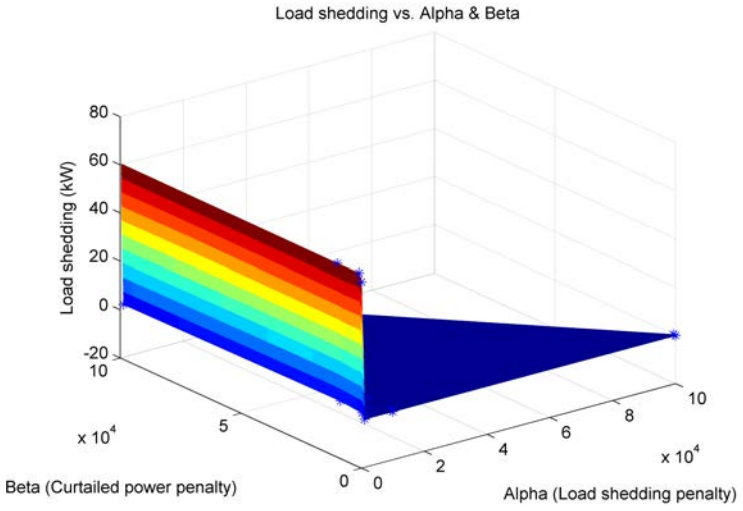

Figure 4.12: Load shedding vs. α & β.

As the only primary energy source is PV, these results are not surprising. The initial energy contained in the BSS and the HSS is however not considered. Case 3 has the largest O&M cost, due to the penalty values combined to LS and PVC. For Case 2A, more fuel cell and hydrogen tanks are needed, which results in the largest capital and total cost.

Simulations also show that the HSS is more appropriate for long term (seasonal) storage, as expected. This is especially valid as FC and electrolyzers have limited dynamics, and require BSS or other fast dynamics storage units to complement them and act as an auxiliary unit. On the other hand, because the discharge and charge power of the HSS are separate, the degradation of the HSS will be slower than for the BSS.

Regarding LS and PVC penalty values, results have shown that values in the range of value $[10^3, 10^5]$ are reasonable and enable limiting the use of LS and PVC only to neces-

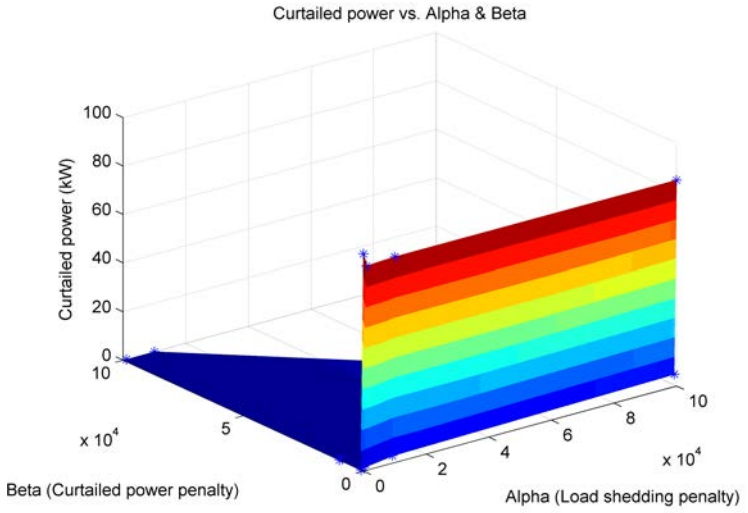

Figure 4.13: Curtailed power vs. α & β.

Table 4.5: Sizing results with different penalty values for Case 1A.

Case 3	$\sum_{t=1}^{T_{hor}} P_{LS}(t)$ [kW]	$\sum_{t=1}^{T_{hor}} P_{curt}(t)$ [kW]	N_{PV}	$P_{fc}^{\max}$ [kW]	$P_{el}^{\max}$ [kW]	V_{H_2} [N.m^3]	C_{bat} [kWh]
$\alpha = 10^5, \beta = 10^3$	0	4.4576	51	7	7	6823	58
$\alpha = 10^5, \beta = 10^1$	0	84.8847	50	7	1	5026	2
$\alpha = 10^4, \beta = 10^1$	0	84.7377	50	7	2	5543	2
$\alpha = 10^4, \beta = 10^3$	0.0839	2.4054	55	7	8	8341	2
$\alpha = 10^4, \beta = 10^4$	0.0352	0	52	6	7	7601	170
$\alpha = 10^4, \beta = 10^5$	0.1297	0	59	7	8	11123	113
$\alpha = 10^3, \beta = 10^1$	0	84.1643	50	7	2	7015	2
$\alpha = 10^3, \beta = 10^3$	2.209	0.7691	52	7	7	7515	2
$\alpha = 10^3, \beta = 10^4$	3.0844	0	52	7	8	10978	11
$\alpha = 10^3, \beta = 10^5$	1.9553	0	54	7	8	8315	38
$\alpha = 10^1, \beta = 10^1$	57.3662	89.4729	50	2	2	5793	2
$\alpha = 10^1, \beta = 10^3$	60.5996	0	50	2	7	9110	1
$\alpha = 10^1, \beta = 10^4$	60.3302	0	50	2	7	9023	2
$\alpha = 10^1, \beta = 10^5$	60.5804	0	50	2	7	9157	2

sary cases. Values larger than 10^5 result in no LS or PVC at all, which can be problematic are they can be seen as flexibility means of last resort.

4.3.7/ COMPARISON WITH A RULE-BASED OPERATION STRATEGY

In order to compare the obtained results with a simpler, reference case, we implement a rule-based operation strategy (RBS) [22, 136]. The outline of the algorithm is shown in Fig. 4.17. The principle is to use the HSS first, and if it is unavailable, to use the BSS. It should be noted that the algorithm does not try to maintain the SOC or LOH level for future use, contrary to the proposed algorithm. Case 1A is run again with the RBS. Results, also given in Table 4.3, show that because using HSS is cheaper, the operation cost is low, but then more BSS capacity is required to ensure power balance. As a consequence, the total capital cost is the largest of all cases.

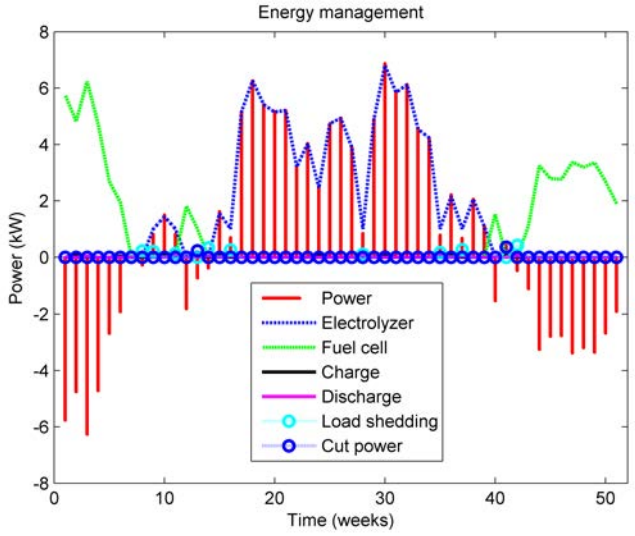

Figure 4.14: Scheduling results for Case 3. The curve labelled “Power” corresponds to the PV output minus the load.

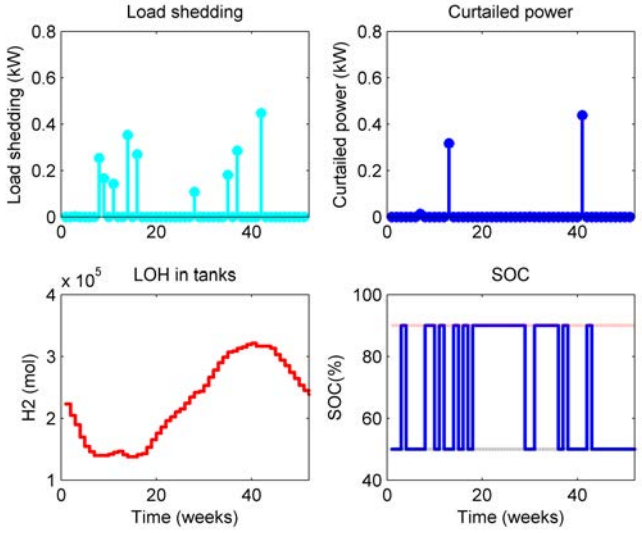

Figure 4.15: Shed and curtailed power, LOH and SOC profiles for Case 3.

4.3.8/ INFLUENCE OF TIME RESOLUTION

In the above simulation, one-week average data is used. A better time resolution (for example, one day or one hour) may provide more accurate results; however, this would also significantly increase computation time to several days or more. In order to check the validity of the obtained results with more precise input data, a rolling-horizon scheduling simulation with a 1-hour time resolution is conducted. This resolution is selected as it is the maximum resolution available for the input data. In summary, the algorithm runs a scheduling task with 1-hour data over 1 day, and repeats this every day for a year.

Results are shown in Figs. 4.18 (SOC, LOH, LS and PVC) and 4.19 (scheduling results from 2000 hour to 2300 hour). From these curves, it can be observed that large LS and

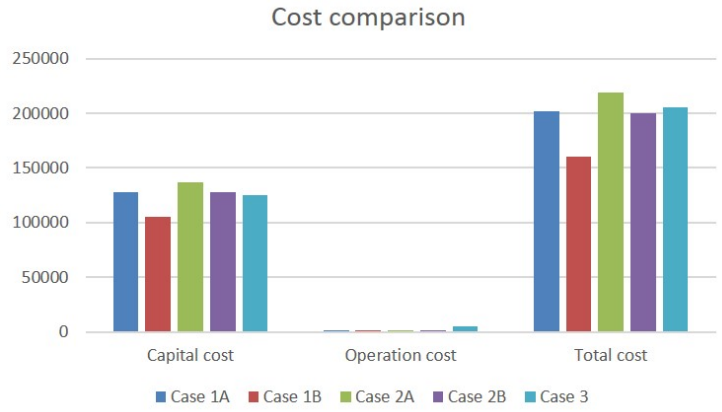

Figure 4.16: Comparison of costs for all cases.

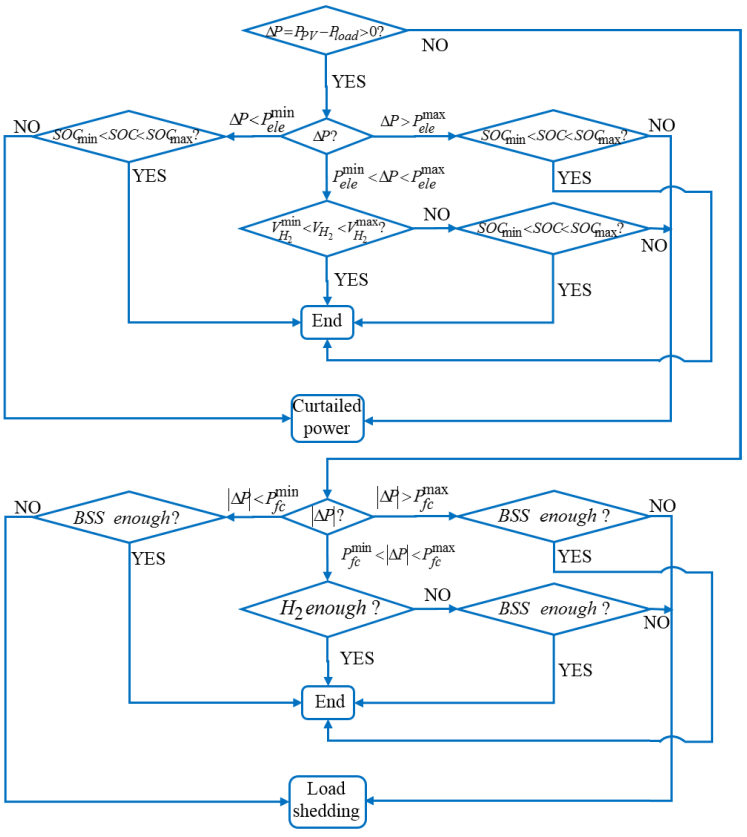

Figure 4.17: Rule-based strategy algorithm.

PVC occur during some periods of the year. As LS and PVC use are supposed to remain rare, this means that the sizing results are insufficient. A reason for this result is that the average data reflects the average load in the system, but does not consider peak load situations. A similar reasoning may be used for PV generation.

In order to adjust sizing results, the difference between PV output and load demand is computed and shown in Fig. 4.20. Then we adopt the maximum shortage value (i.e., the minimum value in Fig. 4.20) as the capacity of the fuel cell, and the maximum surplus value (i.e., the maximum value in Fig. 4.20) as the capacity of the electrolyzer. The sizing

value of the HSS is adjusted, so that $P_{fc}^{max} = 13$, $P_{ele}^{max} = 37$.

After this adjustment, the rolling-horizon simulation is run again. Fig. 4.21 shows the resulting SOC, LOH, LS and PVC, and Fig. 4.22 shows the scheduling results from 2000 hour to 2300 hour with the new sizing values. After adjusting the sizing value based on the peak load demand, no LS or PVC occur. With the adjusted sizing values, we run MILP scheduling for Case 1A, and total cost is €212,160, the operation cost C_{op} is €1,788.7, and the capital cost C_{cap} is €138,080.

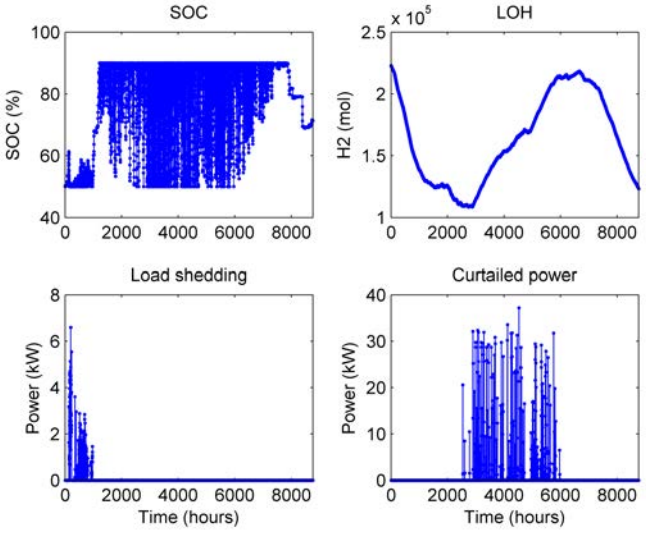

Figure 4.18: One-hour one-day rolling horizon scheduling simulation.

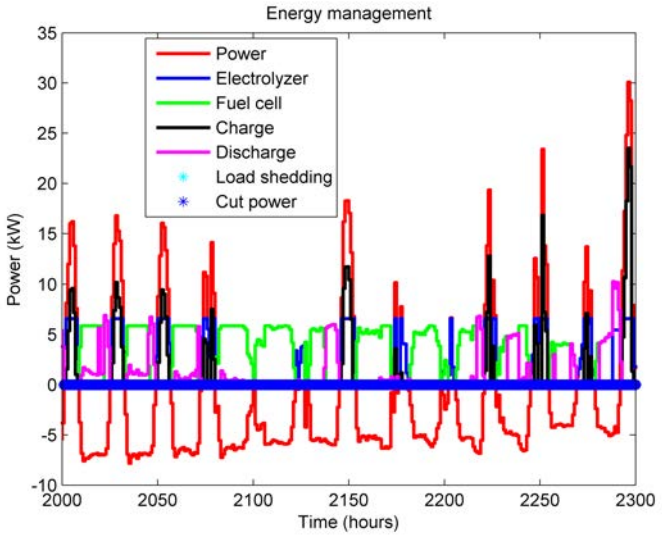

Figure 4.19: One-hour one-day rolling horizon scheduling simulation (2000 h-2300 h). The curve labelled “Power” corresponds to the PV output minus the load.

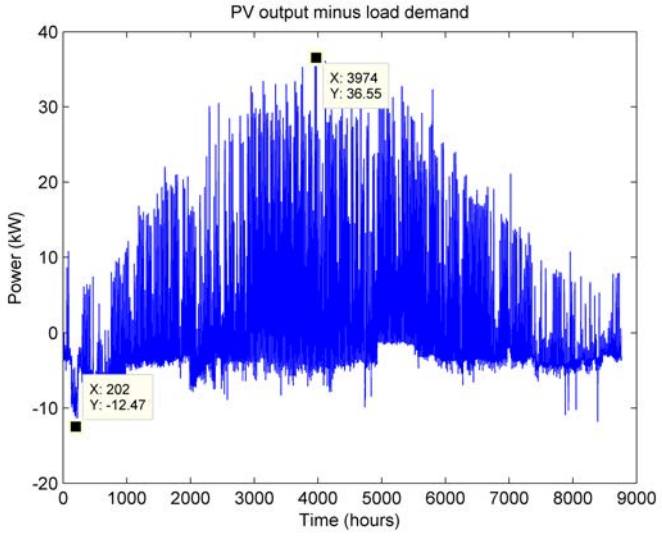

Figure 4.20: PV output minus load demand.

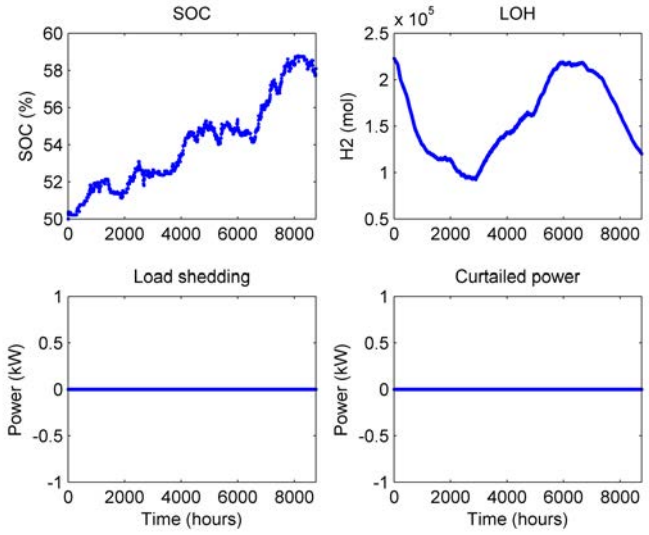

Figure 4.21: One-hour one-day rolling horizon scheduling simulation with the new sizing value of HSS.

4.3.9/ INFLUENCE OF UNCERTAINTY

As discussed earlier, uncertainty on forecasts of PV output and load can impact sizing results. To account for this uncertainty, the upper bound and lower bounds of estimated values are used. In the following, $\widetilde{P_{PV}(t)}$ and $\widetilde{P_{load}(t)}$ are the actual PV output and load values, and Er_{PV} and Er_{load} the error on PV output and load, respectively. The lower and upper bounds are then obtained with $\widetilde{P_{PV}(t)} = P_{PV}(t) \pm P_{PV}(t) \cdot Er_{PV}$ and $\widetilde{P_{load}(t)} = P_{load}(t) \pm P_{load}(t) \cdot Er_{load}$.

Two cases are defined. The worst case (the case where the difference between PV output and load is the largest) is when PV output is equal to the upper bound value, and load is equal to the lower bound value; or when PV output is equal to the lower bound value,

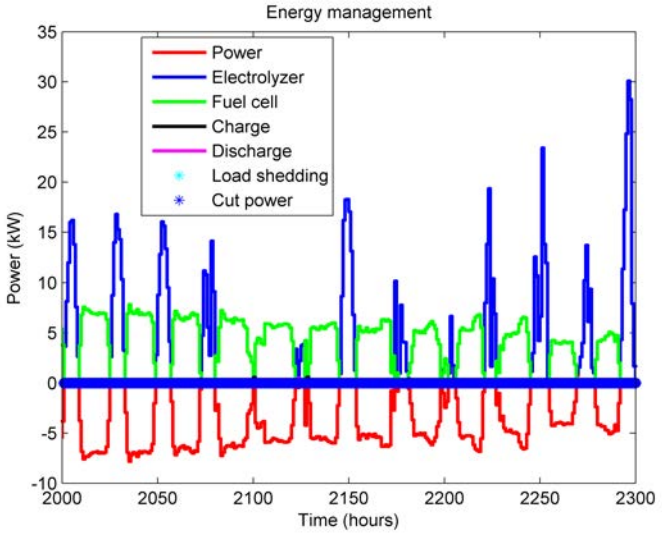

Figure 4.22: One-hour one-day rolling horizon scheduling simulation with the new sizing value of HSS (2000 h-2300 h). The curve labelled “Power” corresponds to the PV output minus the load.

load is equal to the upper bound value. For the best case (the case where the difference between PV output and load is the lowest), the opposite is used.

Values for $\widetilde{P_{PV}(t)}$ minus $\widetilde{P_{load}(t)}$ are shown in Fig. 4.23. If the sizing results can satisfy the worst and best cases, then other cases can also be satisfied by the obtained sizing results. This means that the worst and best case data must be used to run the co-optimization method and obtain the sizing results. Table 4.6 shows the sizing results when $Er_{PV} = Er_{load} = 0.1$. For the worst-case, the HSS is used frequently because it is cheaper than the BSS. For the best case, the BSS is used frequently due to limitations of the HSS (minimum startup power), so more BSS capacity is needed.

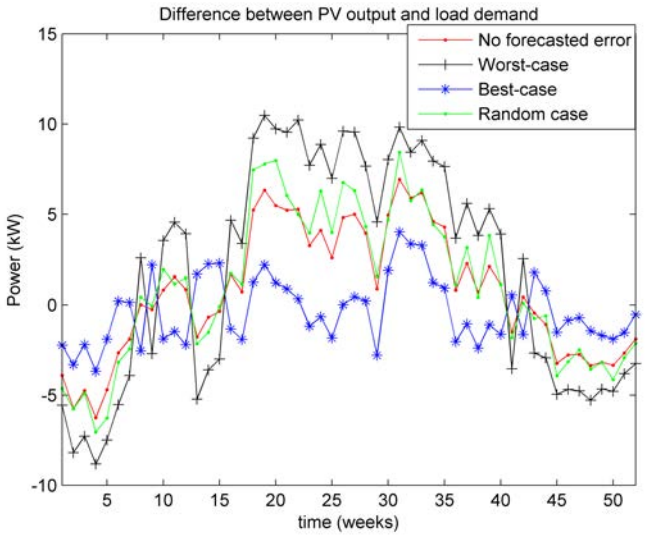

Figure 4.23: Difference between PV output and load demand in 4 cases.

Table 4.6: Sizing results considering uncertainty. The worst case is defined as the case where the difference between PV output and load is the largest, and the lowest for the best case.

Case	Total Cost [€]	C_{op} [€]	C_{cap} [€]	N_{PV}	$P_{fc}^{\max}$ [kW]	$P_{el}^{\max}$ [kW]	V_{H_2} [N.m^3]	C_{bat} [kWh]
Worst case	279270	1761.7	166960	50	8	8	11022	11
Best case	174400	1617.2	113450	50	6	6	5875	269

4.4/ CONCLUSION

In this chapter, we presented a methodology to determine the optimal sizing for a stand-alone microgrid. This methodology combines an EA for sizing and MILP for scheduling, and enables considering advanced energy management strategies, capable of anticipating decisions (especially with respect to storage), compared to classical rule-based approaches. Results showed that the operation strategy, initial conditions, time resolution as well as uncertainty on input data influence the sizing of the components, and consequently the total cost of the microgrid. A comparison with a rule-based operation strategy was run, and sizing results show that co-optimization method performs better. A rolling-horizon simulation was used to adjust the sizing values due to the influence of input data time resolution. At last, forecasting errors are taken into account using a robust method, to further adjust sizing results. With the proposed method and complements, the proposed method can therefore be used for economically sizing a microgrid containing PV panels, a BSS and an HSS.

For the co-optimization sizing method, the main limitation is the run time when the time resolution of forecasted load profiles is increasing. For example, when the time resolution increases from one week to one hour, then the time horizon of the operation optimization increases from 52 to 8760 [3]. It will take much time to solve this large optimization problem.

[3] In our sizing problem, the time range is one year, so there are 52 weeks, 365 days, 8760 hours.

5

SIZING OF MULTI-ENERGY-SUPPLY ISLANDED MICROGRIDS

This chapter is based on the author's published paper: Li Bei, Robin Roche, Damien Paire, and Abdellatif Miraoui. "Sizing of a stand-alone microgrid considering electric power, cooling/heating, hydrogen loads and hydrogen storage degradation." Applied Energy 205 (2017): 1244-1259.

In the previous chapter, a full electric MG was sized. However, there are not only electricity demands, but also several other types of energy in the same time step. In this chapter, we consider microgrids with multiple energies, including electric, thermal and hydrogen loads (Fig. 5.1).

Combined heat and power (CHP) plants are typically efficient and economical, and have applications in the residential and industrial sectors, especially when multiple energies are considered [137, 23, 138]. Similarly, fuel cells are a promising technology for efficient and sustainable energy conversion [24], and are expected to play an important role in future distributed energy generation [6]. Fuel cells are thus considered for a CHP plant. A fuel cell can operate as the main MG power plant to serve the electric and heat load demand of the whole system. Electric loads are powered by PV panels, a fuel cell, and a battery system; heating loads are heated by a solar heating system, a heat boiler, heat from the fuel cell, and a heat storage system; cooling loads are cooled by an air conditioner and an absorption heat chiller. In order to balance the intermittent and varying PV output, a HSS and a battery are used. The fuel cell, the electrolyzer and the hydrogen tanks operate as a long-term storage system, which has several advantages, such as a high storage capacity, and a high energy per unit of volume [5]. The battery system is used as a short-term storage and is inappropriate for long-term storage, due to its low energy density and nonnegligible self-discharge rate [7]. Similarly, heat storage is used to balance heat power (heat from the fuel cell, and intermittent heat from the solar heating system).

A multiple-energy system is a key aspect to evolve toward a cleaner and affordable energy supply system [139] and to improve power system resilience [140]. But how to decide the capacity of each component in this complex system with a given load profile remains a challenge. For example, if the components are oversized, capital and operation costs will be higher, while if the components are undersized, generation curtailment or load shedding may occur. This means that the sizing results are affected not only by the architecture of the system, but also by the operation strategy [129]. Depending on how components are used, the necessary capacity may vary greatly, which in turn impacts sizing results. On the other hand, input data (load demand, PV output) forecasting errors also influence

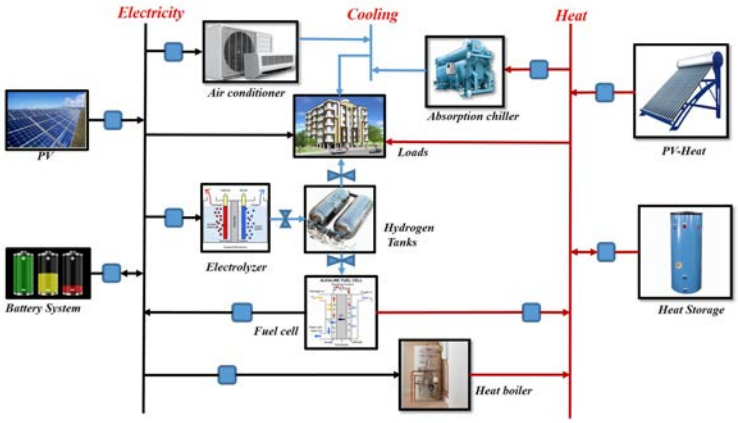

Figure 5.1: Multi-energy supply microgrid structure.

how components are used. This means that forecasting errors must be considered. At last, due to the fact that the fuel cell and the electrolyzer are used as a storage system, as operation time goes, the performance of the fuel cell and the electrolyzer can be expected to decrease, so this degradation process must also be considered [120, 121].

In this chapter, we decompose the sizing problem into a leader-follower problem. The follower problem, namely, the energy management strategy, is formulated as a unit commitment problem, in the form of a mixed integer problem. We use linear programming to obtain the optimal operation strategy. The leader problem, namely, the sizing problem, uses an evolutionary algorithm to search for the best sizing values [32].

The rest of this chapter is structured as follows. Section 5.1 describes the UC strategy and Section 5.2 the EA-based sizing problem formulation. Finally, Section 5.3 presents the simulation results while Section 5.4 concludes the chapter.

5.1/ Operation strategy for multi-enegy-supply microgrid

In this chapter, the operation of MES MG is formulated as an MILP problem. MILP optimization is based on current and future predicted information to optimize the operating points of each component while minimizing a cost function. In this case, the predicted information corresponds to solar radiation and loads, and the cost function is the total cost (including capital cost, maintenance cost and operation cost).

5.1.1/ Cost function

In order to minimize the operation cost, the utilization costs of different components need to be assessed. For the battery storage system (BSS), the utilization cost of charge and discharge are introduced as follows [130]:

$$B_{cost}^{ch,dis}(t) = \frac{C_{ba}^{inv}}{2 \cdot N_{cycles}} \cdot (P_{ch}(t)\eta_{ch} + P_{dis}(t)\eta_{dis}) \tag{5.1}$$

where C_{ba}^{inv} is the investment cost of the battery, and N_{cycles} is the number of cycles over the lifetime.

The hydrogen storage system (HSS) combines an electrolyzer, a fuel cell and hydrogen tanks. The utilization cost can be computed as follows [130]:

$$H_{cost}^{ele}(t) = \left(\frac{C_{ele}^{inv}}{N_{hours}^{ele}} + C_{ele}^{o\&m} \right) \cdot \delta_{ele}(t) + C_{ele}^{startup} \cdot \Delta\delta_{ele}(t) \tag{5.2}$$

$$H_{cost}^{fc}(t) = \left(\frac{C_{fc}^{inv}}{N_{hours}^{fc}} + C_{fc}^{o\&m} \right) \cdot \delta_{fc}(t) + C_{fc}^{startup} \cdot \Delta\delta_{fc}(t) \tag{5.3}$$

where $C_{ele}^{inv}, C_{fc}^{inv}$ are the investment costs of the electrolyzer and the fuel cell, $C_{ele}^{o\&m}$ and $C_{fc}^{o\&m}$ the operation and maintenance costs, and $C_{ele}^{startup}$ and $C_{fc}^{startup}$ the startup costs. Variables $\delta_{ele}(t)$ and $\delta_{fc}(t)$ are the state of the electrolyzer and the fuel cell. When a unit is on, $\delta_i(t) = 1, i = \{ele, fc\}$, otherwise it is set to 0. Equation $\Delta\delta_i(t) = max\{\delta_i(t) - \delta_i(t-1), 0\}, i = \{ele, fc\}$ represents whether the unit started or not.

The heat boiler (HB), air conditioner (AC) and absorption heat chiller (AHC) operation costs are given by [141]:

$$HB_{cost}(t) = \frac{C_{hb}^{inv}}{N_{life}^{hb}} \cdot P_{hb}(t) \tag{5.4}$$

$$AC_{cost}(t) = \frac{C_{ac}^{inv}}{N_{life}^{ac}} \cdot P_{ac}(t) \tag{5.5}$$

$$AHC_{cost}(t) = \frac{C_{ahc}^{inv}}{N_{life}^{ahc}} \cdot P_{ahc}(t) \tag{5.6}$$

For the heat storage (HS) system, the operation cost is:

$$HS_{cost}(t) = \frac{C_{hs}^{inv}}{N_{life}^{hs}} \cdot (Q_{hs}^{ch}(t) + Q_{hs}^{dis}(t)) \tag{5.7}$$

5.1.2/ OPERATION COST FUNCTION

The optimization tries to minimize the overall operation costs over a given horizon of T time steps. The total cost function is then as follows:

$$\begin{aligned} C_{op} = \sum_{t=1}^{T} \{ & B_{cost}^{ch,dis}(t) + H_{cost}^{ele}(t) + H_{cost}^{fc}(t) + a_1 \cdot HB_{cost}(t) + \\ & a_2 \cdot AC_{cost}(t) + AHC_{cost}(t) + HS_{cost}(t) \\ & + \alpha \cdot (LS_{cooling}(t) + LS_{heat}(t) + LS_{power}(t) \\ & + \beta \cdot (cut_{PV}(t) + cut_{solar}(t)) \} \end{aligned} \tag{5.8}$$

where $LS_m(t)$ with $m = \{\text{cooling, heat, power}\}$ are the shed cooling, heat and power loads, and $cut_n(t)$ with $n = \{\text{PV, solar}\}$ are the curtailed PV power and solar heating. α and β are penalty values for load shedding and curtailed power. When there is excess PV

generation, there are four solutions to handle the resulting surplus: using the electrolyzer to store hydrogen, charging the battery, using the heat boiler to store heat, and using the air conditioner to supply cooling demands. The priorities are set as follows: first the electrolyzer, second the battery, then the heat boiler and at last, the air conditioner. Parameters a_1 and a_2 are used to adjust the priorities.

5.1.3/ CONSTRAINTS

The stand-alone microgrid is subject to the following constraints, with $i = \{el, fc\}$ and $j = \{el, fc, bach, badis, hb, ac, ahc, hsch, hsdis\}$, $Z_j(t) = \delta_j(t)P_j(t)$. Variables γ_1^j and γ_2^j are constant real values used to set the minimum and maximum power range of each component:

$$\gamma_1^j P_j^{max} \leq P_j(t) \leq \gamma_2^j P_j^{max} \tag{5.9}$$

$$\delta_j(t) \cdot \gamma_1^j P_j^{max} \leq Z_j(t) \leq \delta_j(t) \cdot \gamma_2^j P_j^{max} \tag{5.10}$$

$$\begin{aligned} Z_j(t) &\leq P_j(t) - (1 - \delta_j(t)) \cdot \gamma_1^j P_j^{max} \\ Z_j(t) &\geq P_j(t) - (1 - \delta_j(t)) \cdot \gamma_2^j P_j^{max} \end{aligned} \tag{5.11}$$

$$\begin{aligned} &\delta_{ele}(t) + \delta_{fc}(t) \leq 1 \\ &\delta_{bach}(t) + \delta_{badis}(t) \leq 1 \\ &\delta_{hsch}(t) + \delta_{hsdis}(t) \leq 1 \end{aligned} \tag{5.12}$$

Equation (5.12) means that the fuel cell and the electrolyzer cannot start up at the same time. The BSS and heat storage system also cannot charge and discharge at the same time.

$\Delta\delta_i(t) = \max\{\delta_i(t) - \delta_i(t-1), 0\}$ can be expressed as $\Delta\delta_i(t) = \delta_i(t) \cdot (1 - \delta_i(t-1))$.

Then, using [133], the above nonlinear equations system can be transformed into the following linear constraints:

$$\begin{aligned} &-\delta_i(t) + \Delta\delta_i(t) \leq 0 \\ &-(1 - \delta_i(t-1)) + \Delta\delta_i(t) \leq 0 \\ &\delta_i(t) + (1 - \delta_i(t-1)) - \Delta\delta_i(t) \leq 1 \end{aligned} \tag{5.13}$$

In order to limit the startup/shutdown times of the fuel cell and the electrolyzer, the following constraints are added: when a fuel cell or electrolyzer starts up, it continues to run for at least k_{run} time steps:

$$\begin{aligned} Ind_i(t) &= \delta_i(t) - \delta_i(t-1) \\ \delta_i(t : t + k_{run}) &\geq Ind_i(t) \end{aligned} \tag{5.14}$$

The power balance equation is written as:

$$\begin{aligned} &PV(t) - cut_{PV}(t) - (L_{power}(t) - LS_{power}(t)) = Z_{ele}(t) \\ &- Z_{fc}(t) + Z_{bach}(t) - Z_{badis}(t) + Z_{ac}(t) + Z_{hb}(t) \end{aligned} \tag{5.15}$$

Similarly, for the heat and cooling balance equations:

$$\begin{aligned} &Q_{sh}(t) - cut_{solar}(t) - (L_{heat}(t) - LS_{heat}(t)) + Q_{fc}(t) \\ &+ Q_{hb}(t) = Q_{hsch}(t) - Q_{hsdis}(t) + Q_{ahc}(t) \end{aligned} \tag{5.16}$$

$$C_{ac}(t) + C_{ahc}(t) = L_{cooling}(t) - LS_{cooling}(t) \tag{5.17}$$

Finally, for the SOC, LOH and HS constraints:

$$\begin{aligned} &SOC_{min} \leq SOC(t) \leq SOC_{max} \\ &LOH_{min} \leq LOH(t) \leq LOH_{max} \\ &HS_{min} \leq HS(t) \leq HS_{max} \end{aligned} \tag{5.18}$$

In summary, for the UC control strategy, the problem can be formulated as:

$$\begin{aligned} &\underset{\widetilde{S}}{min}\{C_{op}\} \\ &s.t.\ (3.10), (3.11), (3.19), (3.20), (3.21), (3.22), (3.23), (5.9) - (5.18) \end{aligned} \tag{5.19}$$

where $\widetilde{S}$ is the set of variables.

5.2/ SIZING METHODOLOGY

Based on the above section, we can describe the power flow in the microgrid system. Our goal is to compute the optimal size value of each component, namely, $N_{PV}, N_{sh}, CB, P_{fc}^{max}, P_{el}^{max}, V_{H_2}^{max}, P_{hb}^{max}, P_{ac}^{max}, Q_{ahc}^{max}, HS_{max}$. Let set U represent these sizing variables. Then the sizing problem is $minF(U)$, with $F(.)$ the total cost function introduced in the following.

In this paper, we use the co-optimization method with an EA [37] to solve the sizing problem, and then MILP to solve the operation problem. The simulation process is shown in Fig. 5.2:

1. First, N candidate solutions are generated for the GA.
2. Each of these solutions is then used with the operation problem. The UC MILP optimization is run to solve problem (5.19). As a one year (8760 hours) MILP optimization would require a large simulation time, we adopt a method based on 12 peak demand days. Each of the 12 days is calculated with the MILP optimization. If no solution is feasible, then a new candidate solution is generated.
3. The GA fitness function value is then computed to determine the total cost of each candidate solution, by calculating (5.22).
4. The process continues until any stopping criterion is met. Here, an adaptive method is selected. Firstly, if the fitness function values for two consecutive steps are the same, then counter Num is incremented. If Num exceeds a given maximum value (here $Num^{max} = 30$), the simulation stops as the fitness function is not improving anymore. The second criterion is on the number of iterations, for which a maximum number (here $Gen^{max} = 100$) is set.

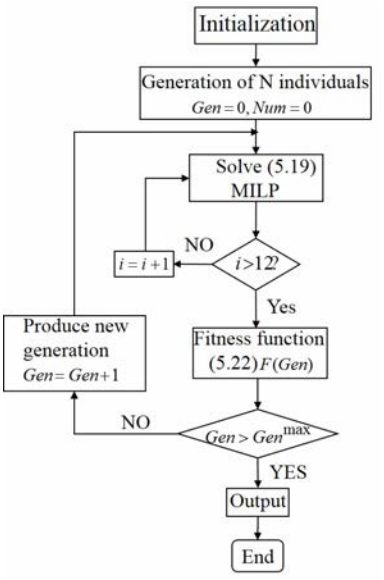

Figure 5.2: Optimization process outline.

The total capital cost corresponds to the cost of buying the equipment, and is given by:

$$\begin{aligned} C_{\text{cap}} = CRF \cdot (&N_{PV} \cdot C_{PV}^{inv} + N_{sh} \cdot C_{sh}^{inv} + P_{fc}^{\max} \cdot C_{fc}^{inv} \\ &+ P_{el}^{\max} \cdot C_{ele}^{inv} + V_{H_2} \cdot C_{tank}^{inv} + C_{bat} \cdot C_{bat}^{inv} \\ &+ P_{hb}^{\max} \cdot C_{hb}^{inv} + P_{ac}^{\max} \cdot C_{ac}^{inv} + P_{ahc}^{\max} \cdot C_{ahc}^{inv} \\ &+ HS_{\max} \cdot C_{hs}^{inv}) \end{aligned} \tag{5.20}$$

where C^{inv} variables represent the prices of each component. $CRF = \frac{r(1+r)^{n_{inv}}}{(1+r)^{n_{inv}}-1}$ is the capital recovery factor (CRF) [32], r is the real interest rate and n_{inv} is the expected life span of the microgrid.

Similarly, the annual maintenance cost is given by:

$$C_{\text{mnt}} = N_{PV} \cdot C_{PV}^{mnt} + V_{H_2} \cdot C_{tank}^{mnt} + C_{bat} \cdot C_{bat}^{mnt} \tag{5.21}$$

where C^{mnt} variables represent the annual maintenance costs of the PV, hydrogen tanks and battery components. As the O&M cost of the FC and the electrolyzer are considered in the operation strategy equations (5.2) to (5.3), they are not included in the annual cost. The maintenance cost of the heat boiler, the air conditioner, the absorbtion heat chiller, and the heat storage are neglected.

The total cost function $F(.)$ is thus:

$$F = C_{\text{cap}} + C_{\text{op}} + C_{\text{mnt}} \tag{5.22}$$

Finally, the overall problem can be formulated as:

$$\begin{aligned} &\min_{U \in \mathbf{U}} \{C_{\text{cap}} + \min_{U^*, \overline{S}} \{C_{\text{op}}\} + C_{\text{mnt}}\} \\ &s.t.\ (3.10), (3.11), (3.19), (3.20), (3.21), (3.22), (3.23), (5.9) - (5.18) \end{aligned} \tag{5.23}$$

5.3/ SIMULATION RESULTS

5.3.1/ SYSTEM SETUP

In order to research about the influence of different operation strategies, we set up three different strategies, shown in Table 5.1. Strategies S1 and S3 are used to compare the influence of minimum startup power of the fuel cell, the electrolyzer and the heat boiler on the sizing results. Strategies S2 and S3 are used to compare different operation durations of the fuel cell and the electrolyzer on the sizing results.

Table 5.1: Three different operation strategies.

Strategy	$\gamma_1^{\{fc,ele\}}$	$\gamma_2^{\{fc,ele\}}$	$k_{run}[h]$
S1	0.1	1	3
S2	0.5	1	5
S3	0.5	1	3

The other main operation parameters are shown in Table 5.2, where ”hb” means heat boiler, ”ac” means air conditioner, ”ahc” means absorbtion heat chiller, ”hy” means hydrogen tanks, and ”hs” means heat storage system.

Table 5.2: Simulation parameters.

Components	γ_1	γ_2
hb	0	1
ac	0.1	0.9
ahc	0	0.9
Components	min	max
battery	$SOC_{min} = 0.5$	$SOC_{max} = 0.9$
hy	$LOH_{min} = 1N.m^3$	–
hs	$HS_{min} = 0$	–

We also set $\alpha = \beta = 10^{10}$. The initial state of hydrogen in tanks is $LOH_{ini} = 10^6$ N.m^3. This large value is chosen in order to make sure there is enough hydrogen to run the fuel cell, and will be adjusted in the following. The initial state of the heat storage is $HS_{ini} = 3 \cdot 10^3$ kWh. The cost parameters are taken from [142, 128, 76]. The degradation parameters are calculated based on [120, 121, 125, 9] and are shown in Table 5.3.

Table 5.3: Degradation parameters.

k_{vd}[V/h]	k_{fcm}[kW/d]	k_{vi}[V/h]	k_{elem}[kW/d]
$3.736 \cdot 10^{-6}$	0.002582	$3 \cdot 10^{-5}$	0.004933

Load demand data (for cooling, heat, electric power and hydrogen) and solar radiation are obtainted from a research building, located in Belfort, France. The 1-h one year profiles of load demands and solar radiation are shown in Figs. 5.3 and 5.4. In order to make the figures readable, the corresponding one day average profiles are shown in Figs. 5.5 and 5.6. Hydrogen is used to run fuel cell research experiments. As no direct data is available,

heating and cooling loads are calculated based on temperature [1]. In order to avoid long simulation times, we adopt 12 days with one hour data as the input profiles. These days correspond to the electricity load demand peak day, the heating load demand peak day, and the cooling load demand peak day for each season. Then, the sizing results are verified based on a 1-hour rolling horizon simulation, and are adjusted if necessary.

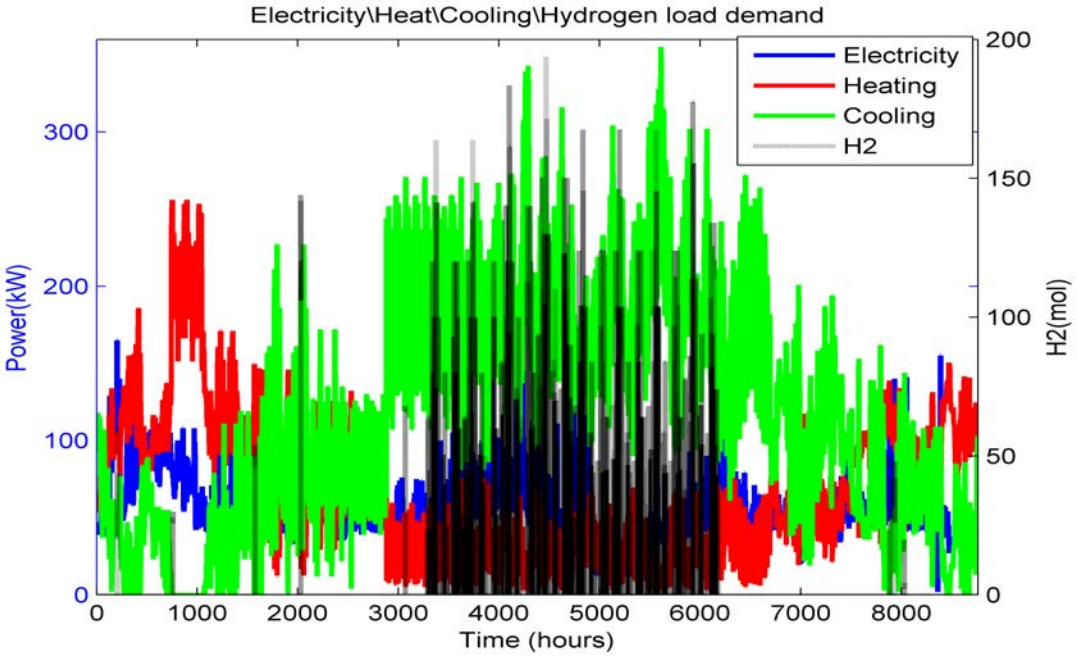

Figure 5.3: Cooling/heat/electricity/hydrogen demand (1 hour).

5.3.2/ GA-BASED SIZING RESULTS

The optimal size values shown in Table 5.4 are obtained. Here $\Delta V_{H_2} = \max\{\Delta V_{H_2}^{rd}\}, rd = \{1, ..., 12\}$, where rd represents the 12 days, and $\Delta V_{H_2}^{rd} = V_{\max}^{rd} - V_{\min}^{rd}$ represents the hydrogen volume change in tanks in the rd^{th} day. Similarly, $\Delta HS = \max\{\Delta HS^{rd}\}, rd = \{1, ..., 12\}$, rd represents the 12 days, and $\Delta HS^{rd} = HS_{\max}^{rd} - HS_{\min}^{rd}$ represents the heat power change in the heat storage system in the rd^{th} day. The hydrogen energy can be expressed in another way: for S1, the hydrogen volume can operate the fuel cell at 100 kW for 24.9 hours; for S2, the duration changes to 28.5 hours; and for S3, to 44.6 hours.

Table 5.4: Sizing results.

Strategy	N_{PV}	$P_{fc}^{\max}$[kW]	$P_{el}^{\max}$[kW]	ΔV_{H_2} [N.m^3]	C_{bat} [kWh]	N_{sh} [m^2]	P_{hb}^{max}	ΔHS[kWh]	P_{ac}^{max}	Q_{ahc}^{max}
S1	121	272	396	1065	383	45	346	3000	117	1207
S2	206	114	584	1220	659	36	123	3000	129	3815
S3	327	131	690	1903	735	43	283	3000	159	686

[1] The following process is used: 1) Obtain the heating demand and average temperature in each 12 month; 2) Calculate the relationship between heat and temperature, i.e., determine heat=f(temperature); 3) Obtain the 1-hour 1-year temperature data, and then based on 2), calculate the 1-hour 1-year heating demand.

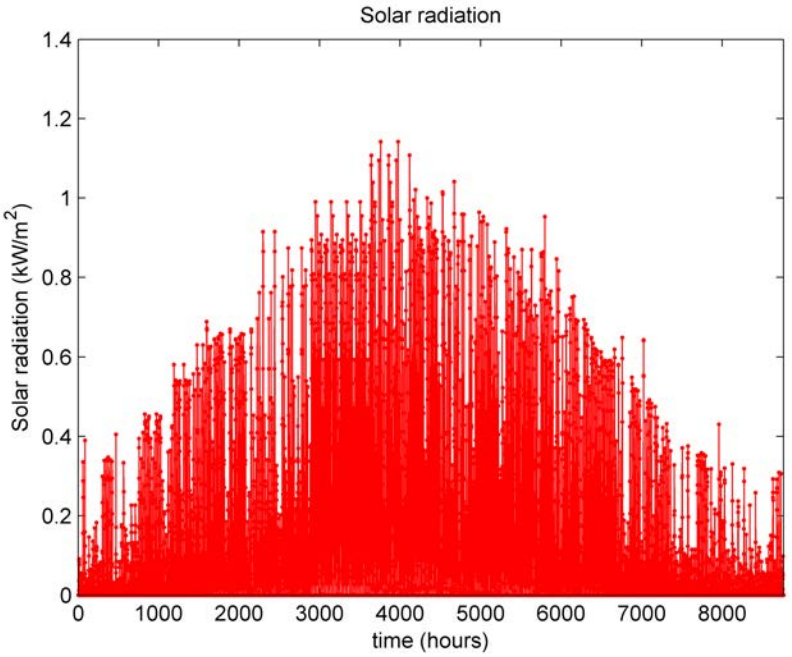

Figure 5.4: Solar radiation (1 hour).

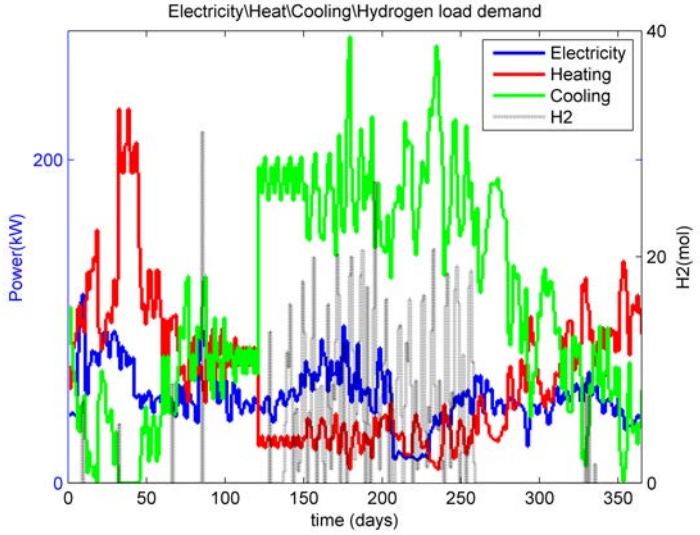

Figure 5.5: Cooling/heat/electricity/hydrogen demand (one day average).

The cost results are shown in Table 5.5. Here, C^*_{total} and C^*_{op} represent real cost of the system, namely, $C^*_{op} = \sum_{day=1}^{12} \sum_{t=1}^{T} \{B^{ch,dis}_{cost}(t) + H^{ele}_{cost}(t) + H^{fc}_{cost}(t) + \alpha \cdot (LS_{cooling}(t) + LS_{heat}(t) + LS_{power}(t)) + \beta \cdot (cut_{PV}(t) + cut_{solar}(t))\}$ (operation cost of heat boiler, air conditioner, absorption heat chiller and heat storage are not considered), $C^*_{total} = C_{cap} + C^*_{op} + C_{mnt}$.

It can be observed that with different operation strategies, the sizing value of each component is different. In strategy S2, the minimum start power of the fuel cell and the electrolyzer is set to be 50% of their maximum power, and the minimum run time of the fuel cell and the electrolyzer is 5 hours. These constraints are strict and must be satisfied

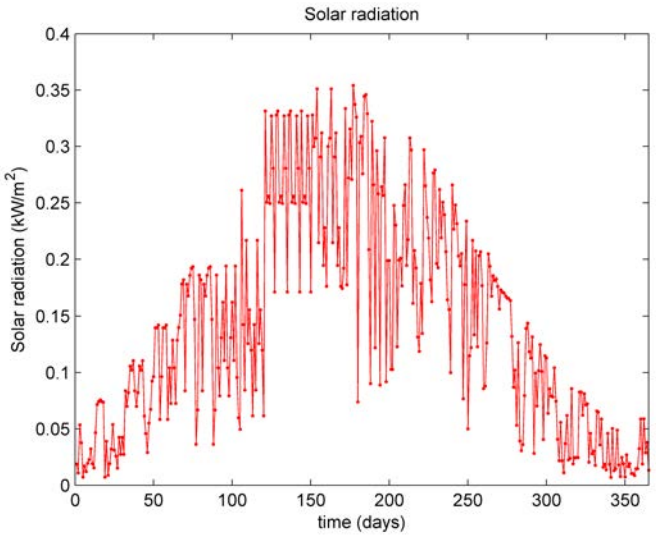

Figure 5.6: Solar radiation (one day average).

Table 5.5: Cost results.

Strategy	C^*_{total} [€]	C_{cap} [€]	C^*_{op} [€]
S1	4.0683e+05	3.6766e+05	3.9171e+04
S2	9.6424e+05	4.7911e+05	4.8513e+05
S3	1.2729e+06	5.3004e+05	7.4290e+05

in the optimization process, leading to a smaller fuel cell, a larger PV and a larger electrolyzer. In strategies S2 and S3, larger PV, electrolyzer, hydrogen tanks and battery are needed, leading to larger capital costs.

Comparing these three operation strategies, we find that if the operation conditions of the HSS are limited (in order to reduce its degradation), the capital cost of the related auxiliary system increases, and the lifetime of the HSS also increases. On the contrary, if the limitations on operation conditions of the HSS are not strict, which means that the HSS can operate in most conditions, the related auxiliary system is smaller, but the life time of HSS also decreases.

Based on the above sizing value, the scheduling results are obtained by running the MILP algorithm. The MILP scheduling is run for one day (electricity peak load demand day in summer) with strategy S2. Scheduling results are shown in Fig. 5.7, which shows the electric power schedule. During the day, a large surplus PV output can be observed. This may show that the number of PV panels is too large (a smaller value may be more appropriate), but as our simulation is based on 12 days, this means that simulation results must be satisfied for all 12 days, so the number of PV panels is chosen from the global view. We observe that the HSS is the main storage system (the fuel cell outputs power at night and the electrolyzer consumes the most power in the day time), with slow variations in output, while the BSS serves as an auxiliary storage system, with shorter and more dynamic charge and discharge periods. The heat boiler and the air conditioner also operate to transfer electricity to heating and cooling power. The fuel cell generates more electricity than the electric load demand, in order to supply the heating and cooling loads.

Fig. 5.8 shows the heating power schedule. During the night, the fuel cell heating and the

heat storage system supply most of the heating load demand, and the absorption heat chiller uses heat to serve the cooling load. During the day, the surplus heating power is stored in the heat storage system and is transferred to cooling load using the AHC. The heat boiler uses electricity to heat water, which can be stored or used in the absorption heat chiller. The fuel cell also generates heat water which can be transferred to rooms through pumps. Similarly, Fig. 5.9 shows the cooling power schedule. The absorption heat chiller and the air conditioner supply all the cooling load.

From the scheduling results, we can see that when there is no PV power output and solar heat output (at night), the fuel cell provides energy for the whole system. It provides electricity to the electric load demand, to the air conditioner to serve the cooling load, and collects heat power to serve the heat load. The heat storage tank provides heating power to the heat load. When there is surplus energy from the PV panels and the solar heating system (during the day), the electrolyzer is used as the main source to consume electricity by producing hydrogen. The heat boiler is also used to consume electricity by producing heat stored in heat tanks.

Regarding storage, Fig. 5.10 shows the change in LOH and stored heat, and Fig. 5.11 the change of SOC. It shows that when there is no PV output, the fuel cell produces power to supply the electric load, and the heat storage tanks provide heat to the heat demand. When there is enough PV output, surplus PV power output and solar heat output are stored in hydrogen tanks and heat tanks, respectively.

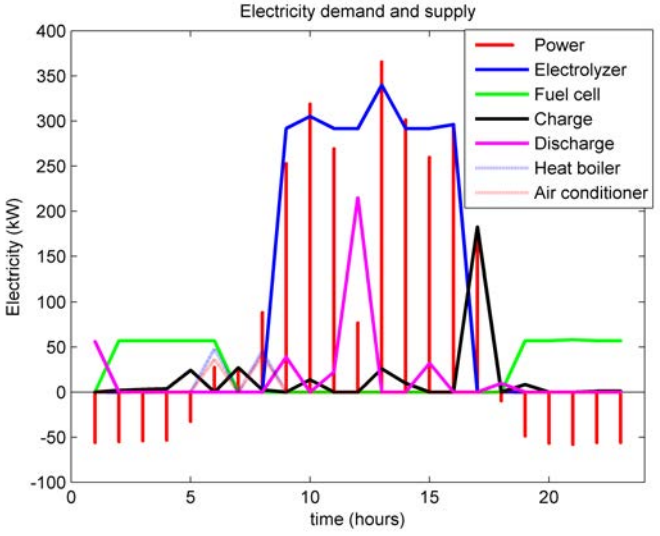

Figure 5.7: Strategy S2, electric power schedule (Power means PV outputs minus electricity load demand; charge/discharge curves are for the battery).

5.3.3/ 1-HOUR ROLLING HORIZON SIMULATION

In order to verify the optimal sizing results, a 1-hour rolling horizon simulation is run. This simulation repeats the 1-hour one day UC scheduling for 365 days. Strategy S2 is adopted. We only use 12 days as the input data to obtain the optimal sizing results. In the rolling horizon simulation, the optimization window moves from the current day to the next day, and then repeats until the last day. So the state of the hydrogen tanks and the heat

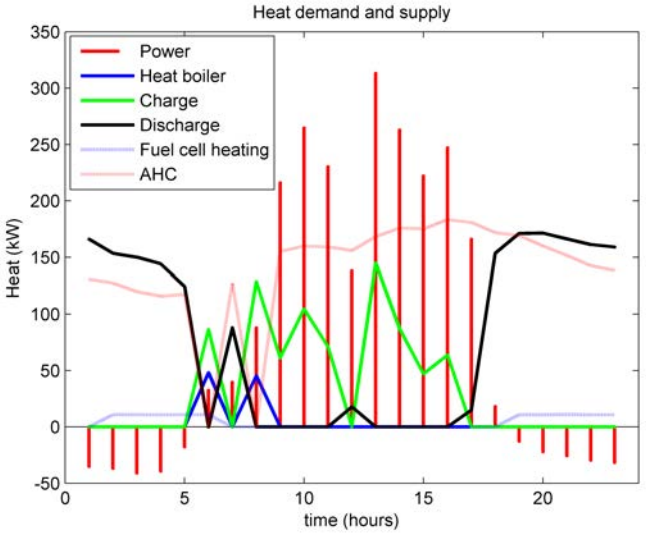

Figure 5.8: Strategy S2, heating power schedule (Power means solar outputs minus heat load demand; charge/discharge curves are for the heat storage system).

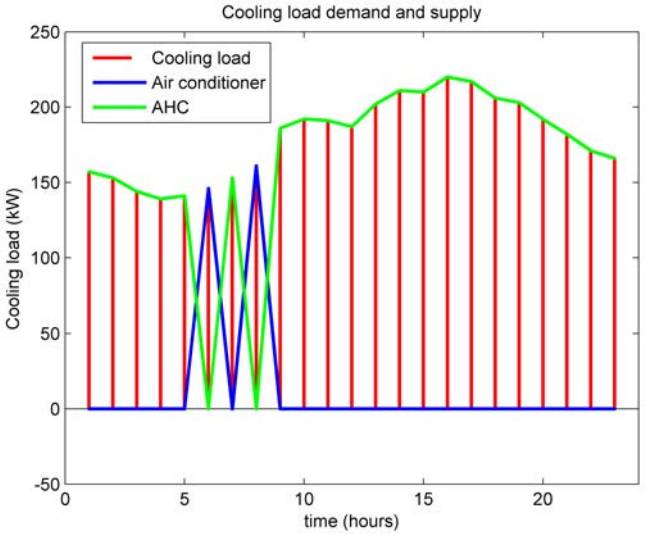

Figure 5.9: Strategy S2, cooling power schedule.

storage system are based on the previous simulation results. To determine the volume of the hydrogen tanks and the heat storage system, we adjust the initial value to a large value. With this new value, the rolling horizon simulation is run, and the results are shown in Fig. 5.12. From Fig. 5.12, we can see that load shedding and curtailed power occur, which means that these sizing values must be adjusted. Firstly, we adjust the sizing value of the heat boiler to be $123 + 209 = 332$ kW, as from Table 5.4, in the second row, we know that the sizing value of the heat boiler is 123 kW, and from Fig. 5.12, we know that the maximum heating shedding power is 209 kW. This means that the curtailed PV power and more fuel cell output power can be transferred to heat. Then, we adjust the fuel cell capacity to satisfy the heat boiler demand: $114 + 209/0.9 = 347$ kW, as from Table 5.4, in the second row, we know that the sizing value of the fuel cell is 114 kW, and the efficiency of the heat boiler is 0.9. With these new sizing values, the 1-hour rolling horizon

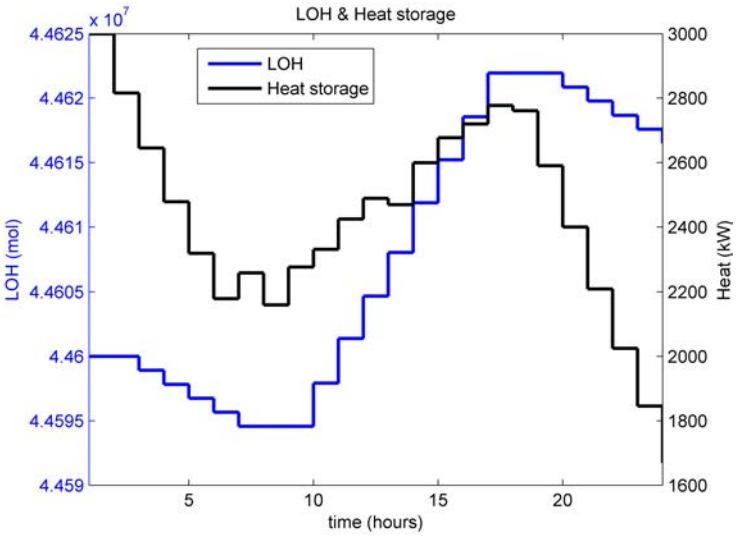

Figure 5.10: LOH and stored heat.

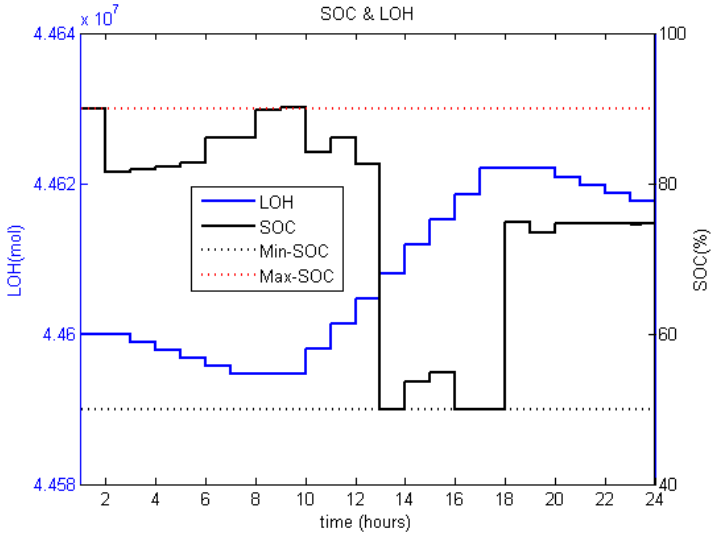

Figure 5.11: LOH and SOC.

simulation results are shown in Figs. 5.13, 5.14, 5.15, and 5.16. We can then calculate the volume of hydrogen tanks: $\max(LOH) - \min(LOH) = 141,270$ N.m^3 [2]. If we do not consider the degradation of the fuel cell, these large amounts of hydrogen can serve a fuel cell operating at 200 kW for 1,750 hours [3]. For the heat storage system, we obtain $\max(ht) - \min(ht) = 4,968$ kWh. After this adjustment, the capital cost of the whole system is 2.2616e+06 €. The large volume of the hydrogen tanks leads to this large capital cost.

[2] Under high pressure $700bar/15^oC$, this volume is about 212.85 $m^3 \approx 12.19m \times 5.96m \times 2.93m (length \times width \times height)$, with a weight of 3,150 kg.

[3] This is 350,000 kWh= 350 MWh energy. Here, we can compare with the lithium-ion battery storage systems. A 1 MWh lithium-ion battery can be installed in a 40-foot shipping container, and weighs 35,000 kg [143]. A 40-foot shipping container is $40ft \times 8ft \times 9.6ft = 12.19m \times 2.44m \times 2.93m$ [144]. This means that a 350 MWh lithium-ion battery occupies about $12.19m \times (2.44m \times 350) \times 2.93m$ of volume, which is about 143.3 times larger than for hydrogen tanks.

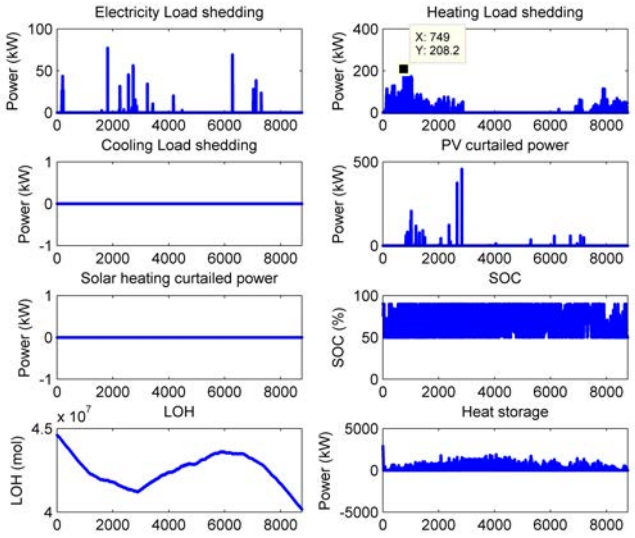

Figure 5.12: 1-hour rolling horizon simulation.

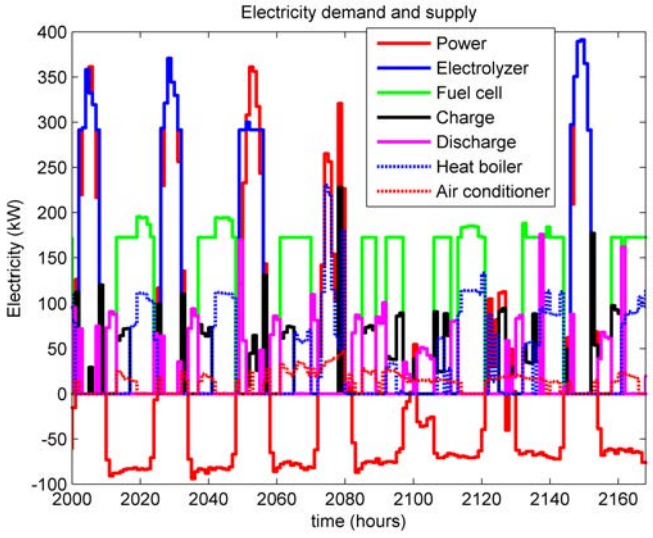

Figure 5.13: 1-hour rolling horizon simulation, electric power schedule (2000-2168h).

5.3.4/ INFLUENCE OF THE DEGRADATION OF THE FUEL CELL, THE ELECTROLYZER AND BATTERY

In this section, the degradation models of the fuel cell, the electrolyzer and battery are considered. 12 days are used as the input profile, and if we consider the degradation of the fuel cell, the electrolyzer and the battery, the maximum output power of the fuel cell, the maximum input power of the electrolyzer, the consumed hydrogen in fuel cell,

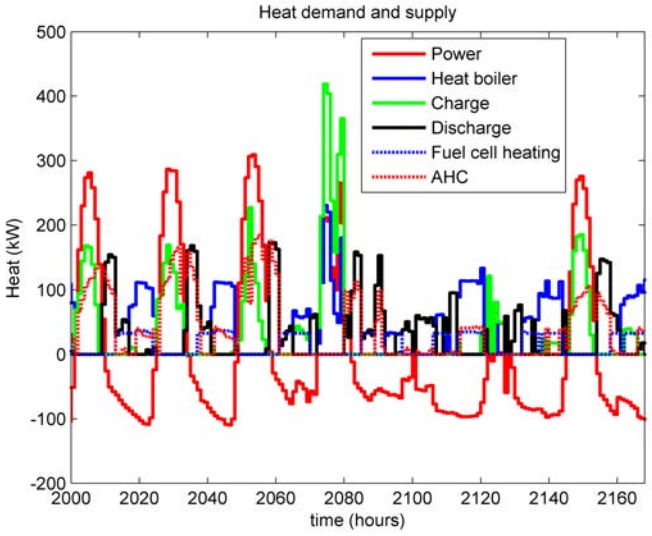

Figure 5.14: 1-hour rolling horizon simulation, heat power schedule (2000-2168h).

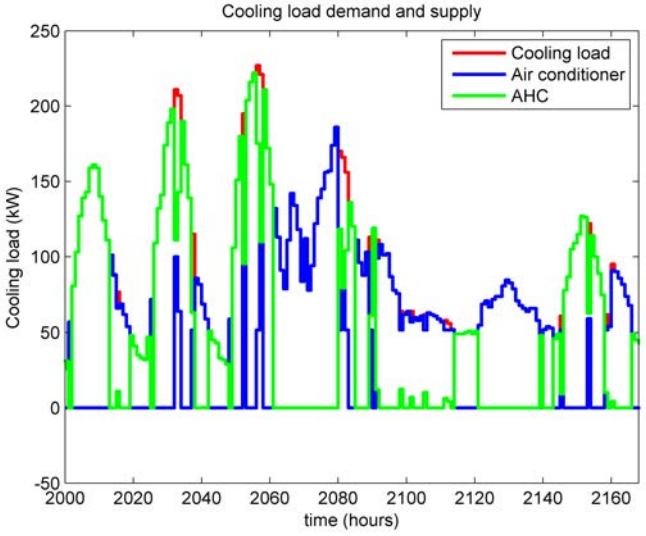

Figure 5.15: 1-hour rolling horizon simulation, cooling power schedule (2000-2168h).

the produced hydrogen in the electrolyzer, the remaining capacity of battery will all be different over these 12 days.

Based on equations (3.10) and (3.11), we can calculate the new parameters for the fuel cell consumed hydrogen and the maximum output power in t_{day}. For the electrolyzer, the new parameters are updated based on (3.19) and (3.20). For the battery, the remaining capacity in each day is updated based on (3.23).

Then the UC optimization problem can be formulated as problem (5.19), and the overall problem is (5.23). We adopt strategy S1. The simulation results are shown in Table 5.6. Deg_{all} means that the degradation of the fuel cell, the electrolyzer and the battery is considered. Deg means considering the degradation of fuel cell and electrolyzer. We can see that in case Deg, due to the degradation of the fuel cell, a larger capacity of fuel cell is needed to satisfy the load demand; a larger heat boiler and air conditioner

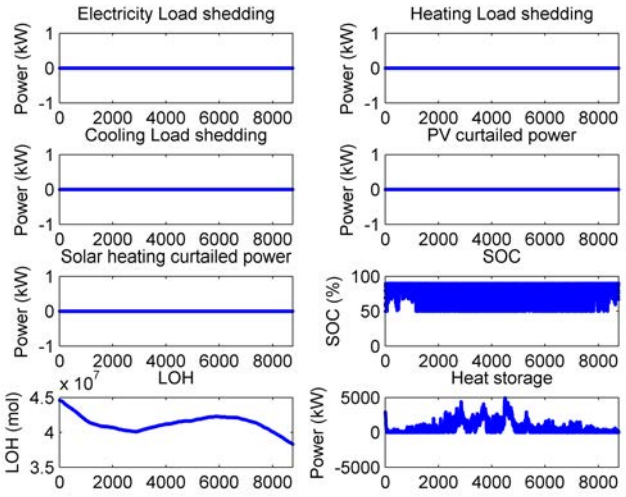

Figure 5.16: 1-hour rolling horizon simulation.

are needed to transfer the PV output power to heat or cooling due to the degradation of the electrolyzer. Then, we consider the degradation of the battery with case Deg_{all}. We can see that the capacity of the battery will increase, also for the capacity of the fuel cell and the electrolyzer, with the larger electrolyzer, then the capacity of the heat boiler and the air conditioner is decreased compared to case Deg. The cost results are shown in Table 5.7. We can see that in case Deg, the operation cost is smaller. This is because the HSS operates more often (because of the larger capacity of the fuel cell), and the utilization cost of the HSS is much smaller, leading to lower operation costs. In case Deg_{all}, due to the large capacity of the storage system, the capital cost of the microgrid is also increased.

Table 5.6: Sizing results considering degradation of the fuel cell, the electrolyzer and the battery.

	N_{PV}	$P_{fc}^{\max}$[kW]	$P_{el}^{\max}$[kW]	ΔV_{H_2} [N.m^3]	C_{bat} [kWh]	N_{sh} [m^2]	P_{hb}^{max}	ΔHS_{max}[kWh]	P_{ac}^{max}	Q_{ahc}^{max}
Deg_{all}	224	498	540	1159	843	43	200	3000	148	542
Deg	103	409	385	1087	101	48	671	3000	843	557
S1	121	272	396	1065	383	45	346	3000	117	1207

Table 5.7: Cost results considering degradation of the fuel cell and the electrolyzer.

Strategy	C_{total}^{*} [€]	C_{cap} [€]	C_{op}^{*} [€]
Deg_{all}	7.8660e+05	5.3978e+05	2.4682e+05
Deg	4.0172e+05	3.8183e+05	1.9887e+04
S1	4.0683e+05	3.6766e+05	3.9171e+04

5.3.5/ INFLUENCE OF UNCERTAINTY

The forecasting errors on PV output and load demand influence the power flow on the whole system, as well as the sizing results of the components. In this section, we adopt

a robust method to research about the influence of uncertainty. We use the upper bound and lower bound to represent the uncertainty. $\widetilde{P_{PV}(t)}, \widetilde{L_{power}(t)}, \widetilde{L_{heat}(t)}, \widetilde{L_{cooling}(t)}, \widetilde{L_{H_2}(t)}$ and $Er_{PV}, Er_{power}, Er_{heat}, Er_{cooling}, Er_{H_2}$ are used to represent the actual values and error bounds of PV output, solar heating output, electric load demand, heating load demand, cooling load demand, and hydrogen load demand respectively. The actual values can be represented as:

$$\begin{aligned}
\widetilde{P_{PV}(t)} &= P_{PV}(t) \pm P_{PV}(t) \cdot Er_{PV}, \\
\widetilde{L_{power}(t)} &= L_{power}(t) \pm L_{power}(t) \cdot Er_{power}, \\
\widetilde{L_{heat}(t)} &= L_{heat}(t) \pm L_{heat}(t) \cdot Er_{heat}, \\
\widetilde{L_{cooling}(t)} &= L_{cooling}(t) \pm L_{cooling}(t) \cdot Er_{cooling}, \\
\widetilde{L_{H_2}(t)} &= L_{H_2}(t) \pm L_{H_2}(t) \cdot Er_{H_2}
\end{aligned} \tag{5.24}$$

Two cases are defined in Fig. 5.17. The worst case (the case where the difference between the PV output and the load is the largest) is when the PV output is equal to the upper bound value, and the load is equal to the lower bound value; or when the PV output is equal to the lower bound value, the load is equal to the upper bound value. For the best case (the case where the difference between the PV output and the load is the lowest), the opposite is used.

If the sizing results can satisfy the worst and best cases, then others cases can also be satisfied by the obtained sizing results. This means that the worst and best case data must be used to run the co-optimization method and obtain the sizing results. Table 5.8 shows the sizing results when $Er_{PV} = Er_{power} = Er_{heat} = Er_{cooling} = Er_{H_2} = 0.1$. Table 5.9 shows the cost results. For the worst-case, the HSS is used frequently because it is cheaper, so larger hydrogen tanks are needed. For the best case, the BSS is used frequently due to limitations of the HSS (minimum startup power and continuous running time), so more BSS capacity is needed. For these two cases, a larger heat storage system is needed to handle the uncertainty.

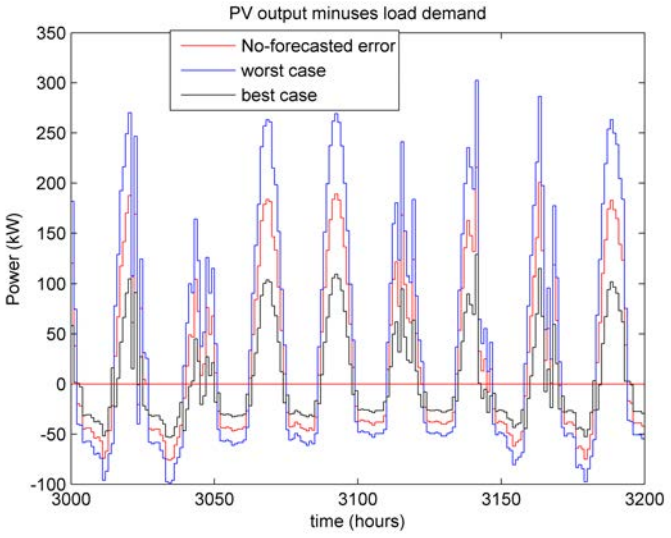

Figure 5.17: PV output minus load demand

Table 5.8: Sizing results considering uncertainty. The worst case is defined as the case where the difference between PV output and load is the largest, and the lowest for the best case.

Strategy	N_{PV}	$P_{fc}^{\max}$[kW]	$P_{el}^{\max}$[kW]	ΔV_{H_2} [N.m^3]	C_{bat} [kWh]	N_{sh} [m^2]	P_{hb}^{max}	ΔHS_{max}[kWh]	P_{ac}^{max}	Q_{ahc}^{max}
Worst case	109	169	307	1199	437	105	323	9072	81	531
Best case	107	191	247	952	652	124	324	8219	337	2728
S1	121	272	396	1065	383	45	346	3000	117	1207

Table 5.9: Cost results considering uncertainty.

Strategy	C_{total}^{*} [€]	C_{cap} [€]	C_{op}^{*} [€]
Worst case	3.9060e+05	3.7248e+05	1.8123e+04
Best case	4.5288e+05	4.2616e+05	2.6729e+04
S1	4.0683e+05	3.6766e+05	3.9171e+04

5.4/ CONCLUSION

In this chapter, we introduced a co-optimization method to size the components of a renewable energy based stand-alone microgrid which combines cooling, heat, electric power and hydrogen loads. The UC optimization method was used for defining the operation strategy, which aims at minimizing the operation cost through an MILP algorithm. A GA was used to compute the sizing value of each component, aiming to minimize the total cost. Three operation strategies were compared, which showed that sizing values are different with different strategies. Then a 1-hour rolling horizon simulation was used to adjust the sizing values of several components. The degradation of the fuel cell, the electrolyzer and the battery was also considered and showed that the sizing values of the fuel cell and the battery increases when considering the degradation. Uncertainty on PV output and load demand was addressed using robust optimization, and results showed that larger volumes of hydrogen tanks and heat storage are needed to tackle these uncertainty factors. This co-optimization method is useful to size complex islanded microgrids, and results show that the optimal size value and operation algorithms are capable of scheduling multiple components and managing flows from different natures (heat/cooling, electricity and hydrogen).

The above two chapters are discussing islanded microgrids, but do not consider the influence of the utility grid. Then, in next chapter, grid-connected microgrids are considered, and the sizing and operation of grid-connected microgrids are presented.

6

SIZING OF GRID-CONNECTED MULTI-ENERGY-SUPPLY MICROGRIDS

This chapter is based on the author's published paper: Li Bei, Robin Roche, Damien Paire, and Abdellatif Miraoui. "Optimal sizing of distributed generation in gas/electricity/heat supply networks." Energy 151 (2018): 675-688.

Today's energy supply systems are large transmission networks, such as the electricity network and gas supply network. Normally, these energy supply networks are planned separately. However, load demands are often with several types of energy in the same time step. For example, when people use gas to cook, people also need electricity to serve electronic devices, and heat energy to heat the room. When these large energy supply systems co-operate together, it can improve the efficiency of the whole energy supply system, because co-operating can make the whole system operate in an optimal state, and in the same time, ensure the power balance of different energy supplies.

On the other hand, at each interconnection node, different types of energy can be converted to each other through power devices. For example, fuel cells can be used to convert H_2 to electricity, electrolyzers can be used to convert electricity to H_2, gas turbines can be used to convert gas to heat, etc. At each node, renewable energy can also be connected, such as with photovoltaic (PV) panels and wind turbines. In this chapter, the focus is on the following problem: how to determine the capacity of these power devices and renewable energy sources at each interconnection node, based on the given hybrid energy network configuration?

In this work, a modified 13-node network is considered (the electricity network is the IEEE 13-node network [145], and the gas and heating networks are assumed to have the same structure as the electricity network, as shown in Fig. 6.1, and three types of gas/electricity/heat load demands are served. In this figure, HS represents a hydrogen storage system (fuel cell + electrolyzer + tanks), which has several advantages, such as a high storage capacity, and a high energy per unit of volume [5]; CHP is a combined heat and power device; ETH is a device that converts electricity to heat, for example, a heat boiler; GTH is a device that converts gas to heat, for example, a gas boiler heater. Black lines represent the gas supply system, blue lines are the electricity supply system, red lines are the heat supply system.

At each node, the devices and load demands can be formed as an MG or an energy hub (EH). In [146], authors design a combined cooling/heat/power and hydrogen MG system, and present a combined GA and MILP method to size such MES MG. GA is used to search for the sizing values, MILP is used to control the operation of MG. In

[147], authors present a smart EH framework to deploy an integrated demand response program (considering electricity and natural gas demands). The goal is to maximize the natural gas and electricity utility companies' profit and to minimize the customers' consumption cost. The problem is formulated as a non-cooperative game.

For MG, the emphasis is on islanded operation ability, which can improve the system resilience when the utility grid is damaged under natural disasters. Authors in [140] use gas-based and hydrogen-based MG to improve resilience to disasters. A hybrid energy supply (electricity/gas/hydrogen) system is built, and Monte Carlo simulation is used to simulate the influence of disasters. For EH, the emphasis is on the energy dispatching efficiency, which can reduce the waste of fuel and improve the energy utilization efficiency, or act as a load serving entity to deploy integrated demand response [147].

In this chapter, renewable energy is integrated and an MG is formed at each node. The detailed structure of the MG at node is shown in Fig. 6.2.

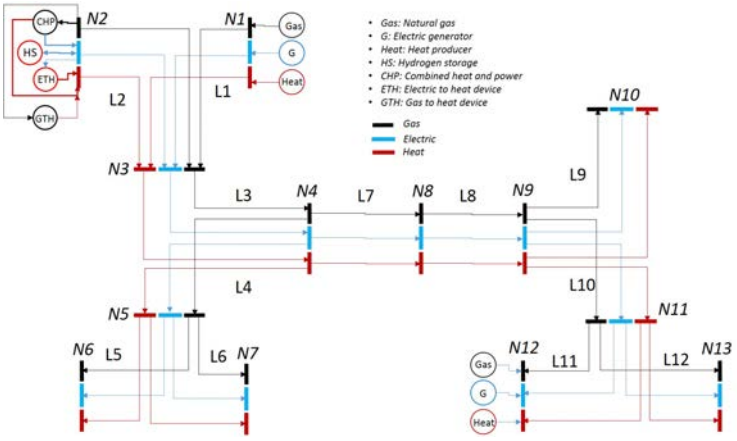

Figure 6.1: Gas/electricity/heat network.

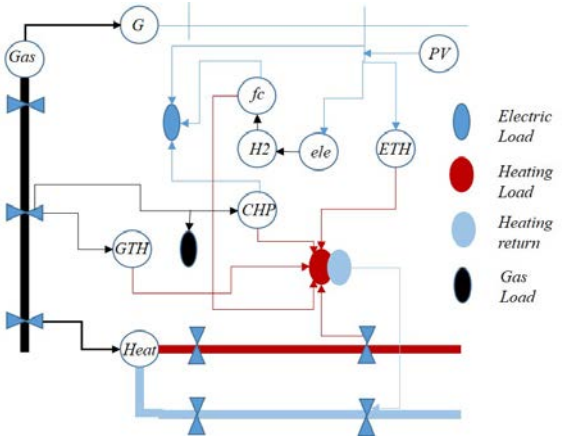

Figure 6.2: Microgrid structure at node.

The MES MG can interconnect with the utility grid, and can also operate in islanded mode. When the utility grid is severely damaged under natural disasters, islanded MG can still operate to supply the load demands (using the local renewable energy and storage system). If the utility grid is partially destroyed, the MG power imports from the utility grid are limited, due to damage on transmission lines or pipelines. This chapter discusses

how such large power devices and PV panels should be installed and sized in each MG. A combined algorithm is presented to size the components in MG to resist to contingency events (namely, some transmission lines are destroyed). Firstly, an optimization method is used to describe the power flow in the whole system, where the objective function is to minimize the investment cost and the unserved load. The constraints are to ensure the power balance and meet capacity limitations. Then, a GA is used to search for the optimal sizing value of each component. After that, two cases are simulated: the first case is a modified 13-node hybrid system, and the second case is a IEEE20 + gas20 + heat14-node hybrid system. Graph theory is used to find the worst case based on betweenness centrality, when the electric system is damaged under contingency events.

The remainder of this chapter is organized as follows. Section 6.1 describes the problem formulation, and Section 6.2, 6.3 the simulation results. Finally, Section 6.4 concludes the paper.

6.1/ PROBLEM FORMULATION

The sizing problem is to give the sizing value of each component, then these sizing values are checked in the operation problem. Based on the results of the operation problem, new sizing values are updated, and this process is repeated until the stopping criterion is satisfied (in this chapter, the stopping criteria is the maximum number of GA iterations).

Assume that a hybrid multi-energy supply network contains N nodes, and at each node $i = 1, ..., N$, we connect PV panels. The capacity of a PV source at each node is noted P^i_{PV}; a fuel cell is used to convert H_2 energy to electricity, the capacity of the fuel cell at each node is $P^{i,max}_{fc}$; an electrolyzer is used to convert electricity to H_2, the capacity of an electrolyzer at each node is $P^{i,max}_{ele}$; H_2 storage tanks are used to store H_2, the capacity of H_2 storage tanks at each node is C^i_{gs}; an ETH device is used to convert electricity to heat, the capacity of an ETH at each node is $P^{i,max}_{ETH}$; a GTH is used to convert gas energy to heat, the capacity of GTH at each node is $P^{i,max}_{GTH}$; a CHP device is used to produce heat and power, the capacity of CHP at each node is $P^{i,max}_{CHP}$. Then the problem is to decide the sizing values of the above components.

6.1.1/ OPERATION PROBLEM

For the operation problem, the goal is to minimize the load shedding of gas/electricity/heat demands, and ensure the reliability of the whole system. The objective function can then be written as:

$$C^{all}_{op} = \alpha \cdot \sum_{i=1}^{N} \sum_{t=1}^{T} LS^{i,t}_{gas} + \beta \cdot \sum_{i=1}^{N} \sum_{t=1}^{T} LS^{i,t}_{el} + \gamma \cdot \sum_{i=1}^{N} \sum_{t=1}^{T} LS^{i,t}_{heat} \tag{6.1}$$

where α, β, γ are penalty values for load shedding of gas/electricity/heat demands; $LS^{i,t}_{gas}, LS^{i,t}_{el}, LS^{i,t}_{heat}$ are the load shedding of gas/electricity/heat demands at node i and time t.

The power devices constraints are:

$$\begin{aligned}
&-P_{line}^{gas,m,n,max} \le P_{line}^{gas,m,n,t} \le P_{line}^{gas,m,n,max} \\
&-P_{line}^{el,m,n,max} \le P_{line}^{el,m,n,t} \le P_{line}^{el,m,n,max} \\
&-P_{line}^{heat,m,n,max} \le P_{line}^{heat,m,n,t} \le P_{line}^{heat,m,n,max} \\
&onoff_{fc}^{i,t} \cdot P_{fc}^{i,min} \le Z_{fc}^{i,t} \le onoff_{fc}^{i,t} \cdot P_{fc}^{i,max} \\
&onoff_{ele}^{i,t} \cdot P_{ele}^{i,min} \le Z_{ele}^{i,t} \le onoff_{ele}^{i,t} \cdot P_{ele}^{i,max} \\
&onoff_{fc}^{i,t} + onoff_{ele}^{i,t} \le 1
\end{aligned} \tag{6.2}$$

$$\begin{aligned}
&0 \le Z_{ETH}^{i,t} \le P_{ETH}^{i,max} \\
&0 \le Z_{GTH}^{i,t} \le P_{GTH}^{i,max} \\
&0 \le Z_{CHP}^{i,t} \le P_{CHP}^{i,max} \\
&0 \le Z_{PS}^{gas,i,t} \le Z_{PS}^{gas,i,max} \\
&0 \le Z_{PS}^{el,i,t} \le Z_{PS}^{el,i,max} \\
&0 \le Z_{PS}^{heat,i,t} \le Z_{PS}^{heat,i,max}
\end{aligned} \tag{6.3}$$

where $P_{line}^{gas,m,n,t}$ is the gas power flow from node m to node n at time t; $P_{line}^{gas,m,n,max}$ is the maximum gas power flow from m to n; $onoff_{fc}^{i,t}$ is the ON/OFF state of the fuel cell at node i and time t; $P_{fc}^{i,min}$ and $P_{fc}^{i,max}$ are the minimum and maximum output of the fuel cell at node i; $P_{ele}^{i,min}$ and $P_{ele}^{i,max}$ are the minimum and maximum input of the electrolyzer at node i; $Z_{fc}^{i,t}$, $Z_{ele}^{i,t}$, $Z_{ETH}^{i,t}$, $Z_{GTH}^{i,t}$, $Z_{CHP}^{i,t}$, are the output power of the fuel cell, electrolyzer, ETH, GTH, CHP at node i and time t; $Z_{PS}^{gas,i,t}$, $Z_{PS}^{el,i,t}$, $Z_{PS}^{heat,i,t}$ are the output power of the gas source, electric generator, and heating source at node i and time t.

The state of H_2 storage tanks can be described as:

$$LOH_{gs}^{i,t} = LOH_{gs}^{i,t-1} + \left(Z_{ele}^{i,t} \cdot eff_{ch} - Z_{fc}^{i,t}\right) \cdot \Delta t / C_{gs}^{i} \tag{6.4}$$

where $LOH_{gs}^{i,t}$ is the state of the H_2 storage tanks at node i and time t, and Δt is the interval time. eff_{ch} is the efficiency to produce H_2 through the electrolyzer.

The H_2 storage tanks constraint is:

$$LOH_{gs}^{i,min} \le LOH_{gs}^{i,t} \le LOH_{gs}^{i,max} \tag{6.5}$$

where $LOH_{gs}^{i,min}, LOH_{gs}^{i,max}$ are the minimal and maximal state of the H_2 storage system at node i.

For the CHP, the following characteristics are used [128]:

- Power generation:

$$Z_{CHP} = \alpha^{GE} Q_{CHP} + \beta^{GE}; \tag{6.6}$$

  Q_{CHP} is the fuel combustion power, in this chapter, the fuel is natural gas; Z_{CHP} is the generated electric power.

- Available waste heat value of flue gas:

$$q^{GAS} = \alpha^{GAS} Q_{CHP} + \beta^{GAS}; \tag{6.7}$$

- Available waste heat value of cylinder water:

$$q^{WA} = \alpha^{WA} Q_{CHP} + \beta^{WA}; \tag{6.8}$$

- The recoverable heat from CHP is:

$$q_{CHP} = eff_{re} \cdot \{q^{GAS} + q^{WA}\} \tag{6.9}$$

- α^{GE}, β^{GE} are the coefficient values to generate electricity; α^{GAS}, β^{GAS} are the coefficient values to produce waste heat from flue gas; α^{WA}, β^{WA} are the coefficient values to produce waste heat from cylinder water; eff_{re} is the heat recovery efficiency; q^{GAS} is the available waste heat value of flue gas; q^{WA} is the available waste heat value of cylinder water; q_{CHP} is the recovery heat from CHP.

The gas power balance constraint is:

$$Z_{PS}^{gas,i,t} - Z_{GTH}^{i,t}/eff_{GTH} - Q_{CHP}^{i,t}/eff_{CHP} - (L_{gas}^{i,t} - LS_{gas}^{i,t}) = P_{line}^{gas,X\to i,t} \tag{6.10}$$

The electricity power balance constraint is:

$$Z_{PS}^{el,i,t} + P_{PV}^{i,t} + Z_{fc}^{i,t} + Z_{CHP}^{i,t} - Z_{ele}^{i,t} - Z_{ETH}^{i,t} - (L_{el}^{i,t} - LS_{el}^{i,t}) = P_{line}^{el,X\to i,t} \tag{6.11}$$

The heat power balance constraint is:

$$Z_{PS}^{heat,i,t} + eff_{heat} \cdot Z_{fc}^{i,t} + eff_{ETH} \cdot Z_{ETH}^{i,t} + Z_{GTH}^{i,t} + q_{CHP}^{i,t} - (L_{heat}^{i,t} - LS_{heat}^{i,t}) = P_{line}^{heat,X\to i,t} \tag{6.12}$$

where $P_{line}^{gas,X\to i,t}$ is the gas power flow from node X to i at time t, X represents all nodes that connect with node i. eff_{GTH} is the efficiency of GTH to produce heat; eff_{CHP} is the gas utilization efficiency of CHP to consume gas; eff_{heat} is the fuel cell efficiency to produce heat; eff_{ETH} is the efficiency of ETH to produce heat. $L_{gas}^{i,t}, L_{el}^{i,t}, L_{heat}^{i,t}$ are the gas/electricity/heat load demands at node i and time t.

6.1.2/ SIZING PROBLEM

For the sizing problem, the objective is to minimize the total investment cost. So the objective function can be written as:

$$\begin{aligned} C_{inv}^{all} = \sum_{i=1}^{N} \{ & C_{inv}^{PV} \cdot P_{PV}^{i} + C_{inv}^{fc} \cdot P_{fc}^{i,max} + C_{inv}^{ele} \cdot P_{ele}^{i,max} \\ & + C_{inv}^{gs} \cdot C_{gs}^{i} + C_{inv}^{ETH} \cdot P_{ETH}^{i,max} + C_{inv}^{GTH} \cdot P_{GTH}^{i,max} \\ & + C_{inv}^{CHP} \cdot P_{CHP}^{i,max} \} \end{aligned} \tag{6.13}$$

where C_{inv} is the investment cost of each component.

U is used to represent the set of the sizing problem variables, namely, $\mathbf{U} = \left\{P^i_{PV}, P^{i,max}_{fc}, P^{i,max}_{ele}, C^i_{gs}, P^{i,max}_{ETH}, P^{i,max}_{GTH}, P^{i,max}_{CHP}\right\}$, $i = 1, ..., N$. **S** represents the set of the operation problem variables. At last, the sizing problem of the hybrid gas/electricity/heat system can be written as:

$$\begin{aligned} &\min_{\mathbf{U}} \left\{ C^{all}_{inv} + \min_{U^*, \mathbf{S}} \left\{ C^{all}_{op} \right\} \right\} \\ &s.t.\ (6.2), (6.3), (6.4), (6.5), (6.6), (6.7), (6.8), (6.9), (6.10), (6.11), (6.12) \end{aligned} \tag{6.14}$$

6.1.3/ CONSIDERING THE CONTINGENCY EVENTS

In large nodes hybrid network, contingency events must be considered. In this section, the influence of contingency events on the sizing results are developed. A large number of contingency events can be listed, and it is impossible to consider all cases. So a robust method can be used to find the worst case. The sizing problem can then be described as:

$$\begin{aligned} &\min_{\mathbf{U}} \left\{ C^{all}_{inv} + \max_{\mathbf{V}} \min_{U^*, \mathbf{S}} \left\{ C^{all}_{op} \right\} \right\} \\ &s.t.\ (6.2), (6.3), (6.4), (6.5), (6.6), (6.7), (6.8), (6.9), (6.10), (6.11), (6.12) \end{aligned} \tag{6.15}$$

where **V** represents the contingency events set.

Then the problem can be described as: search for the best sizing values U^* from **U**, which can make the whole system operate with minimal costs, and at the same time, ensure the whole system resists the worst contingency event.

For this two stage optimization problem, the column-and-constraint generation method [148] is used. In [149], authors use this method to solve a robust microgrid planning problem. In [150], authors solve a distribution network planning problem to minimize the system damage against natural disasters.

For example, in [150], the problem can be summarized as follows:

$$\min_{h \in \mathbf{Y}} \max_{u \in \mathbf{U}} \min_{z \in \mathbf{f}(h,u)} \sum p^{ld} \tag{6.16}$$

$h \in \mathbf{Y}$ is the hardening plans to resist to natural disasters; $u \in \mathbf{U}$ is the natural disasters scenarios; $z \in \mathbf{f}(h, u)$ is the disruption with feasible power flow decisions; $\sum p^{ld}$ is the load shedding.

Then the problem can be described as: search for the hardening plans h^* from **Y**, which can make the whole system operate with minimal load shedding, and at the same time, ensure the whole system resists the worst natural disasters.

Load shedding of the distribution network after hardening lines and DG placement planning (h) and disaster impact (u) can be formulated as: $z = (p, q, v) \in \mathbf{f}(h, u)$. Using an abstract form to describe this feasible set, we have:

$$\mathbf{f}(h, u) = \{z : Ah + Bu + Cz \geq e\} \tag{6.17}$$

Problem 6.16 is a two stage robust optimization problem that can be transferred into two optimization problems, namely, a master problem and a subproblem. The master problem

is:

$$\begin{aligned} &min\ \alpha \\ &s.t.\ h \in \mathbf{Y} \\ &\alpha \geq \sum p^{ld} \\ &z \in \mathbf{f}(h, \widehat{u}) \end{aligned} \tag{6.18}$$

The subproblem is:

$$\max_{u \in \mathbf{U}} \min_{z \in \mathbf{f}(h,u)} \sum p^{ld} \tag{6.19}$$

However, the subproblem is a *maxmin* problem. Then, we need to transfer this *maxmin* problem into a one stage problem. We notice that the inner *min* problem can be transferred to a Lagrange dual problem, which can be shown as follows:

$$\begin{aligned} &\min_{z \in \mathbf{f}(h,u)} z \\ &s.t.\ z \in \mathbf{f}(h, \widehat{u}) \\ &\Rightarrow \\ &\min_{z} z + \pi(e - Ah - Bu - Cz) = (I - \pi C)z + \pi(e - Ah - Bu) \\ &s.t.\ \pi \geq 0 \end{aligned} \tag{6.20}$$

Then the above *min* problem can be represented as the following *max* problem:

$$\begin{aligned} &\max_{\pi} \pi(e - Ah - Bu) \\ &s.t.\ I - \pi C \geq 0 \\ &\pi \geq 0 \end{aligned} \tag{6.21}$$

At last, subproblem 6.19 can be transferred as the following one stage problem:

$$\begin{aligned} &\max_{u \in \mathbf{U}} \min_{z \in \mathbf{f}(h,u)} \sum p^{ld} = \\ &\max_{u \in \mathbf{U}} \max_{\pi} \pi(e - Ah - Bu) = \\ &\max_{u \in \mathbf{U}, \pi} \pi(e - Ah - Bu) \\ &s.t.\ I - \pi C \geq 0 \\ &\pi \geq 0 \end{aligned} \tag{6.22}$$

Based on the above master problem and subproblem, the column & constraint generation (CCG) algorithm is developed based on [150], as follows:

1. solve subproblem 6.23 with the given plan $\widehat{h}$, obtain the objective value of subproblem $objSP$ and disaster scenarios u_k^*;

2. add u_k^* to set $\widehat{U}$, create dispatch variables z^k, and add the corresponding constraints $z^k \in \mathbf{f}(h, u_k^*)$ to master problem 6.18, namely,

$$\begin{aligned} &\alpha \geq z^k \\ &Ah + Cz^k \geq e - Bu^k \end{aligned} \tag{6.23}$$

3. solve master problem 6.18, obtain the objective value of master problem $objMP$ and update the planning plan $\widehat{h}$;

4. repeat this process until the gap between $objMP$ and $objSP$ is less than a small value.

We can see that with the CCG algorithm, the uncertainty set is transferred based on Lagrange dual problem, and two stage optimization is decomposed into a master and a subproblem.

In this chapter, the uncertainty set of disasters is described based on graph theory, and a two stage sizing problem is decomposed into a leader and a follower problem. A comparison between the CCG method and the presented method is summarized in Tab. 6.1.

Table 6.1: Comparison between the CCG method and our method.

Method	Disasters scenarios	Two stage problem	Running	Complexity
CCG [150]	Lagrange dual problem	master & sub problem	iteration repeat	high
Proposed	graph theory	leader & follower problem	iteration repeat	medium

In our method, the worst case is obtained based on graph theory. For the large nodes hybrid network system, the relative importance of each node is ranked. The case where the most important node is destroyed under the contingency event, is the worst case. The relative importance of each node in the graph is described using betweenness centrality [151] of the node:

$$C_B(i) = \sum_{n_i \neq n_k \neq n_l} \frac{n_k \rightarrow n_l, n_i}{n_k \rightarrow n_l} \tag{6.24}$$

where $n_k \rightarrow n_l, n_i$ is 1 if the shortest path between nodes n_k to n_l goes through n_i, and 0 if n_k to n_l does not pass through n_i.

Under the worst case, the new structure of the whole system can be obtained. Then the sizing problem (7.31) is solved based on this new structure, and new sizing values can be obtained.

6.2/ Simulation results for Case I

In this section, the modified 13-node case is tested. Three cases are compared. For the operation problem, the time step is 1 hour, and time horizon is one day (24h).

6.2.1/ System setup

The penalty values are arbitrarily chosen as $\alpha = \beta = \gamma = 10^{10}$ to make sure that the penalty cost of load shedding is larger than that of the total investment cost. Investment costs are shown in Tab. 6.2. The cost parameters are adopted from [145, 142]. The model is implemented in MATLAB and solved with YALMIP [152] and Gurobi. Simulations were run on a computer with an Intel Xeon CPU E3-1220@3.1GHz.

Load demands (peak load) at each node are shown in Tab. 6.3. Source data is shown in Tab. 6.4. The capacity of transportation lines is shown in Tab. 6.5, where the unit is MW.

Table 6.2: Investment costs [145, 142]

Device	Cost
PV	2 M€/MW
Fuel cell	4 M€/MW
Electrolyzer	3.2 M€/MW
H_2 tank	1200 €/MWh
ETH	0.06 M€/MW
GTH	0.15 M€/MW
CHP	1.6 M€/MW

Here the capacity of pipelines in the heat network are assumed to be the same as power lines. In order to reduce the computation time, four typical days (spring, summer, autumn, winter) are used as the load block. In each hour of the typical day, the operation problem (minimizing load shedding) is checked based on the sizing problem. If the constraints of the operation problem are violated, then new sizing values are generated. The simulation flow chart can be seen in Fig. 7.6.

Table 6.3: Load demand (peak load) [145]

Bus	L_{el}[MW]	L_{heat}[MW]	L_{gas}[MW]
1	4.8334	3.8323	1.8251
2	7.0342	6.0123	1.0789
6	5.1668	4.1532	1.1652
7	5.8746	4.8056	1.8487
10	7	6.5642	1.0023
12	5.1668	4.1756	1.1695
13	4.9254	3.9652	1.9362

Table 6.4: Source data [145]

Bus	$Z_{PS}^{el,max}$[MW]	$Z_{PS}^{heat,max}$[MW]	$Z_{PS}^{gas,max}$[MW]
1	5	4	6
8	0	0	90
12	8	7	8

Table 6.5: Feeder data [145]

Line	P_{line}^{el}[MW]	P_{line}^{gas}[MW]	Line	P_{line}^{el}[MW]	P_{line}^{gas}[MW]
1	4.9	11	7	23.6	50
2	7.2	15	8	17.4	37
3	12.2	26	9	7.2	15
4	11.6	24	10	10.8	22
5	5.4	11	11	5.4	11
6	6.2	13	12	5.4	11

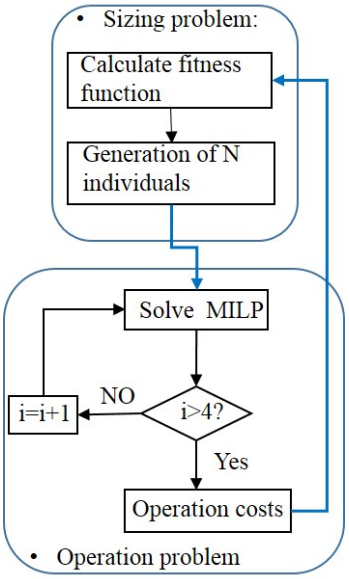

Figure 6.3: Simulation flow chart.

The efficiency parameters are shown in Table 6.6.

Table 6.6: Efficiency values

Efficiency	Value	Efficiency	Value
eff_{ch}	0.5	eff_{GTH}	0.9
eff_{heat}	0.19	eff_{CHP}	0.9
eff_{ETH}	0.9	eff_{re}	0.8

Three cases are compared:

1. case 1: all nodes interconnect the PV panels;
2. case 2: we choose different candidate buses to install PV panels;
3. case 3: the investment cost of the hydrogen storage system is reduced by 50%.

case 1 and case 2 are used to evaluate the influence of PV location on the sizing results (buses 3/4/5/8/9/11 are chosen to install PV panels, because these buses are not load demands central, and have place to install the PV panels). case 1 and case 3 are used to evaluate the influence of hydrogen storage investment costs on the results.

6.2.2/ GENETIC ALGORITHM BASED SIZING RESULTS

In our example, there are 13 nodes, and at each node there are 7 components, so the number of variables is 91. Each population gives the 91 values of each component, then the operation optimization problem is run. Based on the operation results (load shedding) and investment costs, the population is updated.

Tab. 6.7 shows the results of case 1. Tab. 6.8 shows the results of case 2. Tab. 6.9 shows the results of case 3. The unit of each component (PV panels, fuel cell, electrolyzer, ETH, GTH, CHP) in each table is MW, and the unit of H_2 tanks is MWh.

Table 6.7: case1 results

Node	P_{PV}	P_{fc}^{max}	P_{ele}^{max}	P_{ETH}^{max}	P_{GTH}^{max}	P_{CHP}^{max}	C_{gs}
1	7.10	2.41	0.21	0.29	0.72	3.33	84.77
2	2.53	0.60	0.73	3.53	1.52	0.72	57.99
3	4.77	0.02	0.95	1.64	3.49	0.39	4.91
4	3.13	2.60	4.26	0.38	0.32	0.60	63.94
5	3.53	0.01	2.95	2.55	2.72	1.01	89.28
6	8.16	4.45	1.40	0.08	3.14	0.48	89.50
7	5.91	1.92	2.67	0.04	3.65	4.59	13.97
8	2.29	0.20	0.89	2.50	0.03	0.23	19.34
9	3.90	1.47	3.66	2.80	0.16	1.08	76.84
10	6.03	3.11	1.08	2.76	1.71	3.08	15.64
11	4.79	0.81	3.09	1.72	0.98	3.97	78.53
12	6.01	3.96	1.13	4.70	2.16	2.94	30.58
13	2.65	2.20	1.78	2.24	3.41	0.07	50.46
Total	60.78	23.76	24.80	25.23	24.00	22.50	675.76

Table 6.8: case2 results

Node	P_{PV}	P_{fc}^{max}	P_{ele}^{max}	P_{ETH}^{max}	P_{GTH}^{max}	P_{CHP}^{max}	C_{gs}
1	0.00	0.31	1.16	2.73	1.44	3.89	77.93
2	0.00	1.65	0.27	1.38	4.35	3.42	18.82
3	3.24	2.18	0.74	0.41	1.89	1.48	3.69
4	6.96	0.09	0.01	3.60	4.98	0.38	18.97
5	9.41	0.36	3.78	3.71	3.97	2.68	19.75
6	0.00	2.79	4.00	1.12	2.97	1.01	82.38
7	0.00	3.15	0.76	3.43	2.53	0.32	62.97
8	2.57	1.01	3.07	2.40	1.74	0.22	90.56
9	7.74	2.51	0.93	0.71	4.35	2.10	52.50
10	0.00	2.77	0.69	1.64	0.66	4.28	81.83
11	3.03	0.19	4.17	3.26	2.66	2.58	81.33
12	0.00	1.03	0.12	2.67	4.56	0.09	56.10
13	0.00	3.95	4.46	2.09	0.37	0.99	47.04
Total	32.95	22.00	24.15	29.15	36.46	23.43	693.85

Fig. 6.4 shows the comparison of these three cases. In case2, PV is limited to be installed at some nodes which are not load demand centers, so the PV output power must be transferred to the load demand centers based on the power transmission lines, but the capacity of power transmission lines will limit the transferred power. At last, the installed PV power is smaller than that in case1 (decreases 50%). This leads to a smaller capacity for the electrolyzer (which is used to store surplus PV output, and decreases by 3%). The smaller capacity of PV leads to a larger capacity for the H_2 tanks (increases by 2%) and the CHP (increases by 4%). The smaller capacity for electrolyzer leads to a larger

Table 6.9: case3 results

Node	P_{PV}	P_{fc}^{max}	P_{ele}^{max}	P_{ETH}^{max}	P_{GTH}^{max}	P_{CHP}^{max}	C_{gs}
1	3.19	0.56	0.83	3.16	1.08	1.06	13.99
2	8.45	1.58	3.16	2.46	0.05	1.37	59.46
3	8.25	2.95	3.24	4.62	0.84	3.79	83.83
4	3.19	1.13	1.34	4.96	1.21	4.46	64.00
5	6.26	1.65	3.51	0.14	3.96	1.22	7.27
6	4.19	1.42	0.64	3.87	2.44	3.31	81.91
7	6.13	1.69	0.20	1.58	3.48	0.34	64.67
8	2.22	2.45	1.35	4.29	2.26	3.15	2.34
9	5.40	0.81	4.09	0.85	0.28	1.11	79.54
10	4.20	2.58	1.49	2.63	0.25	0.33	77.67
11	4.94	0.67	4.09	3.78	3.96	4.59	95.33
12	6.79	1.55	3.06	2.67	1.00	1.34	59.40
13	6.06	3.70	0.97	0.22	0.40	1.27	1.78
Total	69.27	22.75	27.96	35.23	21.20	27.32	691.20

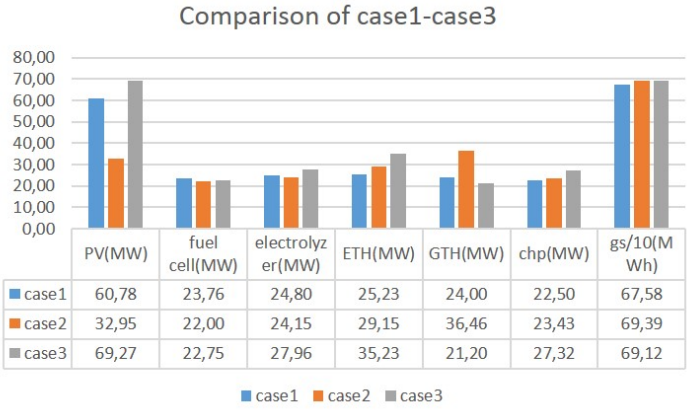

Figure 6.4: Comparison of three cases.

capacity for the ETH (increases by 15%), because both devices are used to consume the electricity, the surplus energy can either be stored in tanks through electrolyzer, or through the ETH to supply the heating demand.

Comparing case1 and case3, it can be seen that in case3, the capacity of PV is larger than that in case1 (increases by 14%). This is because the hydrogen storage system is more competitive (due to the reduction of the investment cost of the fuel cell and tne electrolyzer) and can be used frequently, then more PV panels can be installed, which leads to a larger capacity for the electrolyzer (increases by 13%). More power can be produced by PV, which leads to a larger capacity for the ETH (increases by 40%). A larger capacity for the ETH also leads to a smaller GTH (decreases 13%).

Comparing these three cases, it can be seen that the sizing results of PV, ETH, GTH, and CHP change obviously. This is because their costs are more competitive than that of the fuel cell and the electrolyzer, which has a larger ability to minimize the objective function.

Based on the above simulation results, it can be seen that PV panels' location and the

investment cost of hydrogen storage system are important parameters to influence the sizing values of each component.

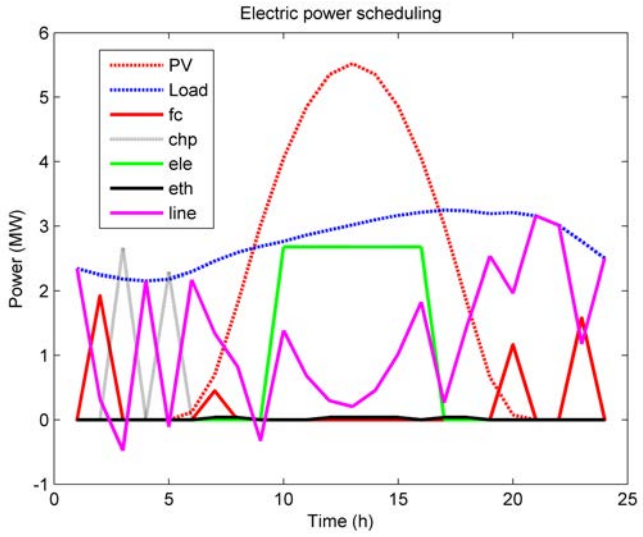

Figure 6.5: Electric power scheduling at node 7 (line is L6).

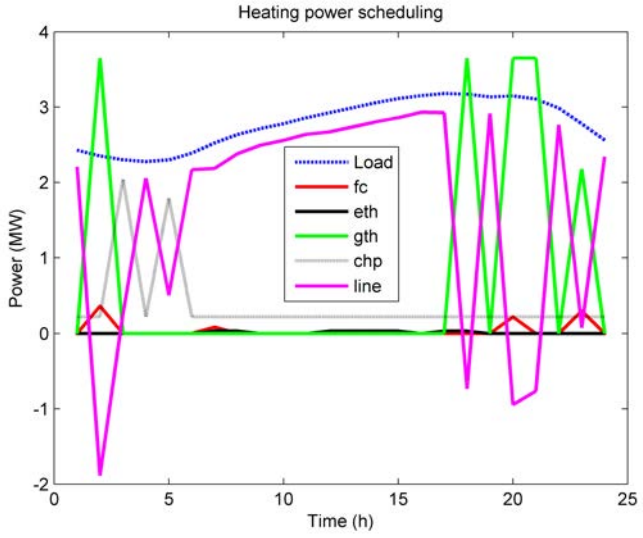

Figure 6.6: Heating power scheduling at node 7 (line is L6).

Figs. 6.5, 6.6, 6.7, 6.8 show one day scheduling results of the three energy systems in a typical spring day. In Fig. 6.5, at node 7, electric energy is exchanged with the other nodes through power line L6. During the night, the fuel cell, and CHP produce electricity to supply the loads. During the day, PV and imported energy are used to supply the loads. The electrolyzer is used to store the surplus energy. In Fig. 6.6, the CHP and GTH produce the main heat energy, and the fuel cell and ETH produce the remaining heat. Imported/exported heating energy through pipeline 6 is also important to keep the energy balance at node 7. Fig. 6.7 shows that gas imports through gas pipeline 6 are the main method to supply gas loads at node 7. Fig. 6.8 shows the state of hydrogen tanks at all nodes. It can be seen that the storage system can be used to keep the power balance of

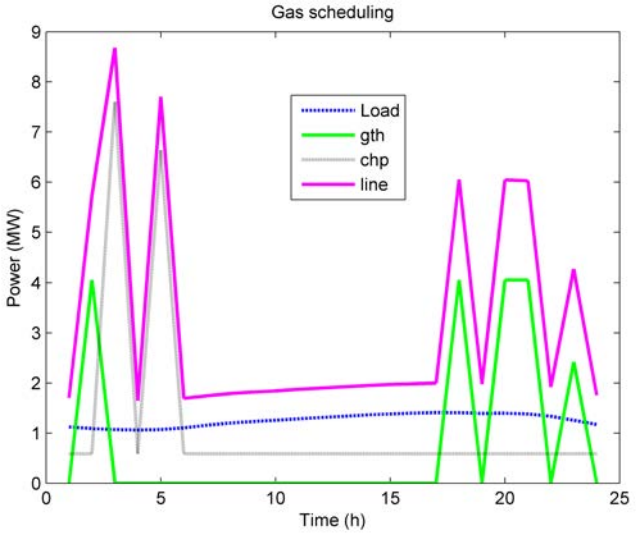

Figure 6.7: Gas scheduling at node 7 (line is L6).

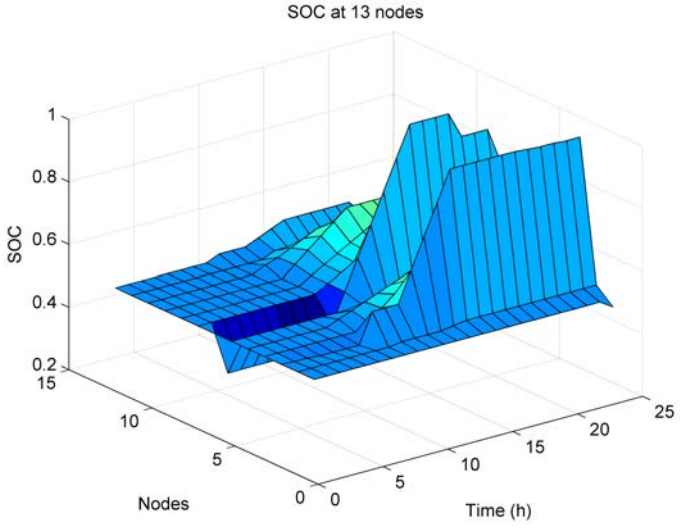

Figure 6.8: SOC at 13 nodes.

the whole system. Through the fuel cell, hydrogen tanks can produce electricity and heat to supply the load demand; through the electrolyzer, the surplus electricity can be stored in hydrogen tanks using H_2.

From the scheduling results, the output of some power devices change fast, especially the lines. For example, in Fig. 6.6, at 2 am, heating pipeline exports heating energy, but at 3 am, heating pipeline imports heating energy. The reason for this phenomenon is that we do not limit the ramp up and ramp down constraints of all components.

6.2.3/ INFLUENCE OF CONTINGENCIES ON THE SIZING RESULTS

Based on section 6.1.3, the worst case can be obtained using graph theory. For this 13-node hybrid network system, we rank the relative importance of each node. The case where the most important node is destroyed under the contingency event is the worst case. The relative importance of each node in the graph is described using the betweenness centrality [151] of the node.

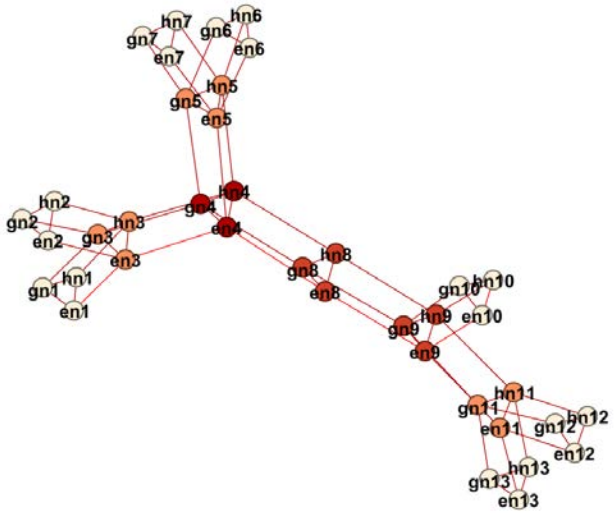

Figure 6.9: Graph structure of the 13-node hybrid network.

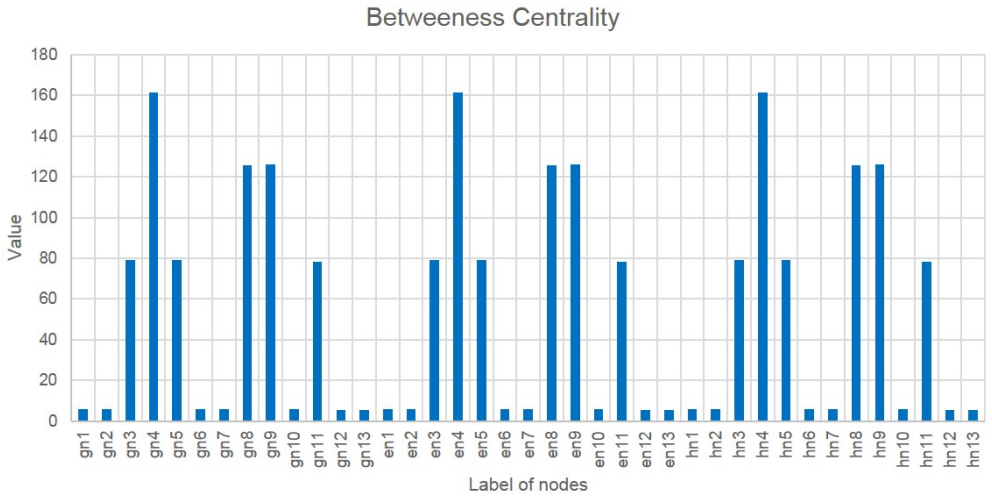

Figure 6.10: Betweenness centrality of the 13-node hybrid network.

Fig. 6.9 shows the graph connection of the 13-node hybrid network. Fig. 6.10 shows the obtained betweenness centrality of the 13-node hybrid network. It can seen that the most important node of the whole system is node 4. The worst case for this network, is thus when the connections between node 4 and the other nodes are removed.

As the failure probability of gas pipelines and heat pipelines are smaller than that of overhead electric power lines [140], for the worst case, only the removal of electric power lines

is considered. Then, the sizing problem needs to check eight cases (the normal condition with four typical days of each season, and the worst case condition with four typical days). Tab. 6.10 shows the sizing results of the whole system when the electric connections between node 4 and the other nodes are removed, namely, we remove electric lines $en3 \leftrightarrow en4$, $en5 \leftrightarrow en4$, $en8 \leftrightarrow en4$. This case is defined as case4.

Table 6.10: case4 results

Node	P_{PV}	P_{fc}^{max}	P_{ele}^{max}	P_{ETH}^{max}	P_{GTH}^{max}	P_{CHP}^{max}	C_{gs}
1	5.55	0.01	2.83	2.55	0.33	3.56	49.85
2	5.58	2.02	3.42	0.74	1.62	0.21	32.59
3	3.98	0.91	2.01	4.44	1.88	0.36	31.51
4	7.30	2.72	4.83	4.67	0.20	0.22	12.83
5	6.05	3.71	0.37	1.88	1.22	1.25	87.38
6	7.25	1.67	2.00	0.77	1.77	2.37	56.29
7	4.09	4.04	3.76	3.95	3.19	1.29	61.96
8	3.92	1.76	1.37	3.09	3.02	2.91	25.46
9	6.03	3.45	3.49	4.73	1.69	1.60	19.71
10	4.86	0.52	0.25	3.81	0.62	1.59	64.03
11	2.09	0.87	3.21	4.10	4.95	3.81	27.16
12	3.45	4.12	2.96	4.20	1.91	0.93	68.01
13	7.69	0.27	2.68	2.43	3.81	1.68	3.89
Total	67.85	26.07	33.19	41.37	26.20	21.78	540.66

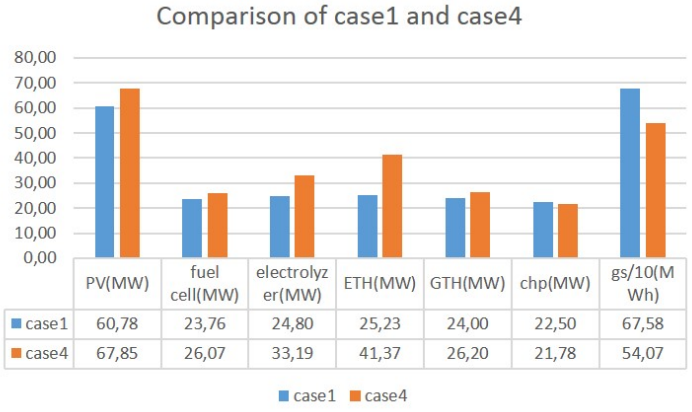

Figure 6.11: Comparison of case1 and case4.

Fig. 6.11 shows a comparison of results for case1 and case4. It can be seen that: 1) at node 4, because the electric loads cannot import/export energy from/to the other nodes, so the capacity of PV, and fuel cell is larger than that in case1 (increase by 12%, and 11% respectively); 2) this worst case divides the electric supply network into four parts: $\{en1, en2, en3\}$, $\{en4\}$, $\{en5, en6, en7\}$, $\{en8, en9, en10, en11, en12, en13\}$. Then each part cannot get electric power from the other parts (through electric power lines), which means that the important task of keeping electric power balance is taken on by the fuel cell, CHP (the main controllable power source) and PV panels. Larger PV panels lead to a larger capacity of electrolyzer (increases by 34%) and ETH (increases by 64%) to consume the surplus energy.

The above simulation shows that the structure of the whole system also influences the sizing results of each component. This is because the interconnection structure of the system can influence the energy flow in the whole system, which will then influence the utilization of the power devices, and at last, the sizing results will be different.

6.2.4/ DISCUSSION

Case 1 to case 3 show that the PV panels location and investment cost of hydrogen storage system influence the sizing value of each component. When the installed capacity of PV panels is reduced by 50%, the capacity of the electrolyzer decreases by 3%, capacity for the H_2 tanks increases by 2%, the CHP increases by 4%, and ETH increases by 15%. When the investment costs of the fuel cell and the electrolyzer decrease by 50%, the capacity of PV increases by 14%, the electrolyzer increases by 13%, ETH increases by 40%, and GTH decreases by 13%.

To resist to contingency events, betweenness centrality is used to find the most important node (worst case). The simulation results (case 4) show that the controllable power sources (fuel cell, CHP), PV panels and the H_2 tanks are the main components to ensure the system power balance. The capacity of PV and fuel cell increase by 12% and 11%, and the electrolyzer increases by 34% while the ETH increases by 64%. After the hybrid network is damaged by contingency events, the whole system is divided into small parts, namely, smaller 'islanded' microgrids. In each part, the main controllable power sources are the fuel cell and CHP. So the size of the PV panels and H_2 tanks is important to enable the whole system to operate normally.

6.3/ SIMULATION RESULTS CASE II

In this section, a benchmark hybrid gas/electric/heat system is presented. The electricity network is an IEEE 30 nodes network [153], shown in Fig. 6.12. At nodes e1 and e2, two gas-generators are connected. MG1, MG2, MG3 and MG4 are connected at nodes e23, e17, e14 and e7. The gas network is a 20-node system, for which the parameters can be found in [154], [155], as shown in Fig. 6.13. A gas-generator is connected at nodes g12 and g19. A heating source is supplied by gas at nodes g11, g12 and g14. MG1, MG2, MG3 and MG4 are connected at nodes g7, g6, g15 and g10. The heating network is a 14-node system [153], shown in Fig. 6.14. Nodes h1, h6 and h11 are heating sources. MG1, MG2, MG3 and MG4 are connected at nodes h9, h10, h4 and h13. The configuration of this hybrid system is summarized in Tab. 6.11.

Two cases are simulated:

1. case5: normal operation state, namely, no connection nodes are removed;
2. case6: operation under contingency events, namely, the most important node is removed;

The obtained sizing values of these four MGs are shown in Tab. 6.12.

Figs. 6.15, 6.16, 6.17, 6.18 show one day scheduling results of MG3 in a typical spring day. Figs. 6.19, 6.20 show the gas flow in the gas supply system and the heat flow in heating supply system.

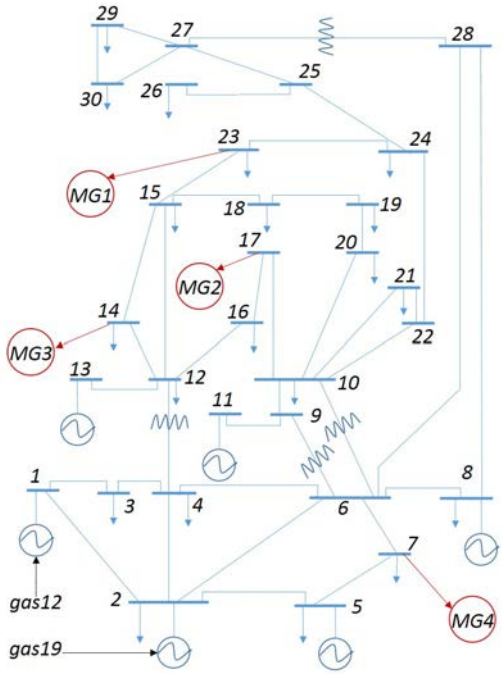

Figure 6.12: IEEE 30-node network.

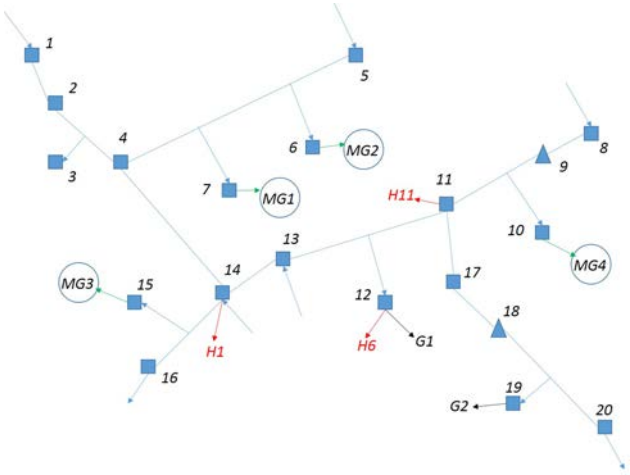

Figure 6.13: Gas 20-node network.

The structure of this hybrid system is then analyzed to obtain the worst case based on graph theory. Fig. 6.21 shows the graph structure of the hybrid system. Fig. 6.22 shows the betweenness centrality, and indicates that the most important node is e6 (electrical network node6). The worst case of this hybrid network is then defined, which is when the connections between node 6 and the other nodes are removed. Here, for the operation problem, 8 cases must be checked (the normal condition with four typical days of each season, and the worst case condition with four typical days).

Tab. 6.13 shows the sizing results when the connections between node 6 and other nodes is removed, namely, remove $e6 \leftrightarrow e2$, $e6 \leftrightarrow e4$, $e6 \leftrightarrow e7$, $e6 \leftrightarrow e8$, $e6 \leftrightarrow e9$, $e6 \leftrightarrow e10$, $e6 \leftrightarrow e28$. Fig. 6.23 shows the comparison of case 5 and case 6. It can be seen that after considering the damage of the electrical network, more PV panels (increases by

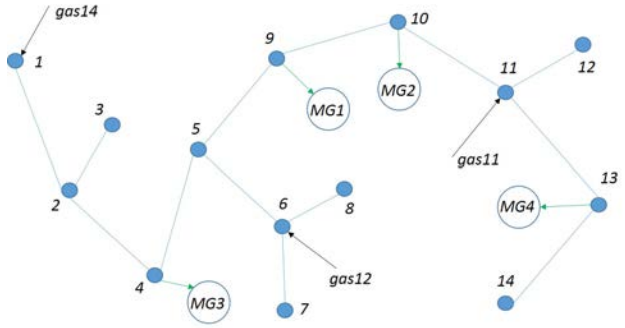

Figure 6.14: Heating 14-node network.

Table 6.11: Configuration

Unit	Electrical bus	Gas node	Heat node
Generator 1	e1	g12	-
Generator 2	e2	g19	-
Heating 1	-	g14	h1
Heating 6	-	g12	h6
Heating 11	-	g11	h11
MG1	e23	g7	h9
MG2	e17	g6	h10
MG3	e14	g15	h4
MG4	e7	g10	h13

Table 6.12: case II results

Node	P_{PV}	P_{fc}^{max}	P_{ele}^{max}	P_{ETH}^{max}	P_{GTH}^{max}	P_{CHP}^{max}	C_{gs}
MG1	3.25	0.97	1.90	1.21	3.78	0.88	3.02
MG2	3.75	0.20	3.22	4.40	1.07	1.32	0.68
MG3	4.29	2.40	0.07	1.73	0.16	0.73	2.87
MG4	3.60	0.46	1.57	4.89	0.21	0.90	4.02
Total	14.89	4.03	6.75	12.24	5.21	3.82	10.59

8%), fuel cell (increases by 11%) and CHP are needed to supply the electricity demands in MGs. The total sizing value of the GTH is decreased, but the sizing value of the ETH (increases by 18%) is increased, because the ETH is used to fill up the position of the GTH to supplement the remaining heating demands. The total volume of hydrogen tanks (increases by 14%) is also increased to supply the electrical demands through fuel cells.

6.4/ CONCLUSION

In this chapter, a co-optimization method was presented to size distributed generation in a hybrid gas/electricity/heat network. MILP was used to control the operation of the whole system, which aims to minimize load shedding. GA was used to search for the sizing values of each component. Case 1 and case 2 showed that the PV panels location influ-

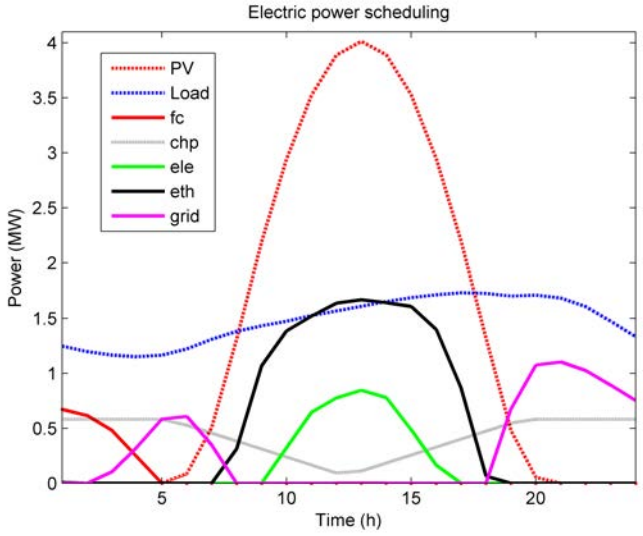

Figure 6.15: Electric power scheduling in MG 3.

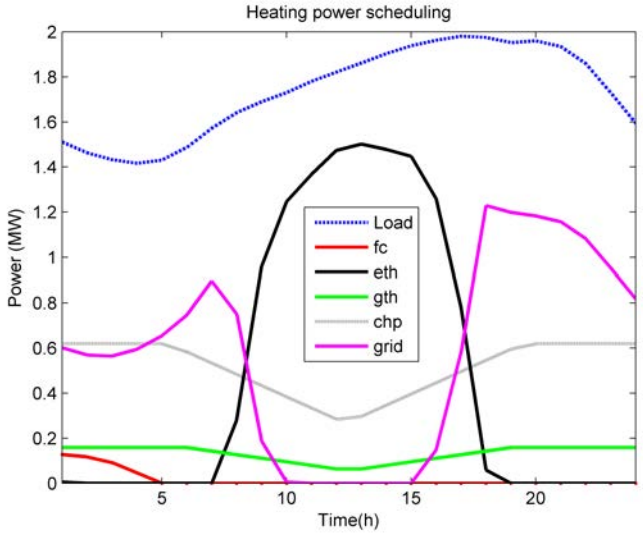

Figure 6.16: Heating power scheduling in MG 3.

Table 6.13: Case II under disasters results

Node	P_{PV}	P_{fc}^{max}	P_{ele}^{max}	P_{ETH}^{max}	P_{GTH}^{max}	P_{CHP}^{max}	C_{gs}
MG1	4.40	2.23	0.03	4.12	0.66	3.54	2.85
MG2	3.62	1.03	3.89	2.98	1.22	0.94	3.75
MG3	4.00	0.36	4.05	3.93	0.37	0.75	3.87
MG4	4.01	0.85	2.62	3.45	0.57	2.38	1.58
Total	16.02	4.48	10.60	14.47	2.82	7.60	12.06

ence the sizing results of each component. This is because the PV panels operating as uncontrollable power sources are playing an important role to ensure the power balance of the whole system. The controllable power devices are all operating encompassly the

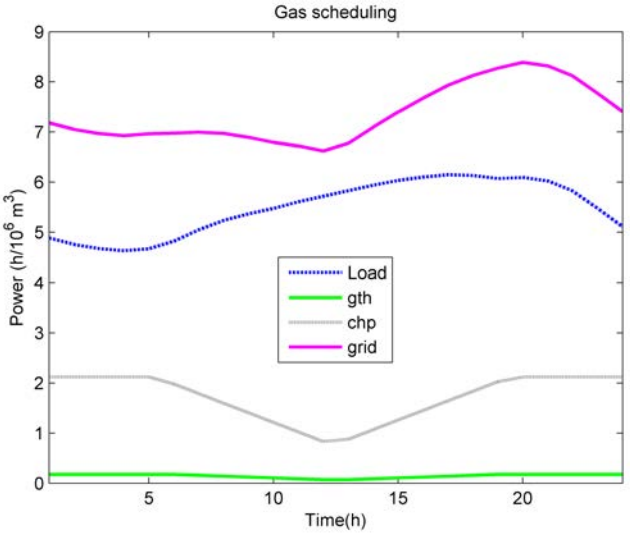

Figure 6.17: Gas scheduling in MG 3.

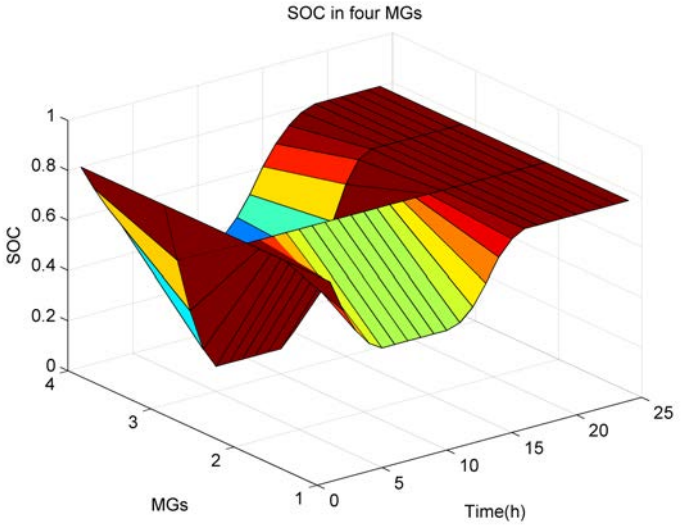

Figure 6.18: SOC in four MGs (the storage system is the hydrogen storage system).

PV panels. At last, with different capacities of PV panels, the sizing results of each component are also different. When the installed capacity of PV panels is reduced by 50%, the capacity of the electrolyzer decreases by 3%, the capacity for the H_2 tanks increases by 2% and the CHP increases by 4% while the ETH increases by 15%.

Case 1 and case 3 showed that the investment cost of the hydrogen storage system also influences the sizing results. This is because the investment costs impact the competitivity of each component to minimize the objective function. When the investment cost of the fuel cell and the electrolyzer decrease by 50%, the capacity of PV increases by 14%, the electrolyzer increases by 13%, ETH increases by 40%, and the GTH decreases by 13%.

A new method based on betweenness centrality was then proposed to find the worst case under contingency events. Case 4 showed that the controllable power sources (fuel cell,

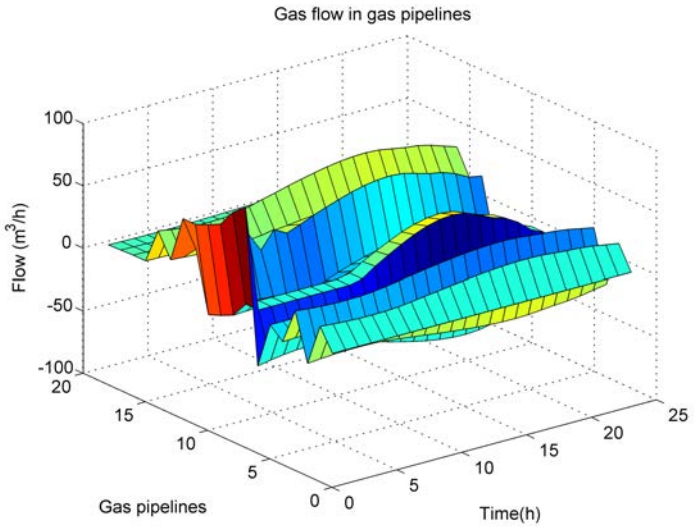

Figure 6.19: Gas flow in gas system.

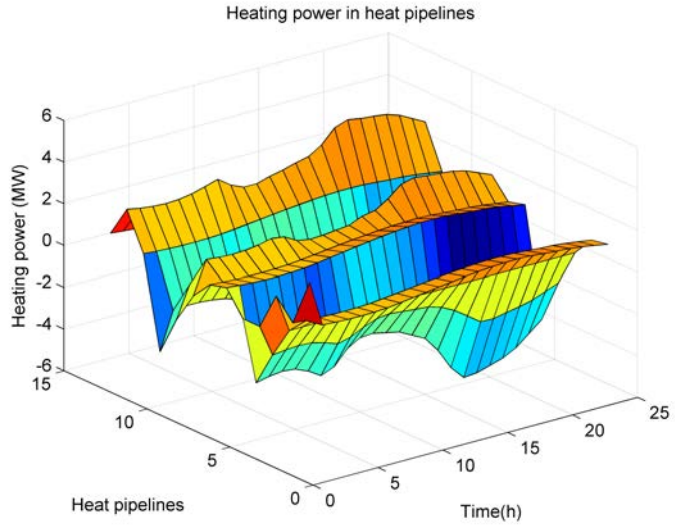

Figure 6.20: Heating flow in heat system.

CHP), PV panels and H_2 tanks are the main factors that influence whether the whole system can operate normally or not. After considering the worst case contingency event, for case 4, the capacity of PV and fuel cell increase by 12% and 11%, and the electrolyzer increases by 34%, while the ETH increases by 64%.

At last, an IEEE30 + Gas20 + Heat14-node network was tested (case 5 and case 6). Case 6 showed that the structure of the power system influences the energy exchanges between the grid and MG, and influence the sizing values in each MG. The results indicate that more power is imported from the gas network when power supply network exports are limited. After considering the worst case contingency event, for case II, the capacity of PV and fuel cell increase by 8% and 11%, and the electrolyzer increases by 57% while the ETH increases by 18%.

This co-optimization method can be used as a guidance for utility companies to build

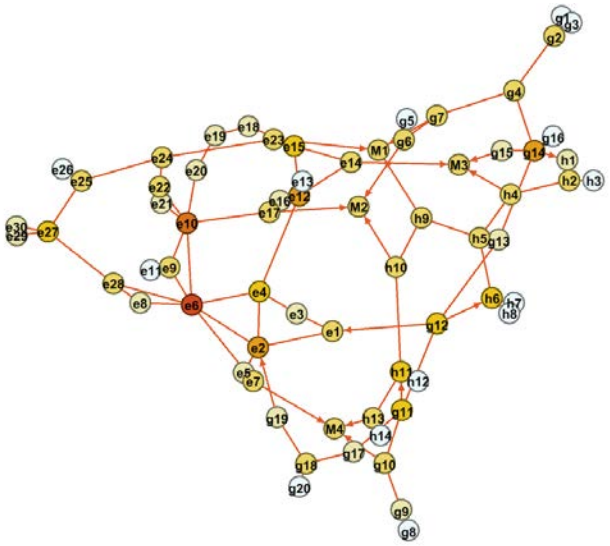

Figure 6.21: Graph structure of hybrid system.

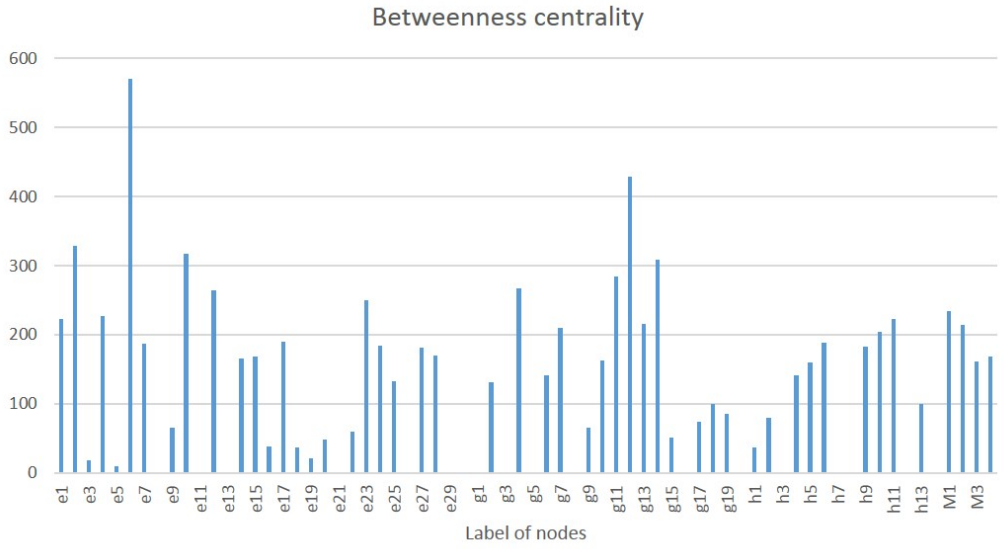

Figure 6.22: Betweenness centrality of hybrid system.

large nodes hybrid gas/electricity/heat supply networks.

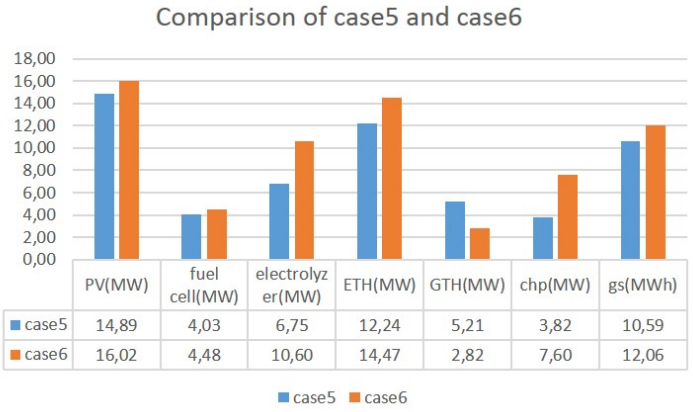

	PV(MW)	fuel cell(MW)	electrolyzer(MW)	ETH(MW)	GTH(MW)	chp(MW)	gs(MWh)
case5	14,89	4,03	6,75	12,24	5,21	3,82	10,59
case6	16,02	4,48	10,60	14,47	2,82	7,60	12,06

Figure 6.23: Comparison of case5 and case6.

7

SIZING AND PRICE DECISION ALGORITHM FOR GRID-CONNECTED MICROGRIDS

The previous chapter discussed about the sizing problem of grid-connected microgrids. But we did not consider the electricity price. Actually, when microgrids interconnect with the utility grid, microgrids will exchange energy with it based on the price. In this chapter, we research about the price decision approach for multiple grid-connected MES MGs. After that, we present a sizing algorithm for grid-connected MES MGs based on the different prices.

Firstly, we introduce the load service entity (LSE) definition. Local generation, local storage systems and renewable energy sources can form an LSE, which can provide ancillary services to the utility grid (UG) and consumers. For example, when there is unbalance power in the regulating power market, an LSE can provide upward/downward power to compensate the imbalances. An LSE can also provide an incentive price to consumers to encourage them to participate in the market [131]. On the other hand, an MG can also sell energy to the UG or LSE to earn profits. Then how the LSE can decide the electricity selling price to multiple MGs, and how the MGs can decide the selling price to LSE are problems. The goal of deciding the prices for LSE and MGs is because prices are the only way to guide the operation of LSE and UGs to arrange their energy scheduling. The operation of the LSE and MGs are significantly influenced by the prices. This means that different goals (such as shifting peak load, or improving the efficiency of the whole system) can be achieved by deploying different prices.

For an LSE, the goal is to maximize the profits, which includes local storage operation costs, electricity buying costs from UG and MGs, and the profit earnings from MGs. For each MG, the goal is to minimize the costs, which includes the operation cost of each component, the electricity buying cost from the UG, and the profit earnings from an LSE. In this chapter, we present a price decision method for multiple MGs considering demand response. MILP is used to control the operation of each MG, and also used to operate the LSE. A GA is used to search for the best price for each MG and the LSE. This combined method is deployed in a decentralized way, namely, each MG runs its own operation problem. Compared to centralized control, the privacy of consumers can be protected.

The structure of the UG-LSE-MGs system is shown in Fig. 7.1. The LSE can purchase electricity from the utility grid, and with local generation and local storage systems, it can also provide services to multiple MGs. In an LSE, renewable energy (PV) is integrated,

and a battery storage system and hydrogen storage system are used to keep the power balance. However, MGs can also sell electricity to LSEs to maximize their profits. The goals of the LSE and MGs are in conflict, namely, the LSE prefers to choose a higher selling price to earn more profits and a lower buying price to/from MGs to decrease costs, but the MGs are actually aiming for the opposite. Thus we introduce an Independent System Operator (i.e., an organization which will not give preference to either side) to decide the reasonable price for the LSE and MGs. The LSE and each MG transfer their costs to the ISO, and then the ISO updates the prices using GA.

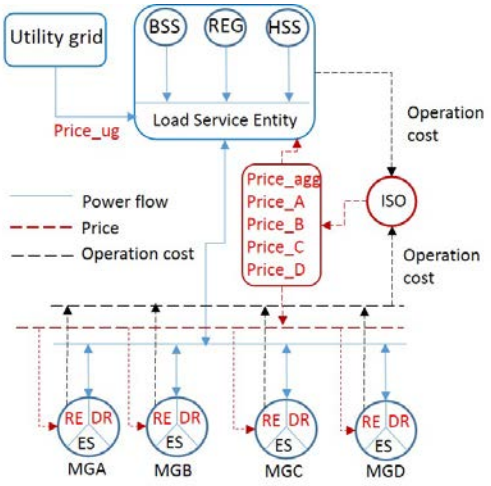

Figure 7.1: Utility grid/Load service entity/microgrids.

The structure of an MES MG is shown in Fig. 7.2. Three types of demands are considered, electricity/heating/cooling. A PV, a battery storage unit, and a hydrogen storage unit are used to provide electricity service; thermal solar, a fuel cell, a heat boiler and a heat storage system are used to serve the heating load demand; an air conditioner and an absorption heat chiller are used to serve the cooling load. More details about this MG can be seen in section 5.

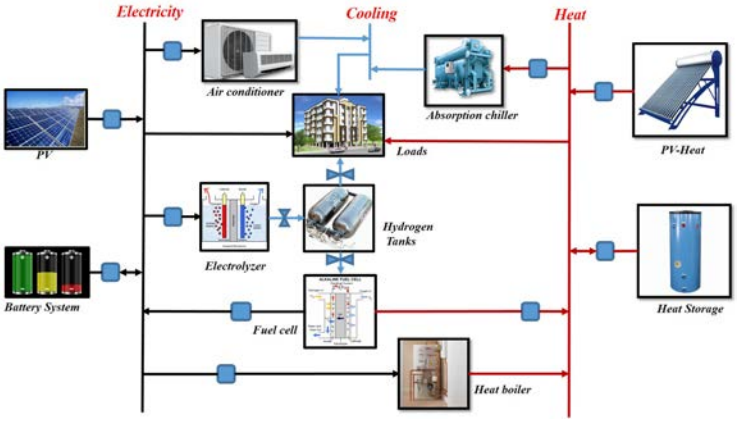

Figure 7.2: Multi-energy-supply microgrid.

When there is a large number of microgrids, the price searching algorithm will take lots of time. Then we present a neural network (NN) model to estimate the performance of the whole system. Based on the NN model, GA is used to search for the best prices.

The remainder of this chapter is organized as follows. Section 7.1 describes the problem formulation, and Section 7.2 and 7.3 the simulation results. Section 7.4 the neural network model. Section 7.5, the discussion of the whole paper. Finally, Section 7.7 concludes the paper.

7.1/ PROBLEM FORMULATION

For the UG-LSE-MGs structure, it includes three aspects: 1) the operation of the LSE; 2) the operation of each MG; 3) prices updating by the ISO.

This structure is formulated as a bilevel structure, which can be seen in Fig. 7.3. In the upper level problem, new prices are updated based on GA; then prices are transferred to the lower level problem, where MGs operation problem are solved. The sold energy and bought energy are then transferred to the LSE, which runs the operation problem, and new prices are updated again. This process is repeated until the stopping criteria are satisfied.

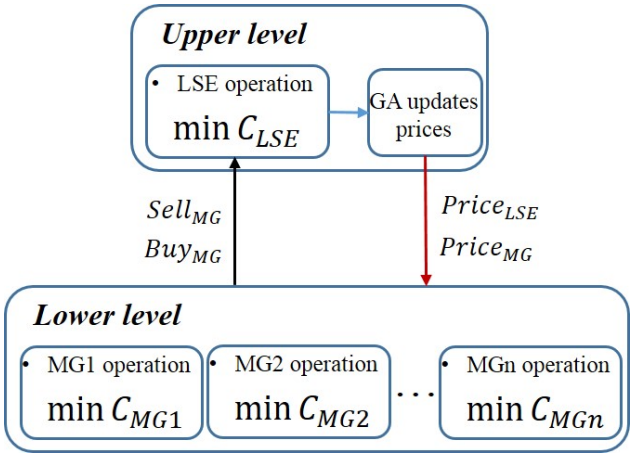

Figure 7.3: The bilevel problem structure.

7.1.1/ OPERATION OF THE LOAD SERVICE ENTITY

For the LSE, three components are included: PV panels, a battery storage system and a hydrogen storage system (Fig. 7.1). The goal is to maximize the profits, which includes the operation cost of storage systems, and the purchasing cost from the utility grid, the purchasing cost from MGs, and the selling profits to MGs. The objective function can be represented as:

$$
\begin{aligned}
&min\, C_{LSE} = \\
&min \sum_{t=1}^{T} \{B_{cost}^{ch,dis}(t) + H_{cost}^{ele}(t) + H_{cost}^{fc}(t) \\
&+ Price_{ug}(t) \cdot ug(t) + \sum_{MG_i=1}^{N} Price_{MG_i}(t) \cdot Buy_{MG_i}(t) \\
&- Price_{LSE}(t) \cdot \sum_{MG_i=1}^{N} Z_{Sell_{MG_i}}(t) \\
&+ \alpha \cdot (LS_{ex}(t)) + \beta \cdot (cut_{PV}(t))\}
\end{aligned}
\tag{7.1}
$$

where the $Price_{LSE}(t)$ is the selling price of LSE, $Price_{MG_i}(t)$ is the selling price of the i^{th} MG. $ug(t)$ is the purchased energy from the utility grid, $Buy_{MG_i}(t)$ is the bought energy from the i^{th} MG. $Z_{Sell_{MG_i}}(t)$ is the sold energy to the i^{th} MG. $LS_{ex}(t)$ is the demands that cannot be supplied by the LSE. $cut_{PV}(t)$ is the curtailed power of PV in the LSE.

For the battery storage system, the utilization cost of charge and discharge can be described as follows [142]:

$$
B_{cost}^{ch,dis}(t) = \frac{C_{ba}^{inv}}{2 \cdot N_{cycles}} \cdot (P_{ch}(t) + P_{dis}(t)) \tag{7.2}
$$

where C_{ba}^{inv} is the investment cost of the battery, and N_{cycles} is the number of cycles over the lifetime.

We use the state-of-charge (SOC) to represent the state of the battery as follows:

$$
\begin{aligned}
SOC(t) =& SOC(t - \Delta t) \\
&+ \frac{\eta_{ch} \cdot P_{ch}(t) \cdot \Delta t}{CB} - \frac{\eta_{dis} \cdot P_{dis}(t) \cdot \Delta t}{CB}
\end{aligned}
\tag{7.3}
$$

where η_{ch} is the charging efficiency, η_{dis} is the discharging efficiency, $P_{ch}(t)$ is the charging power, $P_{dis}(t)$ is the discharging power, Δt is the interval time, and CB is the capacity of the battery.

The hydrogen storage system includes an electrolyzer, a fuel cell and hydrogen tanks. As for the battery storage system, its utilization cost can be computed as follows [142]:

$$
H_{cost}^{ele}(t) = \left(\frac{C_{ele}^{inv}}{N_{hours}^{ele}} + C_{ele}^{o\&m} \right) \cdot \delta_{ele}(t) + C_{ele}^{startup} \cdot \Delta\delta_{ele}(t) \tag{7.4}
$$

$$
H_{cost}^{fc}(t) = \left(\frac{C_{fc}^{inv}}{N_{hours}^{fc}} + C_{fc}^{o\&m} \right) \cdot \delta_{fc}(t) + C_{fc}^{startup} \cdot \Delta\delta_{fc}(t) \tag{7.5}
$$

where $C_{ele}^{inv}, C_{fc}^{inv}$ are the investment costs of the electrolyzer and the fuel cell, $C_{ele}^{o\&m}$ and $C_{fc}^{o\&m}$ the operation and maintenance costs, and $C_{ele}^{startup}$ and $C_{fc}^{startup}$ the startup costs. Variables $\delta_{ele}(t)$ and $\delta_{fc}(t)$ are the state of the electrolyzer and the fuel cell. When a unit is on, $\delta_i(t) = 1, i = \{ele, fc\}$, otherwise it is set to 0. Equation $\Delta\delta_i(t) = max\{\delta_i(t) - \delta_i(t-1), 0\}, i = \{ele, fc\}$ represents whether the unit started or not.

A hydrogen tank is used to store the hydrogen produced by the electrolyzer, as well as to supply hydrogen to the fuel cell. We use the level of hydrogen (LOH) to represent the state of the hydrogen tank:

$$LOH(t) = LOH(t - \Delta t) + \dot{n}_{H2}^{pro} \cdot \Delta t - \dot{n}_{H2}^{con} \cdot \Delta t \tag{7.6}$$

where $\dot{n}_{H2}^{pro}$ is the hydrogen produced by electrolyzer. $\dot{n}_{H2}^{con}$ is the hydrogen consumed by fuel cell. They can be calculated based on the method described in [142].

The electricity power balance equation is:

$$\begin{aligned} & ug(t) + \sum_{MG_i=1}^{N} Buy_{MG_i}(t) + PV(t) - cut_{PV}(t) \\ & - \left(\sum_{MG_i=1}^{N} Z_{Sell_{MG_i}}(t) - LS_{ex}(t) \right) \\ & = Z_{ele}(t) - Z_{fc}(t) + Z_{bach}(t) - Z_{badis}(t) \end{aligned} \tag{7.7}$$

$$0 \leq Buy_{MG_i}(t) \leq Z_{Buy_{MG_i}}(t) \tag{7.8}$$

where $Z_{Buy_{MG_i}}(t)$ is the maximum selling energy of the i^{th} MG at time t, which is obtained from the results of problem (7.9). This means that at time t, an MG can sell $Z_{Buy_{MG_i}}(t)$ amounts of energy, but for the LSE, how much it wants to buy is a variable, namely $Buy_{MG_i}(t)$.

At last, we need to decide the prices of $Price_{LSE}(t)$ and $Price_{MG_i}(t), i = 1, ..., N$.

7.1.2/ OPERATION OF MICROGRID

For each MG, the goal is to minimize the operation costs, which include the operation costs of its own components, the purchasing cost from the LSE, and the selling profits to the LSE. The objective function can be formulated as:

$$\begin{aligned} & min\, C_{MG_i} = \\ & min \sum_{t=1}^{T} \{ B_{cost}^{ch,dis}(t) + H_{cost}^{ele}(t) + H_{cost}^{fc}(t) + a_1 \cdot HB_{cost}(t) + \\ & a_2 \cdot AC_{cost}(t) + AHC_{cost}(t) + HS_{cost}(t) \\ & + \omega \cdot (Z_{DR_{out}}(t) + Z_{DR_{in}}(t)) \\ & + Price_{LSE}(t) \cdot Z_{Sell_{MG_i}}(t) - Price_{MG_i}(t) \cdot Z_{Buy_{MG_i}}(t) \\ & + \alpha \cdot (LS_{cooling}(t) + LS_{heat}(t) + LS_{power}(t)) \\ & + \beta \cdot (cut_{PV}(t) + cut_{solar}(t)) \} \end{aligned} \tag{7.9}$$

where $HB_{cost}(t), AC_{cost}(t), AHC_{cost}(t), HS_{cost}(t)$ are the utilization cost of the heat boiler, the air conditioner, the absorption heat chiller, and heat storage. $Z_{DR_{out}}(t), Z_{DR_{in}}(t)$ are the shift out power and shift in power, and ω is the DR cost. $LS_j(t), j = \{cooling, heat, power\}$ are the load shedding of cooling, heating and electricity. $cut_{PV}(t), cut_{solar}(t)$ are the curtailed

power of PV and thermal solar. α, β are the penalty values of load shedding and curtailed power.

A heat boiler uses electricity to produce heat, as follows:

$$Q_{hb} = \eta_{hb} \cdot P_{hb} \tag{7.10}$$

where P_{hb} is the input power, η_{hb} the efficiency, and Q_{hb} the output heat.

An air conditioner is used to cool air [128]:

$$C_{ac} = \eta_{ac} \cdot P_{ac} \tag{7.11}$$

where P_{ac} is the input power, η_{ac} the efficiency, and C_{ac} the cooling output cooling power.

Similarly, the absorption heat chiller uses heat to produce cooling, so the relation is [128]:

$$C_{ahc} = \eta_{ahc} \cdot Q_{ahc} \tag{7.12}$$

where Q_{ahc} is the input heat, η_{ahc} the efficiency, and C_{ahc} the output cooling power.

The state of the heat storage system is represented by the amount of heat stored [63]:

$$HS(t) = HS(t - \Delta t) + \eta_{hs}^{ch} \cdot Q_{hs}^{ch}(t) \cdot \Delta t - \frac{Q_{hs}^{dis}(t)}{\eta_{hs}^{dis}} \cdot \Delta t \tag{7.13}$$

where $HS(t)$ is the stored heat at time Δt. $Q_{hs}^{ch}(t)$ and $Q_{hs}^{dis}(t)$ are the charge and discharge heating power at time t. η_{hs}^{ch} and η_{hs}^{dis} are the charge and discharge efficiency, respectively.

The heat boiler, air conditioner and absoption heat chiller operation costs are given by [141]:

$$HB_{cost}(t) = \frac{C_{hb}^{inv}}{N_{life}^{hb}} \cdot P_{hb}(t) \tag{7.14}$$

$$AC_{cost}(t) = \frac{C_{ac}^{inv}}{N_{life}^{ac}} \cdot P_{ac}(t) \tag{7.15}$$

$$AHC_{cost}(t) = \frac{C_{ahc}^{inv}}{N_{life}^{ahc}} \cdot P_{ahc}(t) \tag{7.16}$$

For the heat storage system, the operation cost is:

$$HS_{cost}(t) = \frac{C_{hs}^{inv}}{N_{life}^{hs}} \cdot (Q_{hs}^{ch}(t) + Q_{hs}^{dis}(t)) \tag{7.17}$$

The demand response model can be written as:

$$\begin{aligned} &0 \leq Z_{DR_{out}}(t) = \delta_{DR_{out}}(t) \cdot P_{DR_{out}}(t) \leq \delta_{DR_{out}}(t) \cdot P_{load}^{max}(t) \\ &0 \leq Z_{DR_{in}}(t) = \delta_{DR_{in}}(t) \cdot P_{DR_{in}}(t) \leq \delta_{DR_{in}}(t) \cdot P_{in}^{max}(t) \\ &\delta_{DR_{out}}(t) + \delta_{DR_{in}}(t) \leq 1 \end{aligned} \tag{7.18}$$

Shift-out power in each time step $P_{DR_{out}}(t)$ is limited to $P_{load}^{max}(t)$; and shift-in power $P_{DR_{in}}(t)$ is limited to $P_{in}^{max}(t)$. $\delta_{DR_{out}}(t)$ and $\delta_{DR_{in}}(t)$ are binary variables that represent whether shift-out power/shift-in power in this step is allowed or not.

The electricity selling and buying in MG can be written as:

$$\begin{aligned} &0 \leq Z_{Sell_{MG_i}}(t) \leq \delta_{Sell_{MG_i}}(t) \cdot Sell^{max}(t) \\ &0 \leq Z_{Buy_{MG_i}}(t) \leq \delta_{Buy_{MG_i}}(t) \cdot Buy^{max}(t) \\ &\delta_{Sell_{MG_i}}(t) + \delta_{Buy_{MG_i}}(t) \leq 1 \end{aligned} \tag{7.19}$$

where $Z_{Sell_{MG_i}}(t) = \delta_{Sell_{MG_i}}(t) \cdot Sell_{MG_i}(t)$, $Z_{Buy_{MG_i}}(t) = \delta_{Buy_{MG_i}}(t) \cdot Buy_{MG_i}(t)$. $\delta_{Sell_{MG_i}}(t), \delta_{Buy_{MG_i}}(t)$ are binary variables that represent the state of buying energy and selling energy.

The electricity power balance in an MG can be described as:

$$\begin{aligned} &Z_{Sell_{MG_i}}(t) - Z_{Buy_{MG_i}}(t) + PV(t) - cut_{PV}(t) \\ &- (L_{power}(t) - Z_{DR_{out}}(t) + Z_{DR_{in}}(t)) \\ &= Z_{ele}(t) - Z_{fc}(t) + Z_{bach}(t) - Z_{badis}(t) \\ &+ Z_{ac}(t) + Z_{hb}(t) \end{aligned} \tag{7.20}$$

The shift-out power should be equal to the shift-in power:

$$\sum_{t=1}^{T} Z_{DR_{out}}(t) = \sum_{t=1}^{T} Z_{DR_{in}}(t) \tag{7.21}$$

Similarly, for the heat and cooling balance equations:

$$\begin{aligned} &Q_{sh}(t) - cut_{solar}(t) - (L_{heat}(t) - LS_{heat}(t)) + Q_{fc}(t) \\ &+ Q_{hb}(t) = Q_{hsch}(t) - Q_{hsdis}(t) + Q_{ahc}(t) \end{aligned} \tag{7.22}$$

$$C_{ac}(t) + C_{ahc}(t) = L_{cooling}(t) - LS_{cooling}(t) \tag{7.23}$$

Finally, for the SOC, LOH and HS constraints:

$$\begin{aligned} &SOC_{min} \leq SOC(t) \leq SOC_{max} \\ &LOH_{min} \leq LOH(t) \leq LOH_{max} \\ &HS_{min} \leq HS(t) \leq HS_{max} \end{aligned} \tag{7.24}$$

7.1.3/ CONFLICTING GOALS OF LOAD SERVICE ENTITY AND MICROGRIDS

Based on the above, the objective functions of LSE and MGs are all to minimize the operation cost. But from problem (7.1) and problem (7.9), we can see that the decision variables $Price_{LSE}(t)$ and $Price_{MG_i}(t), i = 1, ..., N$ are conflicting variables from the LSE's view and MGs' view. This means that the LSE prefers a higher LSE selling price $Price_{LSE}(t)$ and a lower MGs selling price $Price_{MG_i}(t), i = 1, ..., N$. But MGs prefer a lower LSE selling price $Price_{LSE}(t)$ and a higher MGs selling price $Price_{MG_i}(t), i = 1, ..., N$.

Here, a simulation example is adopted to describe the relationship between price ($Price_{LSE}(t)$, $Price_{MG_i}(t), i = 1, ..., N$) and operation cost. The results can be seen in Fig.

Figure 7.4: Relationship between price ($Price_{LSE}(t)$, $Price_{MG_i}(t), i = 1, ..., N$) and operation cost.

7.4. We can see that, as the price increases, the operation cost of MGs increases, but the operation cost of the LSE is decreasing.

This conflict phenomenon is presented in Fig. 7.5. When the LSE selling price $Price_{LSE}(t)$ is set at $Price1$, the operation cost of the LSE is large, but the operation cost of MGs are small, then the LSE is not satisfied; When the LSE selling price $Price_{LSE}(t)$ is set at $Price2$, the operation cost of the LSE is small, but the operation cost of MGs is large, then MG is not satisfied.

How to deal with this conflict goals of the LSE and MGs? Here, we choose the total cost as the index to make both the LSE and MGs satisfied, namely, when the total cost of the whole system is minimal, both the LSE and MGs are satisfied, and an optimal price $Price^*$ is decided. The total cost of LSE and MGs is a convex function, so an optimal point $Price^*$ is exist.

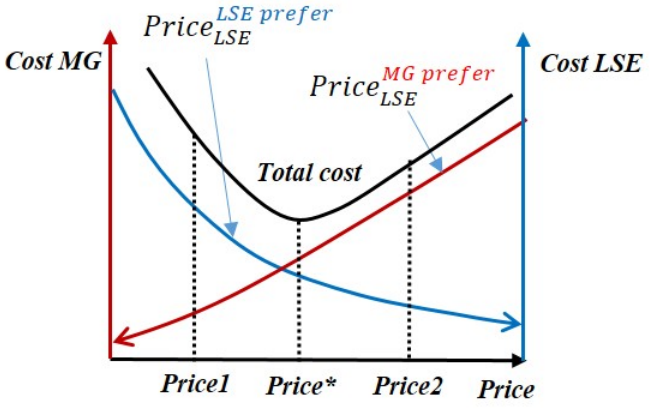

Figure 7.5: Conflict price of $Price_{LSE}(t)$ in LSE and MGs.

7.1.4/ GA SEARCH FOR THE PRICE

The prices $Price_{LSE}(t)$ and $Price_{MG_i}(t), i = 1, ..., N$ are the elements to link the LSE and MGs together. $Price_{LSE}(t)$ is a variable in the LSE optimization problem, but is treated as parameters in MGs optimization problem. $Price_{MG_i}(t), i = 1, ..., N$ are variables in MGs

optimization problem, but are treated as parameters in LSE optimization problem.

It is difficult to solve this bilevel problem. Here we adopt GA to search for the price, namely, $Price_{LSE}(t)$ and $Price_{MG_i}(t), i = 1, ..., N$ are updated by the GA method. This means that in each step optimization of LSE and MGs, variables of $Price_{LSE}(t)$ and $Price_{MG_i}(t), i = 1, ..., N$ are transferred to the decided parameters. The solving method flow chart can be seen in Fig. 7.6.

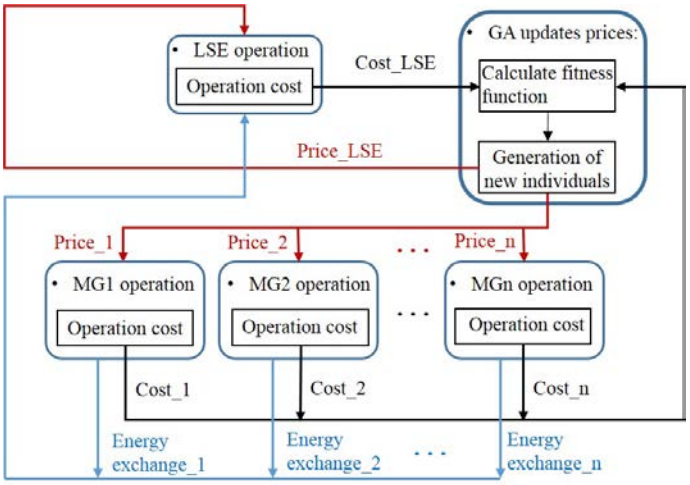

Figure 7.6: Flow chart of the price decision problem.

In each step, firstly, GA gives the values of $Price_{LSE}(t)$ and $Price_{MG_i}(t), i = 1, ..., N$. These price values are sent to each MG, then each MG runs its own optimization problem (7.9). Based on the optimization results of each MG, the total bought energy from the LSE $T_{buy}(t) = \sum_{MG_i=1}^{N} Sell_{MG_i}(t)$ and the total sold energy to the LSE $T_{sell}(t) = \sum_{MG_i=1}^{N} Buy_{MG_i}(t)$ are calculated. After that, the LSE runs its own optimization problem (7.1). Then the objective function results of the LSE and MGs are transferred to the ISO. The ISO updates the new prices of $Price_{LSE}(t)$ and $Price_{MG_i}(t), i = 1, ..., N$ based on fitness function (7.25). This process is repeated until the stopping criterion is satisfied. In our simulation, the stopping criterion is the maximum number of iterations of GA.

The fitness function of the GA is the total cost of LSE and MGs:

$$F = C_{LSE} + \sum_{i=1}^{N} C_{MG_i} \tag{7.25}$$

Then whole problem can be written as:

$$\begin{aligned} \min_{\textbf{Price}} \left\{ \left\{ \sum_{i=1}^{N} \left\{ \min_{price^*, \textbf{exch}} C_{MG_i} \right\} + \min_{price^*, \sum_{i=1}^{N} exch_i^*} C_{LSE} \right\} \right\} \\ s.t.\ (7.2), (7.3), (7.4), (7.5), (7.6), (7.7), (7.8), (7.13), (7.18), (7.19), \\ (7.20), (7.21), (7.23), (7.22), (7.24) \end{aligned} \tag{7.26}$$

$price^* \in$ **Price** is the best price for each MG and LSE. $exch^* \in$ **exch** is the exchanged energy between MG and LSE.

The whole simulation process can be summarized as:

Algorithm 1 Simulation process

initialize set $Price_{LSE}$, $Price_{MG_i}, i = 1, ..., N$;
for $k = 1 : k_{max}$ **do**
each MG solves problem (7.9);
The LSE calculates T_{buy} and T_{sell};
The LSE solves problem (7.1);
The ISO calculates the fitness function (7.25);
The ISO updates price $Price_{LSE}$, $Price_{MG_i}, i = 1, ..., N$ based on GA;
k=k+1;
end for

7.1.5/ EQUILIBRIUM OF THE ABOVE METHOD

The above section presents the solving method. The mathematic flow chart of the method can be seen in Fig. 7.7. This is a closed loop method, but the question is whether this method can reach an equilibrium or not? Namely, whether this method can converge to find the optimal price.

Assume a random price $\widetilde{p}$, which is not the optimal price. Based on this price, the operation cost of MGs can be calculated as $\widetilde{C_{MGi}} = min\, g(\widetilde{p})$, and the exchanged energy is $\widetilde{Q} = arg\, min\, g(\widetilde{p})$. Then, the total exchanged energy is transferred to the LSE, and the operation cost of LSE is calculated as $\widetilde{C_{LSE}} = min\, f(\widetilde{p}, \sum \widetilde{Q}) = min\, f(\widetilde{p}, \sum arg\, min\, g(\widetilde{p}))$. After that, the operation cost of the LSE and total operation cost of MGs are transferred to GA. The fitness value is then calculated as $\widetilde{fitness} = Fitness(\widetilde{C_{LSE}}, \sum \widetilde{C_{MGi}}) = Fitness(min\, f(\widetilde{p}, \sum arg\, min\, g(\widetilde{p})), \sum min\, g(\widetilde{p}))$. Based on the characteristics of GA, because the fitness value $\widetilde{fitness}$ is not the minimum, then a new price $p^{new} = F(\widetilde{fitness})$ is updated, $F(.)$ represents the selection, crossover, and mutation in GA. This means that if price $\widetilde{p}$ is not the optimal price p^*, a new price will be updated until optimal price is reached.

This method is convergent to find the optimal price, when the operation function of MG $min\, g(p)$, the function of LSE $min\, f(p, Q)$ is solvable.

7.1.6/ COMPARISON WITH THE COURNOT MODEL

In this subsection, we compare the combined GA and MILP method with a method based on the Cournot model. In the Cournot model, each player competes on output quantity, and there is a relationship between price p and output quantity Q: $p = P(Q)$. In our model, each MG and LSE also compete on the ouput quantity (exchanged energy). Thus, we developed a price decision method based on Cournot model. The flow chart can be seen in Fig. 7.8.

We assume that the price-quantity relationship $P(p, Q)$ is a linear function: $P: \ p = a - b * Q$. This method can be summarized as follows:

1. Initialize the prices of $Price_{LSE}$ and $Price_{MG}$, iteration number $k = 0$;

2. Each MG calculates optimization (7.9), calculates the operation cost C_{MG_i} and obtains the bought energy from the LSE $Sell_{MG_i}(t)$;

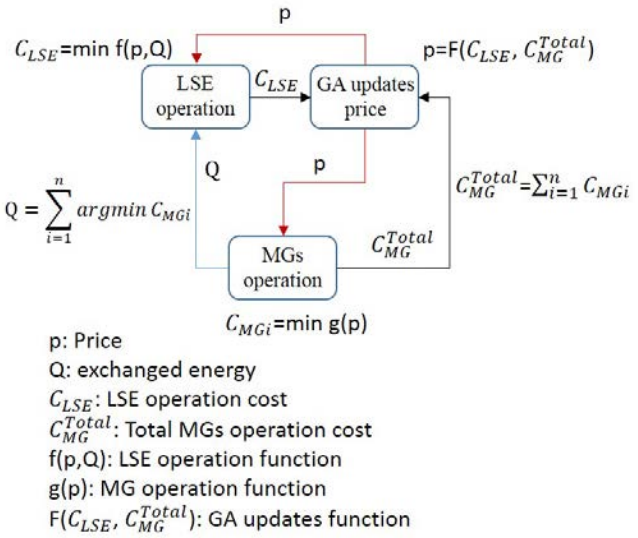

Figure 7.7: Flow chart of the price decision mathematic solving method.

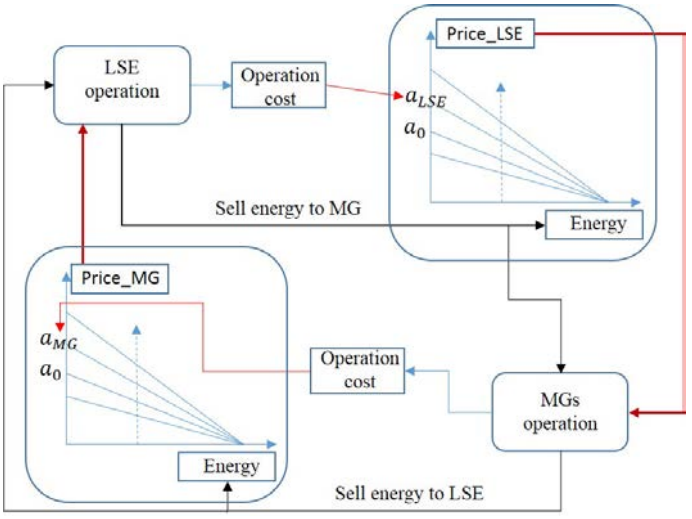

Figure 7.8: Flow chart of the price decision method based on Cournot model.

3. The LSE solves problem (7.1), calculates the operation cost C_{LSE}, and the bought energy from MG $Buy_{MG_i}(t)$;
4. Each MG updates the price-quantity function based on operation cost C_{MG_i}, namely, $a_{MG_i}(k+1) = a_{MG_i}(k)+\gamma\times\frac{C_{MG_i}(k+1)-C_{MG_i}(k)}{C_{MG_i}(k+1)}$, and then calculates new price $Price_{MG_i}(k+1)$;
5. LSE updates the price-quantity function based on operation cost C_{LSE}, namely, $a_{LSE}(k+1) = a_{LSE}(k) + \gamma \times \frac{C_{LSE}(k+1)-C_{LSE}(k)}{C_{LSE}(k+1)}$, and then calculates the new price $Price_{LSE}(k+1)$;
6. $k = k + 1$;
7. Repeat 2)-6), until the maximum iteration number k_{max};

where γ is a coefficient to adjust the value a.

The resulting simulation results are presented in Section 7.2.

7.2/ SIMULATION RESULTS

7.2.1/ SYSTEM SETUP

In our model Case I, there are four MES microgrids, the electricity/heating/cooling demands in one typical day are shown in Fig. 7.9. The penalty values are arbitrarily chosen as $\alpha = \beta = \gamma = 10^{10}$. The capacity of each component in each microgrid is shown in Table 7.1, and is the same for the four MGs. Two different PV panel numbers are adopted to compare the influence of renewable energy penetration on the price: $PV_1 = 50, PV_2 = 100$, the rated power of one PV panel is $0.17kW$ under standard test conditions (STC). This means that the output power of PV can be calculated as $PV \cdot 0.17 \cdot Solar$. $Solar$ is the global solar radiation received by the panels in kW/m^2. The capacity of each component in the LSE is: $PV = 500, P_{fc}^{max} = P_{ele}^{max} = 100kW, Hy = 1000N.m^3, C_{ba} = 100kWh$. The minimum and maximum prices are 0.1 €/kWh and 0.5 €/kWh.

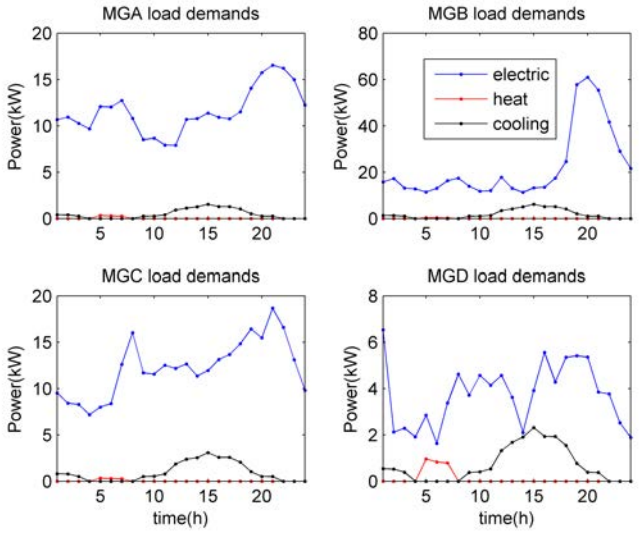

Figure 7.9: Load demand in the four microgrids.

Table 7.1: Capacity of each component in each microgrid

Component	Capacity	Component	Capacity
Fuel cell	10kW	Heat boiler	10kW
Electrolyzer	10kW	Air conditioner	10kW
H_2 tanks	100 $N.m^3$	AHC	10kW
Battery	10 kWh	Heat storage	80 kWh
PV-heat	10	–	–

7.2.2/ SIMULATION RESULTS

For comparisons, we deploy four cases, which is shown in Table 7.2.

- case1a: with TOU (time of use) price, we do not consider the LSE, all MGs connect to the utility grid directly, the PV panels number in each MG is $PV_1 = 50$;
- case1b: we deploy the new searched price in the UG-LSE-MGs system, the PV panels number in each MG is $PV_1 = 50$;
- case2a: TOU price, the PV panels number in each MG is $PV_2 = 100$;
- case2b: we deploy the new searched price, the PV panels number in each MG is $PV_2 = 100$.

Table 7.2: Four different cases.

Case	PV number	price
case1a	$PV_1 = 50$	TOU
case1b	$PV_1 = 50$	new price
case2a	$PV_2 = 100$	TOU
case2b	$PV_2 = 100$	new price

Figs. 7.10, 7.11, 7.12, 7.13, 7.14, 7.15 show the simulation results for case 1b. Fig. 7.10 shows the scheduling results in MGA after deploying the new searched price. The second figure in Fig. 7.10 shows that at each time, MGA either sells energy to the LSE or buys energy from the LSE. Here 'Max sell' is the maximum energy that MGA can sell at each time step. How much the LSE will buy is decided by its operation problem, but can not exceed 'Max sell'. Hydrogen storage system and battery storage system are used to supply the demands inside MGA, also to sell energy outside to LSE. Heat storage system is used to balance the power between heating demands and the thermal solar.

Fig. 7.14 shows the energy exchanged by the LSE. We can see that the LSE operates well in an 'energy exchange pool' role. At time 19:00, MGA, MGC and MGD sell their energy to the LSE (the $1^{st}, 3^{rd}, 4^{th}$ figures in Fig. 7.15), then the LSE imports the other energy from the utility grid (the third figure in Fig. 7.14), and with its local storage systems (the fourth and fifth figure in Fig. 7.14), sells energy to MGB (the 2^{nd} figure in Fig. 7.15). The third figure shows the exchanged energy with the utility grid. The fourth and fifth figures show the energy change in hydrogen tanks and the battery system.

Fig. 7.15 shows the exchanged energy in different MGs. In each time step, each MG either buys energy form the LSE or sells energy to the LSE, or does nothing with the LSE. The 'Max sell' is the maximum energy that can be sold to the LSE in the MG, which is decided by the operation problem of each MG, and is treated as a constraint in the LSE operation problem. The 'Actual sell' is the actual selling energy from an MG to the LSE (cannot exceed the 'Max sell'), which is decided by the operation of LSE (combined with the 'Max sell' constraint).

Table 7.3 shows the objective function results in different cases. Comparing case1a and case1b, we can see that after deploying the new searched price, the operation cost (objective function) of each MG is reduced, which means that the new prices give a better

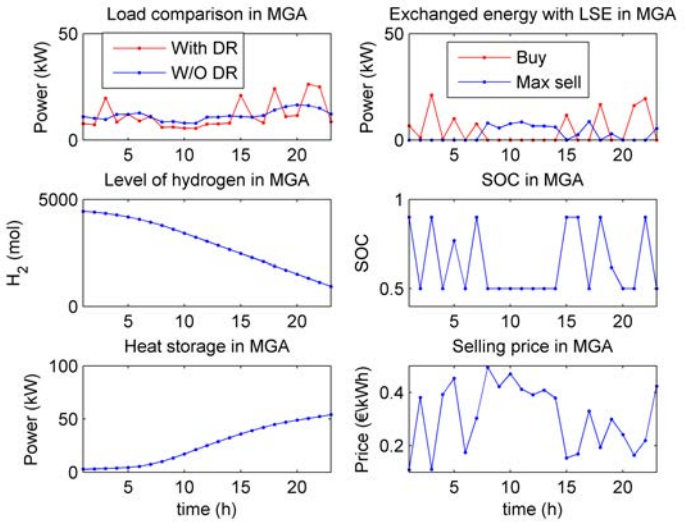

Figure 7.10: Microgrid MGA.

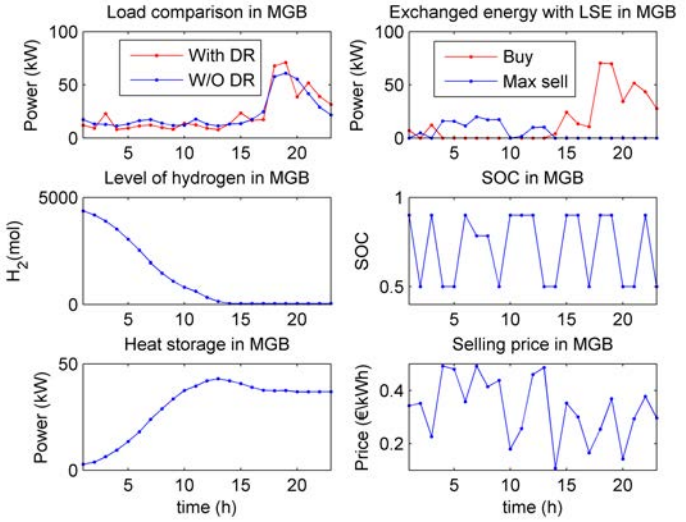

Figure 7.11: Microgrid MGB.

Table 7.3: Objective function results in different cases.

Case	Total cost	MGA	MGB	MGC	MGD
case1a	1.3534e+4	2.5376e+3	1.7478e+4	4.1445e+3	-1.0626e+4
case1b	-2.8603e+4	-4.1863e+3	8.5447e+3	-1.1293e+3	-3.1832e+4
case C	-1.9142e+4	-1.0981e+4	1.3052e+4	3.9076e+3	-2.9410e+4
case2a	2.1244e+3	-3.1483e+2	1.4626e+4	1.2921e+3	-1.3479e+4
case2b	-5.2736e+4	-1.0079e+4	3.1080e+3	-7.6013e+3	-3.8164e+4

guidance for consumers to arrange their demands. The negative values mean that an MG can earn profits. Comparing case1b and case2b, we can see that with higher penetration of renewable energy, the operation cost (objective function) of each MG is reduced more.

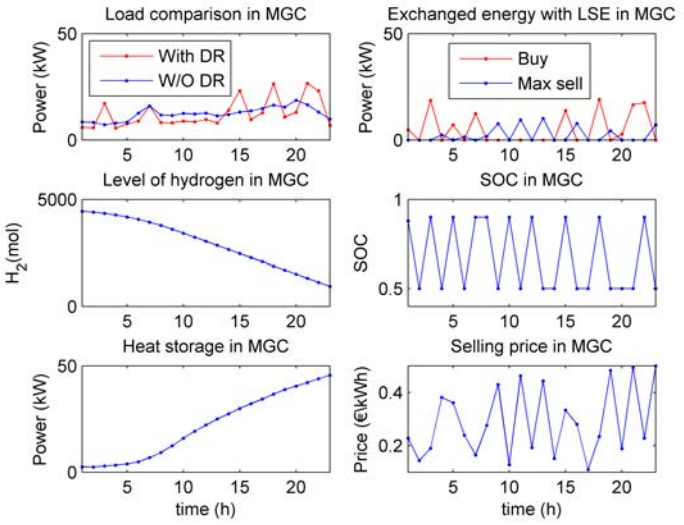

Figure 7.12: Microgrid MGC.

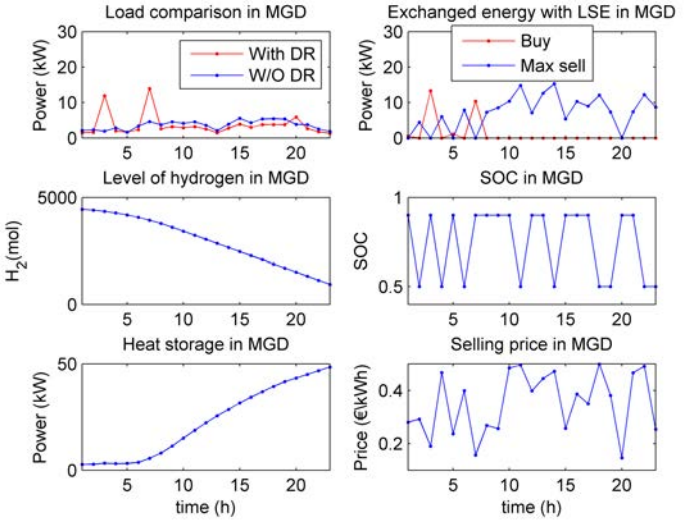

Figure 7.13: Microgrid MGD.

This is because with a higher penetration of renewable energy, on the one hand, an MG can reduce the bought energy from the LSE, and on the other hand, an MG can also sell more energy to the LSE, leading to a smaller operation cost.

Table 7.4: Cost of actual exchanged energy in different cases.

Case	Total cost	MGA	MGB	MGC	MGD	LSE
case1b	70.6965	15.9647	55.7625	15.0009	-16.0315	-57.1048
case2b	67.3723	10.8264	57.0426	11.5537	-12.0505	-36.6018

Table 7.4 shows the cost of actual exchanged energy in case1b and case2b. For MGs, it includes the buying cost from the LSE and the selling profits to the LSE. For the LSE, it includes the buying cost from UG, the buying cost from MGs, and the selling profits to

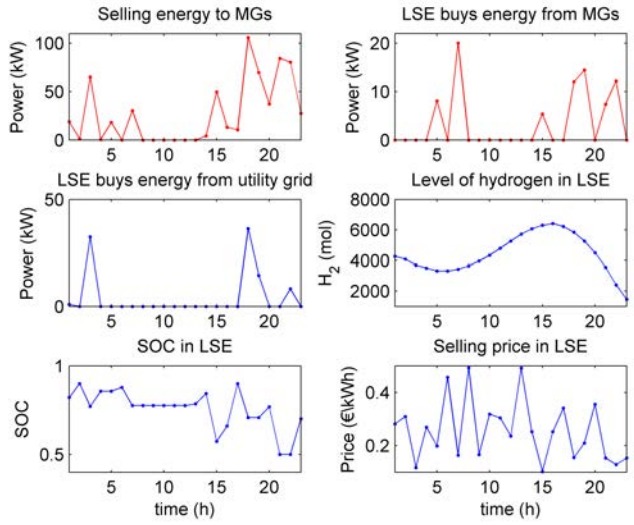

Figure 7.14: Load service entity LSE.

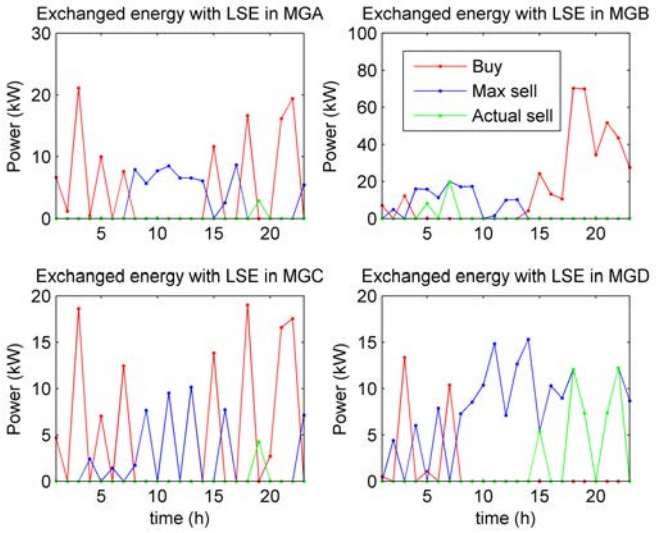

Figure 7.15: Comparision of four microgrids.

MGs. We can see that in both cases, MGD and the LSE earn profits. But in case2b, due to the higher penetration of renewable energy, the bought energy from the LSE will decrease, which leads to the smaller cost of actual exchanged energy in each MG, and also to smaller earned profits by the LSE.

7.2.3/ SIMULATION RESULTS BASED ON THE COURNOT MODEL

Based on the method described in Section 7.1.6, with $\gamma = 0.05, k_{max} = 50$. The simulation results can be seen in Fig. 7.16. The operation costs are shown in Table 7.3, namely, case C. We can see that the searching price based on the Cournot model (case C) is better than the TOU price (case 1a), but worse than that based on GA (case 1b), from the view of the total cost of the whole system. This is because in the GA method, the

operation cost of LSE and MGs are considered at the same time, but in the Cournot method, the LSE and MGs update the prices independently.

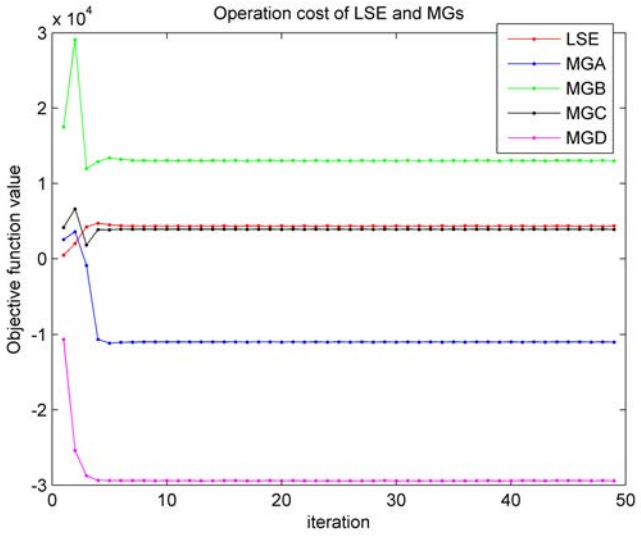

Figure 7.16: Simulation results based on the Cournot model.

The comparison between the GA method and the Cournot method are summarized in Tab. 7.5. For the GA method, in each iteration, it needs to calculate all generations. But for the Cournot method, in each iteration, it just needs to calculate one generation. Thus, the simulation time of the GA method is larger than the Cournot method. An index is defined to estimate the performance of different methods, namely, $Index = \frac{C^{model}_{totalcost} - C^{TOU}_{totalcost}}{C^{TOU}_{totalcost}}$. The $Index$ is smaller, and the total cost is smaller than that with the TOU price. This means that the new searching prices are better than the TOU price. Thus, the performance of the method is better.

Table 7.5: Comparison between the GA method and the Cournot method.

Model	One iteration simulation time	Solving method	$Index$
GA + real model	54.092573 s	branch and bound	-286.35%
Cournot + real model	5.501051 s	branch and bound	-236.89%

7.3/ SIMULATION RESULTS FOR CASE II

In this section, we present a benchmark case. The IEEE 30-node network is taken as the utility grid, and four LSEs are connected directly into the utility grid. In each LSE, four MGs are connected. For this network, there are 16 MGs, and 4 LSEs, each MG/LSE can buy/sell energy to LSE/MG, LSE can also buy energy from the utility grid. Then the problem is how to decide the price for MGs and LSEs. The variables include $price_{aggj}, price_{MGij}, i = \{A, B, C, D\}, j = \{1, 2, 3, 4\}$.

The structure of the IEEE 30-node network can be seen in Fig. 7.17. The whole structure

of this network can be seen in Fig. 7.18. The price range is set between 0.1 €/kWh and 0.2 €/kWh. Two cases are compared, as shown in Tab. 7.6:

Table 7.6: Four different cases.

Case	PV number	price
case3a	$PV_1 = 50$	TOU
case3b	$PV_1 = 50$	new price
case4a	$PV_2 = 100$	TOU
case4b	$PV_2 = 100$	new price

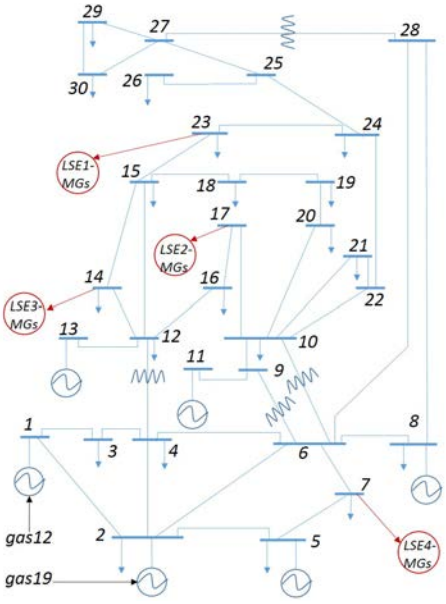

Figure 7.17: IEEE 30 nodes network.

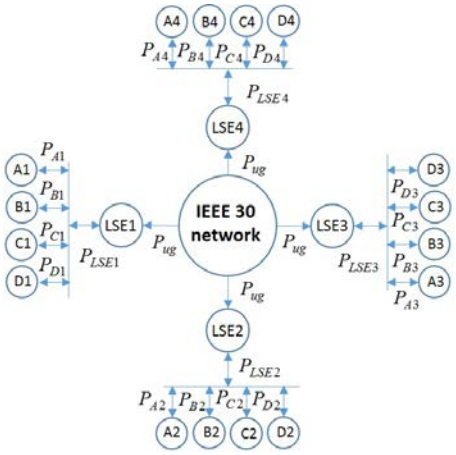

Figure 7.18: IEEE 30 nodes network connecting with LSEs and MGs.

The simulation results are shown in the following. Fig. 7.19 shows the operation of load service entity LSE1. Fig. 7.20 shows the comparison of four MGs in LSE1. Comparing Figs. 7.19 and 7.20, it can be seen that LSE1 plays the role of “energy exchange pool”. At

time 19:00, MGA1 and MGD1 sell enegy to LSE1, then combine with LSE1's local storage system, selling enegy to the other MGs (MGB1 and MGC1 buy energy from LSE1).

Figs. 7.21, 7.22, and 7.23 show the operation of LSE2, LSE3 and LSE4. It can also be seen that the LSEs play the role of the "energy exchange pool" well. It can buy energy from the "surplus" MGs, and sell energy to the "shortage" MGs. This control is achieved by the real-time guidance price. Fig. 7.24 shows the voltage in utility grid, where we can see that the voltage is in the normal range. Fig. 7.25 shows the change of the voltage of nodes at different times.

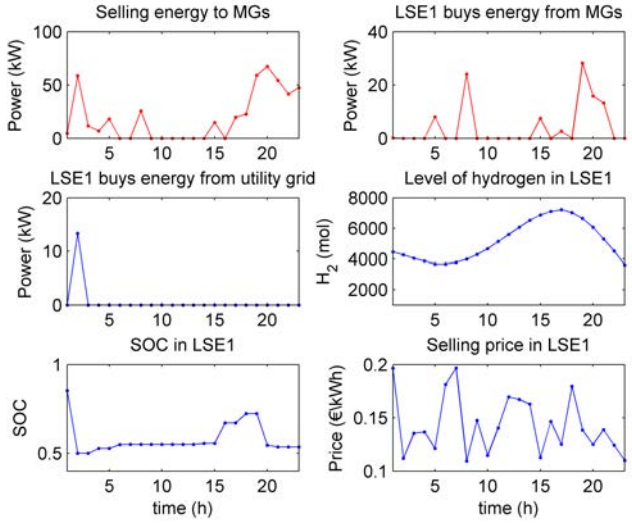

Figure 7.19: Load service entity LSE1

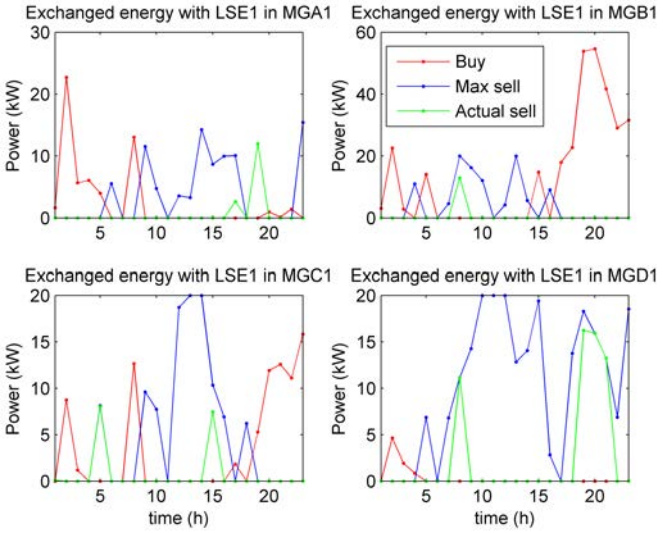

Figure 7.20: Comparision of four microgrids in load service entity LSE1.

Tab. 7.7 shows the detailed objective function results in each MG and LSE. Tab. 7.8 shows the total objective function and the cost of the utility grid in each case. It can be seen that after deploying the new real-time price, the total cost of the whole system is reduced, which means that the new price gives a better guidance for the users to

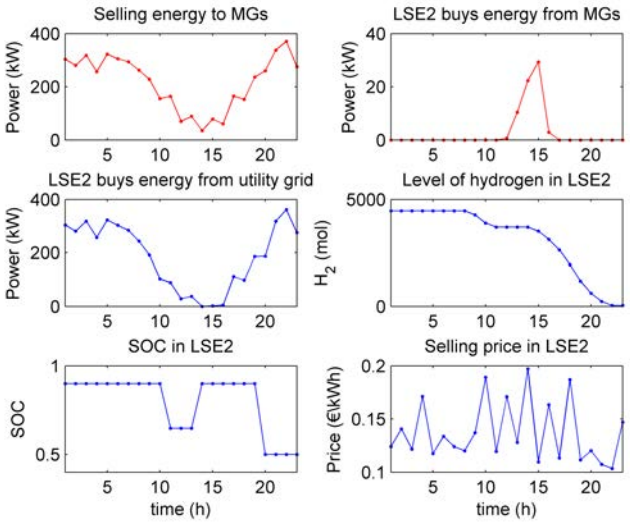

Figure 7.21: Load service entity LSE2

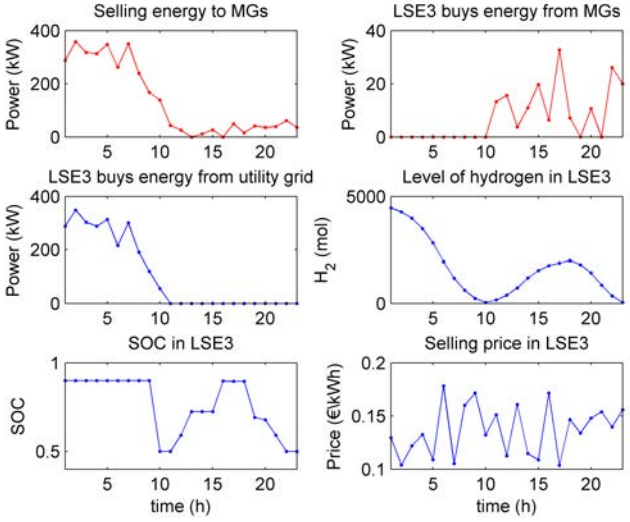

Figure 7.22: Load service entity LSE3

rearrange their load demand profiles. On the other hand, it can also be seen that not all MGs reduce their operation cost. For example, case3a and case3b for MGB3. This is because the fitness function in GA is the sum of all objective functions (see equation (7.25)), we can not guarantee to reduce each objective function, but only the sum of all objective functions can be guaranteed to be reduced. Fig. 7.26 shows the comparison of the objective function results in case II. It can be seen that the tendency of the operation cost in the four cases is: $case3a \geq case3b \geq case4a \geq case4b$. Tab. 7.9 shows the cost of actual exchanged energy.

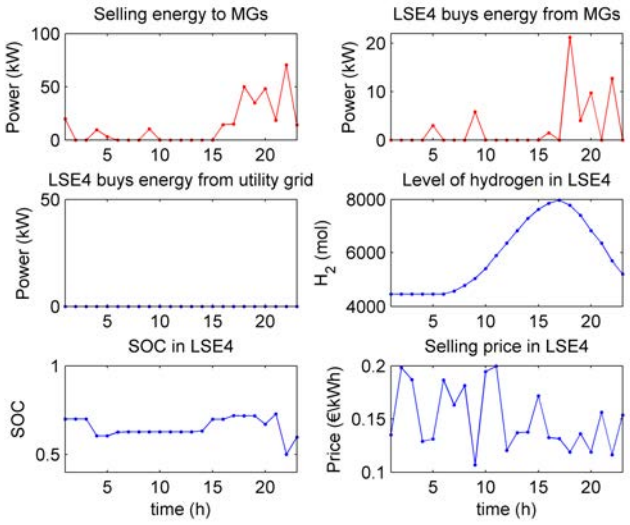

Figure 7.23: Load service entity LSE4

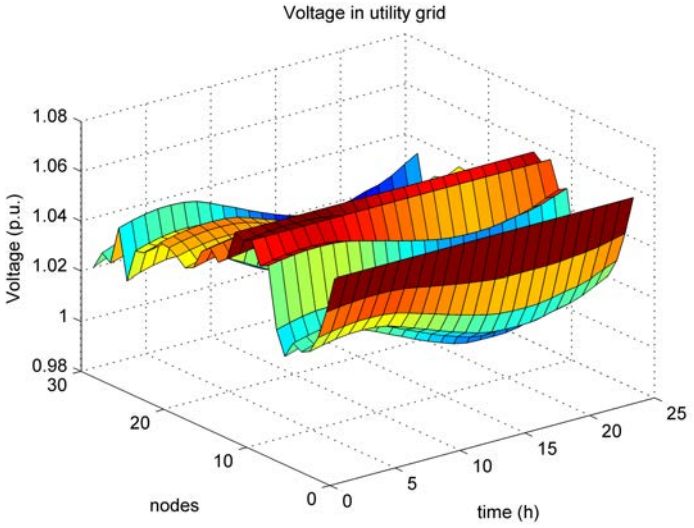

Figure 7.24: Voltage in utility grid

7.4/ SIMULATION BASED ON THE NEURAL NETWORK MODEL

After we deploy the above 16 microgrids test model, we need to consider another problem, namely that when there are hundreds of microgrids, it will take a long simulation time to search for the price. For example, if there are 150 microgrids, in the GA, there needs to be $150 * 20 * 100 = 3 * 10^5$ optimizations for the whole process (20 generations, 100 iterations), which will take a long simulation time. So how to solve this problem?

In this section, we developed a neural network based price searching model. We use a neural network to estimate the performance of the whole system [156]. Then, GA is used to search for the best price. This model can be seen in Fig. 7.27.

For the neural network model, firstly, we need to train the model based on the training

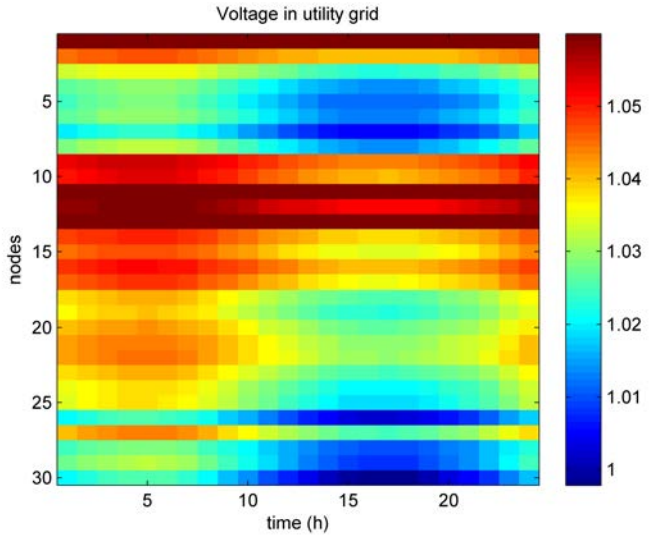

Figure 7.25: Voltage in utility grid (color change)

Table 7.7: Detailed objective function results in case3 and case4.

Case	MGs total	MGA1	MGB1	MGC1	MGD1	LSE1
case3a	1.7201e+3	-1.4027e+3	1.7481e+4	204.9639	-1.4563e+4	968.5433
case3b	-3.5613e+3	-2.7844e+3	1.5494e+4	-1.6485e+3	-1.4622e+4	1.7565e+3
case4a	-9.6897e+3	-4.2551e+3	1.4628e+4	-2.6475e+3	-1.7415e+4	901.5402
case4b	-1.4147e+4	-3.9681e+3	1.2044e+4	-3.2717e+3	-1.8952e+4	939.6796
Case	MGs total	MGA2	MGB2	MGC2	MGD2	LSE2
case3a	1.2841e+6	1.3085e+5	2.8670e+5	3.0801e+5	5.5859e+5	1.7364e+5
case3b	1.2753e+6	1.2964e+5	2.8346e+5	3.0590e+5	5.5628e+5	1.7517e+5
case4a	1.2727e+6	1.2799e+5	2.8385e+5	3.0516e+5	5.5572e+5	1.6713e+5
case4b	1.2456e+6	1.2537e+5	2.7653e+5	2.9772e+5	5.4595e+5	1.7239e+5
Case	MGs total	MGA3	MGB3	MGC3	MGD3	LSE3
case3a	7.4718e+5	7.3250e+4	1.5729e+5	1.8024e+5	3.3641e+5	9.5585e+4
case3b	7.4882e+5	7.2636e+4	1.5830e+5	1.7997e+5	3.3791e+5	9.7462e+4
case4a	7.3577e+5	7.0398e+4	1.5444e+5	1.7738e+5	3.3355e+5	9.2892e+4
case4b	7.2611e+5	6.8116e+4	1.5235e+5	1.7473e+5	3.3092e+5	9.1794e+4
Case	MGs total	MGA4	MGB4	MGC4	MGD4	LSE4
case3a	-1.6521e+3	-4.7333e+3	1.1209e+4	3.4823e+3	-1.1610e+4	176.1018
case3b	-7.8929e+3	-6.0900e+3	9.8742e+3	2.2700e+3	-1.3947e+4	1.4929e+3
case4a	-1.3062e+4	-7.5857e+3	8.3568e+3	629.8449	-1.4463e+4	281.7876
case4b	-1.7517e+4	-8.2467e+3	7.0429e+3	-188.6105	-1.6124e+4	643.2442

data. We use the prices as the input data, and the target is the optimization results (objective function results) of each MG and LSE. The input and target matrix can be shown as in Fig. 7.28.

The training data is obtained based on the simulation results from the real model (Fig. 7.18). There are 80 training cases, the neural network is trained based on the neural network tool in matlab. After the training model is completed, then we can use this model to estimate the performance of the whole system. We still use GA to search for the price.

Table 7.8: Total objective function results in case3 and case4.

Case	Total cost	cost of the utility grid
case3a	2.3018e+6	1.9930e+5
case3b	2.2885e+6	1.9929e+5
case4a	2.2469e+6	1.9932e+5
case4b	2.2058e+6	1.9932e+5

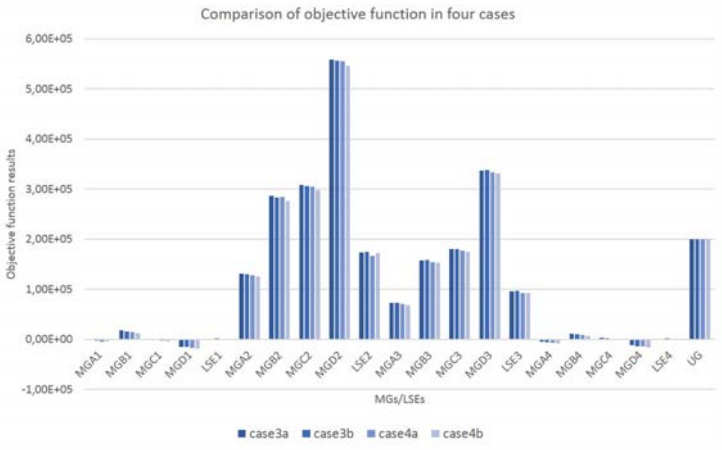

Figure 7.26: Comparison of objective function results in case II.

Table 7.9: Cost of actual exchanged energy in case3 and case4.

Case	MGs total	MGA1	MGB1	MGC1	MGD1	LSE1
case3b	48.2784	12.6390	36.3526	12.2915	-13.0048	-46.5969
case4b	40.1218	4.2615	37.8066	7.4564	-9.4027	-38.4526
Case	MGs total	MGA2	MGB2	MGC2	MGD2	LSE2
case3b	700.9898	60.1388	161.6076	192.8246	286.4188	-72.4367
case4b	643.6114	51.8099	148.3537	177.0427	266.4050	-30.2215
Case	MGs total	MGA3	MGB3	MGC3	MGD3	LSE3
case3b	426.7232	36.9526	91.0320	122.2066	176.5319	-80.8314
case4b	386.9503	33.5274	76.5852	111.7526	165.0852	-60.9570
Case	MGs total	MGA4	MGB4	MGC4	MGD4	LSE4
case3b	25.2160	4.5121	15.8618	9.0177	-4.1757	-25.2160
case4b	29.3022	7.8656	20.4954	8.4728	-7.5316	-29.3022

The simulation results can be seen in Tab. 7.10. case4a is the operation results based on time of use price, case4b is the operation results based on the real model with the GA searching price, case5 is the operation results based on the neural network model with the GA searching price, case6 is the operation results based on the real model with the price from case5, namely, to check the obtained price from case5 with the real model. It can be seen that, comparing case5 and case6, the error is about 6.5%. Comparing case4b and case6, we can see that, based on the real model, better results are obtained. Comparing case4a and case6, we can see that, based on the NN model, the obtained

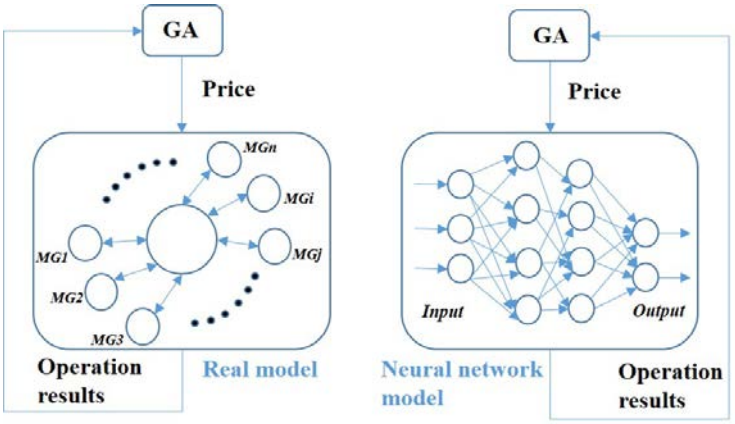

Figure 7.27: Neural network simulation model.

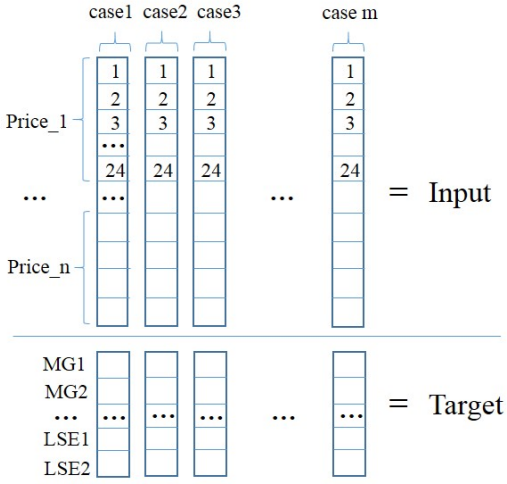

Figure 7.28: Neural network input and target matrix.

prices are still better than TOU price.

Actually, the accuracy of the NN model is highly dependent on the obtained training data and the use of the NN model. But this method can still provide some estimated results and provide guidance for consumers and utility grid.

Table 7.10: Total objective function results in different cases.

Case	Total cost	cost of the utility grid
case4a (TOU price)	2.2469e+6	1.9932e+5
case4b (Real model)	2.2058e+6	1.9932e+5
case5 (NN model)	2.0788e+6	1.9930e+5
case6 (Real model check)	2.2233e+6	1.9928e+5

The simulation results based on the real model and the neural network model are compared in Tab. 7.11. For the real model (Fig. 7.18), in each iteration, GA gives the prices, then the optimization problem of LSEs, MGs and utility grid are run to calculate the operation costs. The simulation time for one iteration is about 102.995639 seconds. For the

neural network model, for each iteration, GA gives the prices, then the operation costs of the whole system is calculated based on NN model, the simulation time for one iteration is about 1.758580 seconds. This is because in the NN model, the complex system is fitted into a hyper-function f_{NN} based on the training cases, which means that in each iteration of GA,the NN model is actually to calculate the results of hyper-function f_{NN}. This leads to a shorter simulation time.

Table 7.11: Comparison between real model and neural network model.

Model	One iteration time	Solving method	Error
GA + real model	102.995639 s	branch and bound	0%
GA + NN model	1.758580 s	function f_{NN}	6.5%

7.5/ DISCUSSION

For the future electricity grid, large numbers of renewable energy resources and storage systems will be integrated, which will make the operation of the whole system a complex problem. For example, a small capacity of distributed renewable energy resources will be integrated in smart homes/smart buildings, and a large capacity of centralized renewable energy resources will be integrated in load service entities. So how to make this system operate is a difficult problem.

In this chapter, we provide an interesting exploration. We use the prices as the only guidance to make the whole system operate well. Firstly, each MG runs the energy management optimization based on prices. After that, the LSE runs the energy management optimization based on the demands from MGs and the prices. Then, the utility grid, based on the demands from LSEs, runs the optimal power flow optimization to schedule the generators which connect with the utility grid.

On the other hand, we can also see that, after the penetration percentage of the renewable energy in MGs and LSEs are increased, the bought energy from the utility grid is reduced. This means that if we make a good guidance for MGs, we can just import small amount of energy from the utility grid, which can improve the resilience of the whole system. If the utility grid is damaged, MGs and LSEs can operate together to supply the load demands.

The above method can provide better prices for the whole system to reduce the operation cost compared to the time of use price. But when there are large numbers of microgrids, the price searching algorithm will take a long time. Thus we presented a NN model to estimate the performance of the whole system. The simulation results show that the error between the real model and the NN model is about 6.5%. Although the searching price based on NN model is not better than the searching price based on the real model, it is better than the time of use price.

7.6/ SIZING OF GRID-CONNECTED MICROGRID CONSIDERING PRICE

The above sections discussed about the price decision method for multiple grid-connected MES MGs. It should be noticed that the sizing values of each component in each MG and LSE are given. Based on these given sizing values (rated capacity), we can search for the best price, which can make the whole system operate in minimal cost.

In this section, we discuss about the sizing problem based on different prices. Namely, with the given prices, we search for the best sizing values for each MG and LSE to design the whole system under minimal total cost.

7.6.1/ PROBLEM FORMULATION

The goal is to compute the optimal size value of each component for MGs, namely, $N_{PV}^{MG,i}, N_{sh}^{MG,i}, C_{bat}^{MG,i}, P_{fc}^{MG,i,max}, P_{el}^{MG,i,max}, V_{H_2}^{MG,i,max}, P_{hb}^{MG,i,max}, P_{ac}^{MG,i,max}, Q_{ahc}^{MG,i,max}$, $HS_{MG,i,max}$, and for the LSE, namely, $N_{PV}^{LSE}, N_{sh}^{LSE}, CB^{LSE}, P_{fc}^{LSE,max}, P_{el}^{LSE,max}, V_{H_2}^{LSE,max}$. Let set U represent these sizing variables. Then the sizing problem is $minF(U)$, with $F(.)$ the total cost function introduced in the following.

The total capital cost corresponds to the cost of buying the equipment for MG i, given by:

$$\begin{aligned} C_{cap}^{MG,i} = CRF \cdot (&N_{PV}^{MG,i} \cdot C_{PV}^{inv} + N_{sh}^{MG,i} \cdot C_{sh}^{inv} + P_{fc}^{\mathrm{MG,i,max}} \cdot C_{fc}^{inv} \\ &+ P_{el}^{\mathrm{MG,i,max}} \cdot C_{ele}^{inv} + V_{H_2}^{MG,i,max} \cdot C_{tank}^{inv} + C_{bat}^{MG,i} \cdot C_{bat}^{inv} \\ &+ P_{hb}^{\mathrm{MG,i,max}} \cdot C_{hb}^{inv} + P_{ac}^{\mathrm{MG,i,max}} \cdot C_{ac}^{inv} + P_{ahc}^{\mathrm{MG,i,max}} \cdot C_{ahc}^{inv} \\ &+ HS_{\mathrm{MG,i,max}} \cdot C_{hs}^{inv}) \end{aligned} \tag{7.27}$$

The capital cost for the LSE can be written as:

$$C_{cap}^{LSE} = CRF \cdot (N_{PV}^{MG,i} \cdot C_{PV}^{inv} + P_{fc}^{\mathrm{MG,i,max}} \cdot C_{fc}^{inv} + P_{el}^{\mathrm{MG,i,max}} \cdot C_{ele}^{inv} + V_{H_2}^{MG,i,max} \cdot C_{tank}^{inv} + C_{bat}^{MG,i} \cdot C_{bat}^{inv}) \tag{7.28}$$

Similarly, the annual maintenance cost is given by:

$$C_{mnt} = N_{PV} \cdot C_{PV}^{mnt} + V_{H_2} \cdot C_{tank}^{mnt} + C_{bat} \cdot C_{bat}^{mnt} \tag{7.29}$$

The total cost function $F(.)$ is thus:

$$\begin{aligned} F &= \sum_{i=1}^{N} \left\{ C_{cap}^{MG,i} + C_{MG_i} + C_{mnt}^{MG,i} \right\} + \left\{ C_{cap}^{LSE} + C_{LSE} + C_{mnt}^{LSE} \right\} \\ &= C_{inv}^{all} + \sum_{i=1}^{N} C_{MG_i} + C_{LSE}; \\ C_{inv}^{all} &= \sum_{i=1}^{N} \left\{ C_{cap}^{MG,i} + C_{mnt}^{MG,i} \right\} + \left\{ C_{cap}^{LSE} + C_{mnt}^{LSE} \right\} \end{aligned} \tag{7.30}$$

Then the whole problem can be written as:

$$\begin{aligned} \min_{\mathbf{U}} & \left\{ C_{inv}^{all} + \left\{ \sum_{i=1}^{N} \left\{ \min_{U^*, price^*, \mathbf{exch}} C_{MG_i} \right\} + \min_{U^*, price^*, \sum_{i=1}^{N} exch_i^*} C_{LSE} \right\} \right\} \\ & s.t.\ (7.2), (7.3), (7.4), (7.5), (7.6), (7.7), (7.8), (7.13), (7.18), (7.19), \\ & (7.20), (7.21), (7.23), (7.22), (7.24) \end{aligned} \tag{7.31}$$

$U^* \in \mathbf{U}$ is the best sizing values for each MG and LSE. $price^*$ is the given price. $exch^* \in \mathbf{exch}$ is the exchanged energy between MG and LSE.

This sizing problem can be described as: under the given price $price^*$, searching for the best sizing values $U^* \in \mathbf{U}$ which can make the whole system operate under minimal total cost, and at the same time, ensure the energy exchange between MGs and LSE. It should be pointed out that the price is a given parameter. This is because only with the given price, the energy flow in the whole system can be decided, then the sizing values can be searched.

The simulation flow chart can be seen in Fig. 7.29.

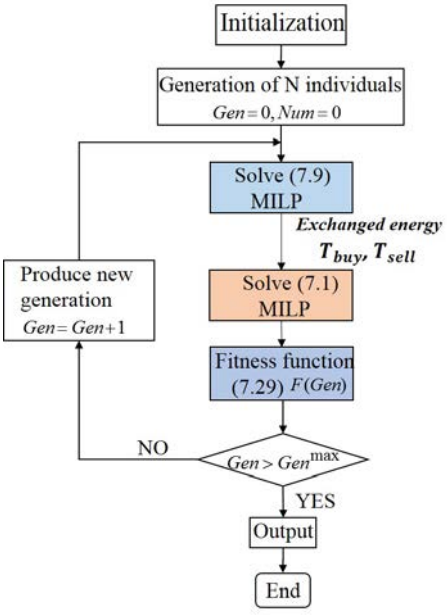

Figure 7.29: Flow chart for sizing problem considering price.

With the given sizing values from the GA algorithm, firstly, each MG runs its operation problem (7.9). Then, the total bought energy T_{buy} and sold energy T_{sell} are transferred to the LSE. Next, the LSE runs its operation problem (7.1). After that, the fitness functions (total cost) 7.30 are calculated; and at last, GA updates the new population of sizing values. This process is repeated until the stopping criteria are satisfied.

7.6.2/ SIMULATION RESULTS

We take Case I as the example. In Case I, there are 4 MGs and 1 LSE. GA generates the sizing values for 4 MG and 1 LSE, there are 45 variables (10 components in each MG, 5 components in the LSE). Two cases are compared:

- case s1: The given price is the TOU, namely, $Price_{ug} = Price_{LSE} = Price_A = Price_B = Price_C = Price_D$;
- case s2: The given price is the searching price from case 1b.

To reduce the simulation time, we just adopt one day (Fig. 7.9) to check the sizing results (in practice, several typical days should be checked). Sizing results of each MG and LSE are shown in Tab. 7.12 and Tab. 7.13.

Table 7.12: Sizing results for case s1.

Strategy	N_{PV}	$P_{fc}^{\max}$[kW]	$P_{el}^{\max}$[kW]	V_{H_2} [N.m^3]	C_{bat} [kWh]	N_{sh} [m^2]	P_{hb}^{max}	HS[kWh]	P_{ac}^{max}	Q_{ahc}^{max}
MGA	57.1	97.5	12.5	318.5	31.1	17.8	64.1	47.9	84.6	41.7
MGB	56.8	42.0	29.2	905.5	43.3	11.0	64.9	56.0	92.2	41.3
MGC	55.2	9.2	37.3	165.1	35.6	13.2	36.7	51.1	34.6	30.5
MGD	54.3	68.7	42.0	219.2	33.5	14.3	60.8	76.0	14.2	76.9
LES	419.8	176.1	110.8	1853.9	143.8	–	–	–	–	–

Table 7.13: Sizing results for case s2.

Strategy	N_{PV}	$P_{fc}^{\max}$[kW]	$P_{el}^{\max}$[kW]	V_{H_2} [N.m^3]	C_{bat} [kWh]	N_{sh} [m^2]	P_{hb}^{max}	HS[kWh]	P_{ac}^{max}	Q_{ahc}^{max}
MGA	64.1	103.7	121.3	287.9	388.8	30.9	81.5	98.6	59.6	7.2
MGB	63.4	103.7	10.8	676.1	231.6	17.6	38.4	69.4	36.2	9.4
MGC	58.2	13.9	182.7	282.7	42.7	11.8	12.3	77.8	7.1	30.3
MGD	79.1	14.4	61.4	353.9	797.9	5.7	57.8	53.3	90.8	23.8
LES	343.6	118.0	81.5	731.5	159.7	–	–	–	–	–

We compare the sizing results of the two cases. Fig. 7.30 shows the sizing results for MGA under two different prices (TOU price and searching price from case 1b). We can see that, with different given prices, the sizing results are significantly different. This is because the price decides the power flow inside MGs and LSE, which then influences the sizing results. Fig. 7.31 shows the sizing results for the LSE under two different prices (TOU price and searching price from case 1b). We can see that the sizing results for the LSE in case 2s is smaller than that in case 1s. This is because in case 2s, the LSE bought more power from utility grid (because it is cheaper than utilizing its own storage energy), leading to a smaller capapcity of installed power source and storage system.

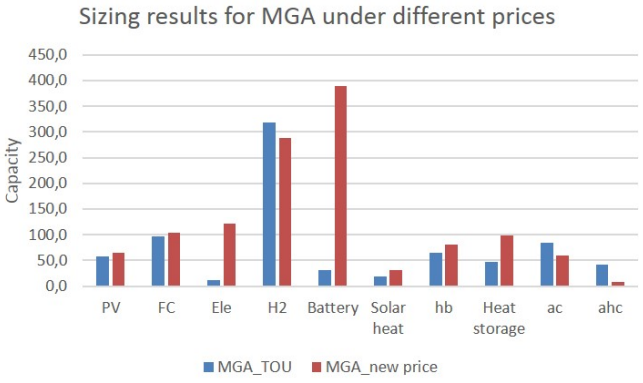

Figure 7.30: Sizing results for MGA under two different prices (TOU price and searching price from case 1b).

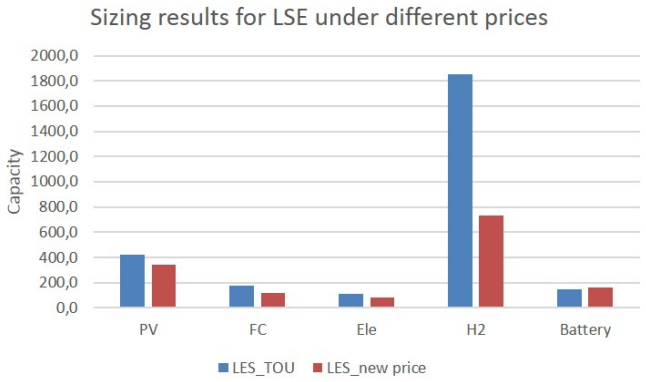

Figure 7.31: Sizing results for LSE under two different prices (TOU price and searching price from case 1b).

7.7/ CONCLUSION

In this chapter, we presented a bidding price decision approach for multiple MES microgrids considering DR. The LSE was introduced to play a middle agent role, which can benefit both utility grid and consumers. The LSE integrates the local generation, energy storage systems and renewable energy, which can not only provide auxiliary service to regulating power market, but also provide an incentive price to consumers. On the other hand, the MG integrates with renewable energy can also sell energy to UG/LSE. Then how to decide the electricity selling prices for LSE and each MG are problems.

A combined GA and MILP method was proposed to solve this problem. MILP is used to control the operation of LSE and each MG. GA is used to search for the best prices. Then a four MES MGs model was used, and four cases were compared to research about the influence of PV penetration and different prices on the operation costs. We then developed a decentralized optimization method, namely, each MG just runs its own optimization problem, then the LSE runs its own operation problem, at last, operation cost of LSE and each MG are transferred to an ISO to update the prices based on GA. The simulation results showed that the new searched price works better than the TOU price, which can reduce the operation cost of the whole system. Also with higher penetration of renewable energy in MG, the bought energy from the utility grid was reduced.

A large system was tested, in which 4 LSEs, 16 MGs and IEEE30-node network are considered. The simulation results also showed the effectiveness of the proposed algorithm.

In order to reduce the GA searching time, a neural network model was presented to estimate the performance of the whole system, the simulation results showed that the searching prices based on the NN model was better than the TOU price.

After that, the sizing algorithm for grid-conneted MES MGs under different prices were presented. With different given prices, power flow inner MGs and LSE was different, then the sizing values in MGs and LSE were different. Two different price cases were compared, the results showed that, price significantly influenced the sizing values. Especially for LSE, when selling price of MG was high, LSE preferred buying energy from utility grid, and leading to smaller installed capacity of power source and storage system.

III

CONCLUSION

8

CONCLUSION

This chapter is the conclusion of the whole dissertation. It discusses four aspects: 1) a summary of this dissertation; 2) the list of contributions; 3) the practical application of the proposed co-optimization sizing method; and 4) future works.

8.1/ SUMMARY

In this dissertation, we focused on the sizing and operation problem of hydrogen-based microgrids. We considered islanded microgrids (sections 4 and 5), and grid-connected microgrids (section 6). Then we solved this problem while considering different specific aspects, including the operation strategy (2.2), the sizing method (2.3), the uncertainty on load demands (2.2.1), the degradation of energy storage system (5.3.4), and the results validation (4.3.8, 5.3.3). For grid-connected microgrids, we also considered the influence of contingency events on the utility grid (sections 6.2.3, 6.3). Finally, a prices decision approach was also studied (section 7).

Firstly, for the operation strategies, we determined that three methods are often used: the rule-based strategy, the evolutionary algorithm, and the deterministic algorithm (such as LP, MILP). We reviewed related operation strategies of microgrids in section 2.2. In this thesis, the MILP operation strategy was adopted to control the operation of microgrid models.

Secondly, for the sizing method, the leader-follower (co-optimization) structure is often adopted. Related works about sizing methods was summarized in section 2.3. The leader is typically the sizing problem, which uses a searching algorithm to search for the best sizing values. The follower is the operation problem, which uses a deterministic algorithm to solve the operation problem based on the sizing values from the leader. In this thesis, GA was used as the searching algorithm, and MILP was used to control the operation of the microgrid, solved by a branch-and-bound algorithm.

Thirdly, for the uncertainty on the load demands and PV output, robust optimization was adopted, namely, to find the worst and the best case based on the uncertainty level, which is presented in section 2.2.1. The worst case (the case where the difference between the PV output and the load is the largest) is when the PV output is equal to the upper bound value, and the load is equal to the lower bound value. For the best case (the case where the difference between the PV output and the load is the lowest), when the PV output is equal to the lower bound value, the load is equal to the upper bound value.

The degradation of the energy storage system was discussed in section 5.3.4. We considered the degradation model of hydrogen storage system and the battery storage system. The simulation results showed that after we consider the degradation model, the sizing values were significantly influenced. We especially notice an increase in the capacity of hydrogen storage and battery storage systems.

For the sizing results check, one-hour one-day rolling horizon optimization was adopted, as discussed in sections 4.3.8 and 5.3.3. As in the co-optimization, we often choose several typical days to check whether sizing values are appropriate or not. We used rolling horizon optimization to check these obtained results, and test whether there was any necessary load shedding or curtailed power. In cases where these occured, adjustments to the sizing values were required.

Sixth, we looked at the influence of contingency events on the utility grid, as shown in sections 6.2.3 and 6.3. We used the betweenness centrality index to describe the relative importance of each node for the whole system. Then we defined a worst case, namely, when the most important node was destroyed. We included the worst case in the sizing problem to research about the influence of utility grid contingency events on the sizing values.

After that, for the price decision approach, we adopted the combined GA and MILP method to obtain the best prices to reduce the operation cost of the whole system, which can be found in section 7. MILP was used to control the operation of the microgrid and the load service entity, and GA was used to search for the best price. At last, a neural network was also developed to estimate the performance of the whole system and accelerate computation time.

At last, a sizing algorithm for grid-connected MES MGs under different prices was presented, as shown in section 7.6. With different given prices, power flow between MGs and LSE was different, and so the sizing values in MGs and LSE were different. Two different price cases were compared, and the results showed that price significantly influenced the sizing values.

8.2/ LIST OF CONTRIBUTIONS

Based on the previous elements, we list the main contributions of this thesis as follows:

1. A bi-level optimization method to perform microgrid sizing. A genetic algorithm is used to compute the sizing of the components to minimize the total annual cost (capital, maintenance and operation) of the system. Each candidate solution (set of components sizes) is evaluated with an MILP algorithm for scheduling validation;
2. A study on two types of microgrid architectures: a full-electric hydrogen-based microgrid and a multi-energy supply hydrogen-based microgrid;
3. A model of the hydrogen storage system, integrating a degradation model for the fuel cell and the electrolyzer;
4. An MILP model to control energy flows, which considers technical and economic criteria, such as the operation costs of the components, the startup costs of the fuel cell and the electrolyzer, the state-of-charge of the BSS, and the level-of-hydrogen of hydrogen tanks.

5. A 1-h resolution rolling-horizon simulation used to verify the validity of the obtained sizing solutions, and to adjust the sizing values if required;
6. A multi-node gas/electricity/heat network model, where a hydrogen storage system is used to keep the power balance;
7. In order to resist to contingency events, the use of betweenness centrality to find the worst case under contingency events, and research about the influence of contingencies on the sizing results;
8. A decentralized price decision approach for UG-LSE-MGs, in which each MG and LSE runs its own operation problem;
9. A neural network model to estimate the performance (operation cost) of the whole system;
10. A sizing algorithm for grid-connected MES MGs under different prices is presented.

8.3/ PRACTICAL APPLICATIONS

In this section, we discuss how to use the proposed combined GA and MILP algorithm in practical applications. It can be used in two aspects: the planning problem and the bilevel price decision problem.

For the planning problem, we need to find the best values of each component to make the whole system cost-effective. This is a non-convex combinational optimization problem, where we need to consider not only the long term planning period (such as 1 year), but also the short term operation period (such as 1 hour), which makes the planning problem challenging. Then we can use the presented combined planning algorithm, namely, using GA to search for the sizing values, and the MILP (or the other operation strategy) to control the operation of the whole system. After that, we can use the 1-hour one day rolling horizon optimization to check the obtained sizing results, and to adjust the sizing values if required.

For the price decision problem. We need to consider both suppliers and consumers interests. The price is the link between suppliers and consumers. This is a bilevel problem, namely, the upper-level problem (the supplier operation is the upper-level problem) and the lower-level problem (the MGs operation is the lower-level problem), which means that price is often the decision variable in the upper-level problem, and is treated as a parameter in the lower-level problem. We can use the presented combined GA and MILP algorithm to solve the price decision problem. GA is used to search for the prices, and the MILP is used to control the operation of suppliers and consumers. Based on this combined method, we can obtain the best prices, which can both benefit the energy suppliers and the consumers.

8.4/ FUTURE WORK

In this thesis, we have presented a combined GA and MILP algorithm to solve the planning and price decision problem. But there are still many problems to be solved in the future, which can be concluded in as follows:

1. The modeling of the hydrogen storage system. The consumed hydrogen of the fuel cell and produced hydrogen of electrolyzer will influence the sizing volume of hydrogen tanks. In this thesis, we use a linear model to describe the consumed hydrogen of a fuel cell and the produced hydrogen of a electrolyzer. However, more precise models can be built, such as nonlinear models, which will be a future work;

2. The running time of the combined algorithm. Evolutionary algorithms need to search the "optimal" points in a large searching space, which makes the combined algorithm cost lots of time. Especially, when the inner operation problem is complex to solve, such as the MINLP operation problem, the whole simulation time will be very long. Then, in the future, how to reduce the simulation time is a problem;

3. Other methods to solve the bilevel sizing problem. Two stage sizing optimization problem can be solved based on Benders decomposition method [157]. The inner problem is the operation MILP problem, which can be transferred into a Lagrange dual problem. Solving the inner Lagrange dual problem, a Benders type cutting plan can be generated based on dual variables. Then, these Benders cuts are added to the outer level problem. Using the Benders decomposition method to solve the sizing problem will be a future work;

4. The uncertainty of the load demands, renewable energy sources (such as PV, WT), and failure of power devices. In this thesis, we just consider the forecasted error of the electricity load demands and PV generation, but actually, in the multi-energy supply microgrid, there are different types of load demands. This means that when we consider multiple forecasted error from different types of loads, the problem is harder to solve;

5. The artificial intelligence model to estimate the performance of the power system integrating large numbers of renewable energy resources. In the last sections of this thesis, we presented a neural network to estimate the performance of the IEEE 30 network integrating microgrids. The error is about 6.5%, and how to reduce the error will be researched in the future work.

BIBLIOGRAPHY

[1] WANG, Y., CHEN, C., WANG, J., AND BALDICK, R. **Research on resilience of power systems under natural disasters-a review**. *IEEE Transactions on Power Systems 31*, 2 (2016), 1604–1613.

[2] CHEN, C., WANG, J., QIU, F., AND ZHAO, D. **Resilient distribution system by microgrids formation after natural disasters**. *IEEE Transactions on Smart Grid 7*, 2 (March 2016), 958–966.

[3] CHEN, H., CONG, T. N., YANG, W., TAN, C., LI, Y., AND DING, Y. **Progress in electrical energy storage system: A critical review**. *Progress in Natural Science 19*, 3 (2009), 291–312.

[4] SHUKLA, A., AND PREM KUMAR, T. **Nanostructured electrode materials for electrochemical energy storage and conversion**. *Wiley Interdisciplinary Reviews: Energy and Environment 2*, 1 (2013), 14–30.

[5] JARAMILLO, L. B., AND WEIDLICH, A. **Optimal microgrid scheduling with peak load reduction involving an electrolyzer and flexible loads**. *Applied Energy 169* (2016), 857–865.

[6] KAZEMPOOR, P., DORER, V., AND OMMI, F. **Evaluation of hydrogen and methane-fuelled solid oxide fuel cell systems for residential applications: system design alternative and parameter study**. *international journal of hydrogen energy 34*, 20 (2009), 8630–8644.

[7] CAU, G., COCCO, D., PETROLLESE, M., KÆR, S. K., AND MILAN, C. **Energy management strategy based on short-term generation scheduling for a renewable microgrid using a hydrogen storage system**. *Energy Conversion and Management 87* (2014), 820–831.

[8] WIKIPEDIA. **Hydrogen production**, 2018.

[9] BERTUCCIOLI, L., CHAN, A., HART, D., LEHNER, F., MADDEN, B., AND STANDEN, E. **Development of water electrolysis in the european union**. *Fuel Cells and Hydrogen Joint Undertaking* (2014), 83.

[10] WIKIPEDIA. **Fuel cell**, 2018.

[11] DEPARTMENT OF ENERGY, U. **fuel cells comparison**, 2018.

[12] LIDULA, N., AND RAJAPAKSE, A. **Microgrids research: A review of experimental microgrids and test systems**. *Renewable and Sustainable Energy Reviews 15*, 1 (2011), 186–202.

[13] HATZIARGYRIOU, N., ASANO, H., IRAVANI, R., AND MARNAY, C. **Microgrids**. *IEEE power and energy magazine 5*, 4 (2007), 78–94.

[14] KATSIGIANNIS, Y. A., GEORGILAKIS, P. S., AND KARAPIDAKIS, E. S. **Hybrid simulated annealing–tabu search method for optimal sizing of autonomous power systems with renewables**. *IEEE Transactions on Sustainable Energy 3*, 3 (2012), 330–338.

[15] KYRIAKARAKOS, G., DOUNIS, A. I., ROZAKIS, S., ARVANITIS, K. G., AND PAPADAKIS, G. **Polygeneration microgrids: a viable solution in remote areas for supplying power, potable water and hydrogen as transportation fuel**. *Applied Energy 88*, 12 (2011), 4517–4526.

[16] ABBEY, C., CORNFORTH, D., HATZIARGYRIOU, N., HIROSE, K., KWASINSKI, A., KYRIAKIDES, E., PLATT, G., REYES, L., AND SURYANARAYANAN, S. **Powering through the storm: microgrids operation for more efficient disaster recovery**. *IEEE power and energy magazine 12*, 3 (2014), 67–76.

[17] AKHIL, A. A., HUFF, G., CURRIER, A. B., KAUN, B. C., RASTLER, D. M., CHEN, S. B., COTTER, A. L., BRADSHAW, D. T., AND GAUNTLETT, W. D. **Electricity storage handbook**. Tech. rep., DOE/EPRI in collaboration with NRECA, 2013.

[18] KYRIAKARAKOS, G., PIROMALIS, D. D., ARVANITIS, K. G., DOUNIS, A. I., AND PAPADAKIS, G. **On battery-less autonomous polygeneration microgrids: Investigation of the combined hybrid capacitors/hydrogen alternative**. *Energy Conversion and Management 91* (2015), 405–415.

[19] LARMINIE, J., DICKS, A., AND MCDONALD, M. S. **Fuel cell systems explained**, vol. 2. Wiley New York, 2003.

[20] TESFAHUNEGN, S. G. **Fuel cell assisted photovoltaic power systems**.

[21] LAJNEF, T., ABID, S., AND AMMOUS, A. **Modeling, control, and simulation of a solar hydrogen/fuel cell hybrid energy system for grid-connected applications**. *Advances in Power Electronics 2013* (2013).

[22] UZUNOGLU, M., ONAR, O., AND ALAM, M. **Modeling, control and simulation of a pv/fc/uc based hybrid power generation system for stand-alone applications**. *Renewable Energy 34*, 3 (2009), 509–520.

[23] LIU, M., SHI, Y., AND FANG, F. **Combined cooling, heating and power systems: A survey**. *Renewable and Sustainable Energy Reviews 35* (2014), 1–22.

[24] FACCI, A. L., CIGOLOTTI, V., JANNELLI, E., AND UBERTINI, S. **Technical and economic assessment of a sofc-based energy system for combined cooling, heating and power**. *Applied Energy* (2016).

[25] TSE, L. K. C., WILKINS, S., MCGLASHAN, N., URBAN, B., AND MARTINEZ-BOTAS, R. **Solid oxide fuel cell/gas turbine trigeneration system for marine applications**. *Journal of Power Sources 196*, 6 (2011), 3149 – 3162.

[26] BANIASADI, E., AND ALEMRAJABI, A. A. **Fuel cell energy generation and recovery cycle analysis for residential application**. *International Journal of Hydrogen Energy 35*, 17 (2010), 9460 – 9467.

[27] MENG, L., SANSEVERINO, E. R., LUNA, A., DRAGICEVIC, T., VASQUEZ, J. C., AND GUERRERO, J. M. **Microgrid supervisory controllers and energy management systems: A literature review**. *Renewable and Sustainable Energy Reviews 60* (2016), 1263–1273.

[28] BAO, Z., ZHOU, Q., YANG, Z., YANG, Q., XU, L., AND WU, T. **A multi time-scale and multi energy-type coordinated microgrid scheduling solution—part i: Model and methodology**. *IEEE Transactions on Power Systems 30*, 5 (2015), 2257–2266.

[29] LUO, Z., WU, Z., LI, Z., CAI, H., LI, B., AND GU, W. **A two-stage optimization and control for cchp microgrid energy management**. *Applied Thermal Engineering* (2017).

[30] MASHAYEKH, S., STADLER, M., CARDOSO, G., AND HELENO, M. **A mixed integer linear programming approach for optimal der portfolio, sizing, and placement in multi-energy microgrids**. *Applied Energy 187* (2017), 154–168.

[31] MALEKI, A., AND ASKARZADEH, A. **Comparative study of artificial intelligence techniques for sizing of a hydrogen-based stand-alone photovoltaic/wind hybrid system**. *international journal of hydrogen energy 39*, 19 (2014), 9973–9984.

[32] MALEKI, A., AND POURFAYAZ, F. **Optimal sizing of autonomous hybrid photovoltaic/wind/battery power system with lpsp technology by using evolutionary algorithms**. *Solar Energy 115* (2015), 471–483.

[33] FETANAT, A., AND KHORASANINEJAD, E. **Size optimization for hybrid photovoltaic–wind energy system using ant colony optimization for continuous domains based integer programming**. *Applied Soft Computing 31* (2015), 196–209.

[34] MALEKI, A., AND ASKARZADEH, A. **Artificial bee swarm optimization for optimum sizing of a stand-alone pv/wt/fc hybrid system considering lpsp concept**. *Solar Energy 107* (2014), 227–235.

[35] MALEKI, A., AMERI, M., AND KEYNIA, F. **Scrutiny of multifarious particle swarm optimization for finding the optimal size of a pv/wind/battery hybrid system**. *Renewable Energy 80* (2015), 552–563.

[36] ZHAO, B., ZHANG, X., LI, P., WANG, K., XUE, M., AND WANG, C. **Optimal sizing, operating strategy and operational experience of a stand-alone microgrid on dongfushan island**. *Applied Energy 113* (2014), 1656–1666.

[37] ATIA, R., AND YAMADA, N. **Optimization of a pv-wind-diesel system using a hybrid genetic algorithm**. In *Electrical Power and Energy Conference (EPEC), 2012 IEEE* (2012), IEEE, pp. 80–85.

[38] ROSS, M., HIDALGO, R., ABBEY, C., AND JOÓS, G. **Energy storage system scheduling for an isolated microgrid**. *IET renewable power generation 5*, 2 (2011), 117–123.

[39] MARZBAND, M., PARHIZI, N., SAVAGHEBI, M., AND GUERRERO, J. M. **Distributed smart decision-making for a multimicrogrid system based on a hierarchical interactive architecture**. *IEEE Transactions on Energy Conversion 31*, 2 (2016), 637–648.

[40] MARZBAND, M., AZARINEJADIAN, F., SAVAGHEBI, M., AND GUERRERO, J. M. **An optimal energy management system for islanded microgrids based on multiperiod artificial bee colony combined with markov chain**. *IEEE SYSTEMS JOURNAL* (2015).

[41] MARZBAND, M., YOUSEFNEJAD, E., SUMPER, A., AND DOMÍNGUEZ-GARCÍA, J. L. **Real time experimental implementation of optimum energy management system in standalone microgrid by using multi-layer ant colony optimization**. *International Journal of Electrical Power & Energy Systems 75* (2016), 265–274.

[42] MURTY, P. **Operation and control in power systems**. BS Publications, 2011.

[43] HEMMATI, R., AND SABOORI, H. **Short-term bulk energy storage system scheduling for load leveling in unit commitment: modeling, optimization, and sensitivity analysis**. *Journal of advanced research 7*, 3 (2016), 360–372.

[44] DETROJA, K. P. **Optimal autonomous microgrid operation: A holistic view**. *Applied Energy 173* (2016), 320–330.

[45] GUO, L., LIU, W., CAI, J., HONG, B., AND WANG, C. **A two-stage optimal planning and design method for combined cooling, heat and power microgrid system**. *Energy Conversion and Management 74* (2013), 433–445.

[46] KIM, J. S., AND EDGAR, T. F. **Optimal scheduling of combined heat and power plants using mixed-integer nonlinear programming**. *Energy 77* (2014), 675–690.

[47] MARZBAND, M., SUMPER, A., DOMÍNGUEZ-GARCÍA, J. L., AND GUMARA-FERRET, R. **Experimental validation of a real time energy management system for microgrids in islanded mode using a local day-ahead electricity market and minlp**. *Energy Conversion and Management 76* (2013), 314–322.

[48] DANESHI, H., AND SRIVASTAVA, A. K. **Security-constrained unit commitment with wind generation and compressed air energy storage**. *Generation, Transmission & Distribution, IET 6*, 2 (2012), 167–175.

[49] PARHOUDEH, S., BAZIAR, A., MAZAREIE, A., AND KAVOUSI-FARD, A. **A novel stochastic framework based on fuzzy cloud theory for modeling uncertainty in the micro-grids**. *International Journal of Electrical Power & Energy Systems 80* (2016), 73–80.

[50] ZAKARIAZADEH, A., JADID, S., AND SIANO, P. **Smart microgrid energy and reserve scheduling with demand response using stochastic optimization**. *International Journal of Electrical Power & Energy Systems 63* (2014), 523–533.

[51] XIANG, Y., LIU, J., AND LIU, Y. **Robust energy management of microgrid with uncertain renewable generation and load**. *IEEE Transactions on Smart Grid 7*, 2 (2016), 1034–1043.

[52] KUZNETSOVA, E., LI, Y.-F., RUIZ, C., AND ZIO, E. **An integrated framework of agent-based modelling and robust optimization for microgrid energy management**. *Applied Energy 129* (2014), 70–88.

[53] HUSSAIN, A., BUI, V.-H., AND KIM, H.-M. **Robust optimization-based scheduling of multi-microgrids considering uncertainties**. *Energies 9*, 4 (2016), 278.

[54] LIU, G., AND TOMSOVIC, K. **Robust unit commitment considering uncertain demand response**. *Electric Power Systems Research 119* (2015), 126–137.

[55] VALENCIA, F., COLLADO, J., SÁEZ, D., AND MARÍN, L. G. **Robust energy management system for a microgrid based on a fuzzy prediction interval model**. *IEEE Transactions on Smart Grid 7*, 3 (2016), 1486–1494.

[56] JAYASEKARA, S., AND HALGAMUGE, S. **A review on optimization strategies of combined cooling heating and power generation**. In *2012 IEEE 6th International Conference on Information and Automation for Sustainability* (2012), IEEE, pp. 302–307.

[57] FANG, F., WANG, Q. H., AND SHI, Y. **A novel optimal operational strategy for the cchp system based on two operating modes**. *IEEE Transactions on Power Systems 27*, 2 (2012), 1032–1041.

[58] KAVVADIAS, K., TOSIOS, A., AND MAROULIS, Z. **Design of a combined heating, cooling and power system: Sizing, operation strategy selection and parametric analysis**. *Energy Conversion and Management 51*, 4 (2010), 833–845.

[59] CHANG, L., WENG, G., HU, J., AND MAO, M. **Operation and configuration optimization of a cchp system for general building load**. In *Power Electronics and Motion Control Conference (IPEMC-ECCE Asia), 2016 IEEE 8th International* (2016), IEEE, pp. 1799–1805.

[60] KYRIAKARAKOS, G., PIROMALIS, D. D., DOUNIS, A. I., ARVANITIS, K. G., AND PAPADAKIS, G. **Intelligent demand side energy management system for autonomous polygeneration microgrids**. *Applied Energy 103* (2013), 39–51.

[61] MOHAMMADI-IVATLOO, B., MORADI-DALVAND, M., AND RABIEE, A. **Combined heat and power economic dispatch problem solution using particle swarm optimization with time varying acceleration coefficients**. *Electric Power Systems Research 95* (2013), 9–18.

[62] BASU, M. **Artificial immune system for combined heat and power economic dispatch**. *International Journal of Electrical Power & Energy Systems 43*, 1 (2012), 1–5.

[63] MOTEVASEL, M., SEIFI, A. R., AND NIKNAM, T. **Multi-objective energy management of chp (combined heat and power)-based micro-grid**. *Energy 51* (2013), 123–136.

[64] PIPERAGKAS, G., ANASTASIADIS, A., AND HATZIARGYRIOU, N. **Stochastic pso-based heat and power dispatch under environmental constraints incorporating chp and wind power units**. *Electric Power Systems Research 81*, 1 (2011), 209–218.

[65] WEI, D., CHEN, A., SUN, B., AND ZHANG, C. **Multi-objective optimal operation and energy coupling analysis of combined cooling and heating system**. *Energy 98* (2016), 296–307.

[66] BORNAPOUR, M., HOOSHMAND, R.-A., KHODABAKHSHIAN, A., AND PARASTEGARI, M. **Optimal stochastic coordinated scheduling of proton exchange membrane fuel cell-combined heat and power, wind and photovoltaic units in micro grids considering hydrogen storage**. *Applied Energy 202* (2017), 308–322.

[67] CHEN, X., KANG, C., O'MALLEY, M., XIA, Q., BAI, J., LIU, C., SUN, R., WANG, W., AND LI, H. **Increasing the flexibility of combined heat and power for wind power integration in china: Modeling and implications**. *IEEE Transactions on Power Systems 30*, 4 (2015), 1848–1857.

[68] BISCHI, A., TACCARI, L., MARTELLI, E., AMALDI, E., MANZOLINI, G., SILVA, P., CAMPANARI, S., AND MACCHI, E. **A detailed milp optimization model for combined cooling, heat and power system operation planning**. *Energy 74* (2014), 12–26.

[69] LOZANO, M. A., RAMOS, J. C., AND SERRA, L. M. **Cost optimization of the design of chcp (combined heat, cooling and power) systems under legal constraints**. *Energy 35*, 2 (2010), 794–805.

[70] ARCURI, P., FLORIO, G., AND FRAGIACOMO, P. **A mixed integer programming model for optimal design of trigeneration in a hospital complex**. *Energy 32*, 8 (2007), 1430–1447.

[71] SACHS, J., AND SAWODNY, O. **Multi-objective three stage design optimization for island microgrids**. *Applied Energy 165* (2016), 789–800.

[72] HOWARD, B., AND MODI, V. **Examination of the optimal operation of building scale combined heat and power systems under disparate climate and ghg emissions rates**. *Applied Energy 185* (2017), 280–293.

[73] GUROBI. **gurobi**, 2018.

[74] ZHOU, W., LOU, C., LI, Z., LU, L., AND YANG, H. **Current status of research on optimum sizing of stand-alone hybrid solar–wind power generation systems**. *Applied Energy 87*, 2 (2010), 380–389.

[75] CONNOLLY, D., LUND, H., MATHIESEN, B. V., AND LEAHY, M. **A review of computer tools for analysing the integration of renewable energy into various energy systems**. *Applied Energy 87*, 4 (2010), 1059–1082.

[76] DUFO-LÓPEZ, R., BERNAL-AGUSTÍN, J. L., AND CONTRERAS, J. **Optimization of control strategies for stand-alone renewable energy systems with hydrogen storage**. *Renewable energy 32*, 7 (2007), 1102–1126.

[77] KHODAEI, A., AND SHAHIDEHPOUR, M. **Microgrid-based co-optimization of generation and transmission planning in power systems**. *IEEE transactions on power systems 28*, 2 (2013), 1582–1590.

[78] KHODAEI, A., BAHRAMIRAD, S., AND SHAHIDEHPOUR, M. **Microgrid planning under uncertainty**. *IEEE Transactions on Power Systems 30*, 5 (2015), 2417–2425.

[79] ZHANG, J., LI, K.-J., WANG, M., LEE, W.-J., AND GAO, H. **A bi-level program for the planning of an islanded microgrid including caes**. In *Industry Applications Society Annual Meeting, 2015 IEEE* (2015), IEEE, pp. 1–8.

[80] EBRAHIMI, M., AND KESHAVARZ, A. **Climate impact on the prime mover size and design of a cchp system for the residential building**. *Energy and Buildings 54* (2012), 283–289.

[81] RUAN, Y., LIU, Q., LI, Z., AND WU, J. **Optimization and analysis of building combined cooling, heating and power (bchp) plants with chilled ice thermal storage system**. *Applied Energy 179* (2016), 738–754.

[82] BEIHONG, Z., AND WEIDING, L. **An optimal sizing method for cogeneration plants**. *Energy and Buildings 38*, 3 (2006), 189–195.

[83] SHANEB, O., COATES, G., AND TAYLOR, P. **Sizing of residential μchp systems**. *Energy and Buildings 43*, 8 (2011), 1991–2001.

[84] SANAYE, S., AND KHAKPAAY, N. **Simultaneous use of mrm (maximum rectangle method) and optimization methods in determining nominal capacity of gas engines in cchp (combined cooling, heating and power) systems**. *Energy 72* (2014), 145–158.

[85] WANG, J., SUI, J., AND JIN, H. **An improved operation strategy of combined cooling heating and power system following electrical load**. *Energy 85* (2015), 654–666.

[86] WANG, J., LU, Y., YANG, Y., AND MAO, T. **Thermodynamic performance analysis and optimization of a solar-assisted combined cooling, heating and power system**. *Energy 115* (2016), 49–59.

[87] ZHU, Q., LUO, X., ZHANG, B., AND CHEN, Y. **Mathematical modelling and optimization of a large-scale combined cooling, heat, and power system that incorporates unit changeover and time-of-use electricity price**. *Energy Conversion and Management* (2016).

[88] PRAKASH, P., AND KHATOD, D. K. **Optimal sizing and siting techniques for distributed generation in distribution systems: A review**. *Renewable and Sustainable Energy Reviews 57* (2016), 111–130.

[89] JORDEHI, A. R. **Allocation of distributed generation units in electric power systems: A review**. *Renewable and Sustainable Energy Reviews 56* (2016), 893–905.

[90] ROH, J. H., SHAHIDEHPOUR, M., AND FU, Y. **Market-based coordination of transmission and generation capacity planning**. *IEEE Transactions on Power Systems 22*, 4 (2007), 1406–1419.

[91] KHAYATIAN, A., BARATI, M., AND LIM, G. J. **Market-based and resilient coordinated microgrid planning under uncertainty**. In *Transmission and Distribution Conference and Exposition (T&D), 2016 IEEE/PES* (2016), IEEE, pp. 1–5.

[92] HEMMATI, R., SABOORI, H., AND SIANO, P. **Coordinated short-term scheduling and long-term expansion planning in microgrids incorporating renewable energy resources and energy storage systems**. *Energy* (2017).

[93] YANG, Y., ZHANG, S., AND XIAO, Y. **Optimal design of distributed energy resource systems coupled with energy distribution networks**. *Energy 85* (2015), 433–448.

[94] ZIDAN, A., GABBAR, H. A., AND ELDESSOUKY, A. **Optimal planning of combined heat and power systems within microgrids**. *Energy 93* (2015), 235–244.

[95] SHAO, C., SHAHIDEHPOUR, M., WANG, X., WANG, X., AND WANG, B. **Integrated planning of electricity and natural gas transportation systems for enhancing the power grid resilience**. *IEEE Transactions on Power Systems* (2017).

[96] ZHANG, X., SHAHIDEHPOUR, M., ALABDULWAHAB, A. S., AND ABUSORRAH, A. **Security-constrained co-optimization planning of electricity and natural gas transportation infrastructures**. *IEEE Transactions on Power Systems 30*, 6 (2015), 2984–2993.

[97] QIU, J., DONG, Z. Y., ZHAO, J. H., MENG, K., ZHENG, Y., AND HILL, D. J. **Low carbon oriented expansion planning of integrated gas and power systems**. *IEEE Transactions on Power Systems 30*, 2 (2015), 1035–1046.

[98] UNSIHUAY-VILA, C., MARANGON-LIMA, J., DE SOUZA, A. Z., PEREZ-ARRIAGA, I. J., AND BALESTRASSI, P. P. **A model to long-term, multiarea, multistage, and integrated expansion planning of electricity and natural gas systems**. *IEEE Transactions on Power Systems 25*, 2 (2010), 1154–1168.

[99] YU, M., AND HONG, S. H. **Supply–demand balancing for power management in smart grid: A stackelberg game approach**. *Applied Energy 164* (2016), 702–710.

[100] REIHANI, E., MOTALLEB, M., THORNTON, M., AND GHORBANI, R. **A novel approach using flexible scheduling and aggregation to optimize demand response in the developing interactive grid market architecture**. *Applied Energy 183* (2016), 445–455.

[101] TUSHAR, W., CHAI, B., YUEN, C., SMITH, D. B., WOOD, K. L., YANG, Z., AND POOR, H. V. **Three-party energy management with distributed energy resources in smart grid**. *IEEE Transactions on Industrial Electronics 62*, 4 (2015), 2487–2498.

[102] WANG, Y., AI, X., TAN, Z., YAN, L., AND LIU, S. **Interactive dispatch modes and bidding strategy of multiple virtual power plants based on demand response and game theory**. *IEEE Transactions on Smart Grid 7*, 1 (2016), 510–519.

[103] BAHRAMI, S., AND SHEIKHI, A. **From demand response in smart grid toward integrated demand response in smart energy hub**. *IEEE Transactions on Smart Grid 7*, 2 (2016), 650–658.

[104] KAMYAB, F., AMINI, M., SHEYKHHA, S., HASANPOUR, M., AND JALALI, M. M. **Demand response program in smart grid using supply function bidding mechanism**. *IEEE Transactions on Smart Grid 7*, 3 (2016), 1277–1284.

[105] ZHONG, H., XIE, L., AND XIA, Q. **Coupon incentive-based demand response: Theory and case study**. *IEEE Transactions on Power Systems 28*, 2 (2013), 1266–1276.

[106] FANG, X., HU, Q., LI, F., WANG, B., AND LI, Y. **Coupon-based demand response considering wind power uncertainty: A strategic bidding model for load serving entities**. *IEEE Transactions on Power Systems 31*, 2 (2016), 1025–1037.

[107] YU, M., AND HONG, S. H. **Incentive-based demand response considering hierarchical electricity market: A stackelberg game approach**. *Applied Energy 203* (2017), 267–279.

[108] DING, Y., PINEDA, S., NYENG, P., ØSTERGAARD, J., LARSEN, E. M., AND WU, Q. **Real-time market concept architecture for ecogrid eu—a prototype for european smart grids**. *IEEE Transactions on Smart Grid 4*, 4 (2013), 2006–2016.

[109] MANSHADI, S. D., AND KHODAYAR, M. E. **A hierarchical electricity market structure for the smart grid paradigm**. *IEEE Transactions on Smart Grid 7*, 4 (2016), 1866–1875.

[110] NGUYEN, D. T., NGUYEN, H. T., AND LE, L. B. **Dynamic pricing design for demand response integration in power distribution networks**. *IEEE Transactions on Power Systems 31*, 5 (2016), 3457–3472.

[111] ZUGNO, M., MORALES, J. M., PINSON, P., AND MADSEN, H. **A bilevel model for electricity retailers' participation in a demand response market environment**. *Energy Economics 36* (2013), 182–197.

[112] ZHANG, C., WANG, Q., WANG, J., KORPS, M., PINSON, P., ØSTERGAARD, J., AND KHODAYAR, M. E. **Trading strategies for distribution company with stochastic distributed energy resources**. *Applied Energy 177* (2016), 625–635.

[113] WANG, Z., CHEN, B., WANG, J., BEGOVIC, M. M., AND CHEN, C. **Coordinated energy management of networked microgrids in distribution systems**. *IEEE Transactions on Smart Grid 6*, 1 (2015), 45–53.

[114] JALALI, M., ZARE, K., AND SEYEDI, H. **Strategic decision-making of distribution network operator with multi-microgrids considering demand response program**. *Energy 141* (2017), 1059–1071.

[115] XIE, M., JI, X., HU, X., CHENG, P., DU, Y., AND LIU, M. **Autonomous optimized economic dispatch of active distribution system with multi-microgrids**. *Energy* (2018).

[116] TESFAHUNEGN, S. G. **Fuel Cell Assisted PhotoVoltaic Power Systems**. PhD thesis, 2012.

[117] LAZAAR, M., BOUADILA, S., KOOLI, S., AND FARHAT, A. **Comparative study of conventional and solar heating systems under tunnel tunisian greenhouses: Thermal performance and economic analysis**. *Solar Energy 120* (2015), 620–635.

[118] LAURENCELLE, F., CHAHINE, R., HAMELIN, J., AGBOSSOU, K., FOURNIER, M., BOSE, T., AND LAPERRIERE, A. **Characterization of a ballard mk5-e proton exchange membrane fuel cell stack**. *Fuel Cells 1*, 1 (2001), 66–71.

[119] SHABANI, B., ANDREWS, J., AND WATKINS, S. **Energy and cost analysis of a solar-hydrogen combined heat and power system for remote power supply using a computer simulation**. *Solar Energy 84*, 1 (2010), 144–155.

[120] LI, J., HU, Z., XU, L., OUYANG, M., FANG, C., HU, J., CHENG, S., PO, H., ZHANG, W., AND JIANG, H. **Fuel cell system degradation analysis of a chinese plug-in hybrid fuel cell city bus**. *International Journal of Hydrogen Energy 41*, 34 (2016), 15295–15310.

[121] MAMAGHANI, A. H., NAJAFI, B., CASALEGNO, A., AND RINALDI, F. **Predictive modelling and adaptive long-term performance optimization of an ht-pem fuel cell based micro combined heat and power (chp) plant**. *Applied Energy* (2016).

[122] PEI, P., AND CHEN, H. **Main factors affecting the lifetime of proton exchange membrane fuel cells in vehicle applications: A review**. *Applied Energy 125* (2014), 60–75.

[123] DIÉGUEZ, P., URSÚA, A., SANCHIS, P., SOPENA, C., GUELBENZU, E., AND GANDÍA, L. **Thermal performance of a commercial alkaline water electrolyzer: experimental study and mathematical modeling**. *international journal of hydrogen energy 33*, 24 (2008), 7338–7354.

[124] ULLEBERG, Ø. **Modeling of advanced alkaline electrolyzers: a system simulation approach**. *International journal of hydrogen energy 28*, 1 (2003), 21–33.

[125] TIETZ, F., SEBOLD, D., BRISSE, A., AND SCHEFOLD, J. **Degradation phenomena in a solid oxide electrolysis cell after 9000 h of operation**. *Journal of Power Sources 223* (2013), 129–135.

[126] KRÜGER, E., AND TRAN, Q. T. **Minimal aging operating strategies for battery energy storage systems in photovoltaic applications**. In *PES Innovative Smart Grid Technologies Conference Europe (ISGT-Europe), 2016 IEEE* (2016), IEEE, pp. 1–6.

[127] OMAR, N., MONEM, M. A., FIROUZ, Y., SALMINEN, J., SMEKENS, J., HEGAZY, O., GAULOUS, H., MULDER, G., VAN DEN BOSSCHE, P., COOSEMANS, T., AND OTHERS. **Lithium iron phosphate based battery–assessment of the aging parameters and development of cycle life model**. *Applied Energy 113* (2014), 1575–1585.

[128] XINWEI, S., YINGDUO, H., SHOUZHEN, Z., ZHENG, J., QINGSHENG, L., AND JING, N. **Comprehensive power-supply planning for active distribution system considering cooling, heating and power load balance**. *Journal of Modern Power Systems and Clean Energy 3*, 4 (2015), 485–493.

[129] MENON, R. P., PAOLONE, M., AND MARÉCHAL, F. **Study of optimal design of polygeneration systems in optimal control strategies**. *Energy 55* (2013), 134–141.

[130] GARCIA, F., AND BORDONS, C. **Optimal economic dispatch for renewable energy microgrids with hybrid storage using model predictive control**. In *Industrial Electronics Society, IECON 2013-39th Annual Conference of the IEEE* (2013), IEEE, pp. 7932–7937.

[131] HANSEN, T. M., ROCHE, R., SURYANARAYANAN, S., MACIEJEWSKI, A. A., AND SIEGEL, H. J. **Heuristic optimization for an aggregator-based resource allocation in the smart grid**. *IEEE Transactions on Smart Grid 6*, 4 (2015), 1785–1794.

[132] ROCHE, R., SURYANARAYANAN, S., HANSEN, T. M., KILICCOTE, S., AND MIRAOUI, A. **A multi-agent model and strategy for residential demand response coordination**. In *PowerTech, 2015 IEEE Eindhoven* (June 2015), pp. 1–6.

[133] FERRARI-TRECATE, G., GALLESTEY, E., LETIZIA, P., SPEDICATO, M., MORARI, M., AND ANTOINE, M. **Modeling and control of co-generation power plants: a hybrid system approach**. *IEEE Transactions on Control Systems Technology 12*, 5 (2004), 694–705.

[134] COLSON, B., MARCOTTE, P., AND SAVARD, G. **An overview of bilevel optimization**. *Annals of operations research 153*, 1 (2007), 235–256.

[135] LAGORSE, J., PAIRE, D., AND MIRAOUI, A. **Sizing optimization of a stand-alone street lighting system powered by a hybrid system using fuel cell, {PV} and battery**. *Renewable Energy 34*, 3 (2009), 683 – 691.

[136] CASTAÑEDA, M., CANO, A., JURADO, F., SANCHEZ, H., AND FERNANDEZ, L. M. **Sizing optimization, dynamic modeling and energy management strategies of a stand-alone pv/hydrogen/battery-based hybrid system**. *International journal of hydrogen energy 38*, 10 (2013), 3830–3845.

[137] WU, D., AND WANG, R. **Combined cooling, heating and power: a review**. *progress in energy and combustion science 32*, 5 (2006), 459–495.

[138] GU, W., WU, Z., BO, R., LIU, W., ZHOU, G., CHEN, W., AND WU, Z. **Modeling, planning and optimal energy management of combined cooling, heating and power microgrid: A review**. *International Journal of Electrical Power & Energy Systems 54* (2014), 26–37.

[139] MANCARELLA, P. **Mes (multi-energy systems): An overview of concepts and evaluation models**. *Energy 65* (2014), 1–17.

[140] LI, B., ROCHE, R., AND MIRAOUI, A. **System resilience improvement using multiple energy supply systems under natural disasters**. In *Industrial Electronics Society, IECON 2016-42nd Annual Conference of the IEEE* (2016), IEEE, pp. 3912–3917.

[141] REN, H., GAO, W., AND RUAN, Y. **Optimal sizing for residential chp system**. *Applied Thermal Engineering 28*, 5 (2008), 514–523.

[142] LI, B., ROCHE, R., AND MIRAOUI, A. **Microgrid sizing with combined evolutionary algorithm and milp unit commitment**. *Applied Energy 188* (2017), 547–562.

[143] WESOFF, E. **Update: Ionex has a 1 mw battery ready for the grid, epri issues ess rfi**, 2011.

[144] CONTAINERS, S. **High cube shipping containers**, 2018.

[145] MITRA, J., VALLEM, M. R., AND SINGH, C. **Optimal deployment of distributed generation using a reliability criterion**. *IEEE Transactions on Industry Applications 52*, 3 (2016), 1989–1997.

[146] LI, B., ROCHE, R., PAIRE, D., AND MIRAOUI, A. **Sizing of a stand-alone microgrid considering electric power, cooling/heating, hydrogen loads and hydrogen storage degradation**. *Applied Energy 205* (2017), 1244–1259.

[147] SHEIKHI, A., BAHRAMI, S., AND RANJBAR, A. M. **An autonomous demand response program for electricity and natural gas networks in smart energy hubs**. *Energy 89* (2015), 490–499.

[148] ZENG, B., AND ZHAO, L. **Solving two-stage robust optimization problems using a column-and-constraint generation method**. *Operations Research Letters 41*, 5 (2013), 457–461.

[149] WANG, Z., CHEN, B., WANG, J., KIM, J., AND BEGOVIC, M. M. **Robust optimization based optimal dg placement in microgrids**. *IEEE Transactions on Smart Grid 5*, 5 (2014), 2173–2182.

[150] YUAN, W., WANG, J., QIU, F., CHEN, C., KANG, C., AND ZENG, B. **Robust optimization-based resilient distribution network planning against natural disasters**. *IEEE Transactions on Smart Grid 7*, 6 (2016), 2817–2826.

[151] CHANDA, S., AND SRIVASTAVA, A. K. **Defining and enabling resiliency of electric distribution systems with multiple microgrids**. *IEEE Transactions on Smart Grid 7*, 6 (2016), 2859–2868.

[152] LÖFBERG, J. **Automatic robust convex programming**. *Optimization methods and software 27*, 1 (2012), 115–129.

[153] SHABANPOUR-HAGHIGHI, A., AND SEIFI, A. R. **Simultaneous integrated optimal energy flow of electricity, gas, and heat**. *Energy Conversion and Management 101* (2015), 579–591.

[154] DE WOLF, D., AND SMEERS, Y. **The gas transmission problem solved by an extension of the simplex algorithm**. *Management Science 46*, 11 (2000), 1454–1465.

[155] MARTINEZ-MARES, A., AND FUERTE-ESQUIVEL, C. R. **A unified gas and power flow analysis in natural gas and electricity coupled networks**. *IEEE Transactions on Power Systems 27*, 4 (2012), 2156–2166.

[156] XIA, L., MA, Z., KOKOGIANNAKIS, G., WANG, Z., AND WANG, S. **A model-based design optimization strategy for ground source heat pump systems with integrated photovoltaic thermal collectors**. *Applied Energy 214* (2018), 178–190.

[157] ZHAO, L., AND ZENG, B. **Robust unit commitment problem with demand response and wind energy**. In *Power and Energy Society General Meeting, 2012 IEEE* (2012), IEEE, pp. 1–8.

List of Figures

List of Tables

IV

APPENDIX

A

List of publications by the author

Journal:

- Li Bei, Robin Roche, and Abdellatif Miraoui. “Microgrid sizing with combined evolutionary algorithm and MILP unit commitment.” Applied energy 188 (2017): 547-562.
- Li Bei, Robin Roche, Damien Paire, and Abdellatif Miraoui. “Sizing of a stand-alone microgrid considering electric power, cooling/heating, hydrogen loads and hydrogen storage degradation.” Applied Energy 205 (2017): 1244-1259.
- Li Bei, Robin Roche, Damien Paire, and Abdellatif Miraoui. “Optimal sizing of distributed generation in gas/electricity/heat supply networks.” Energy 151 (2018): 675-688.

Conference:

- Li Bei, Robin Roche, Damien Paire, and Abdellatif Miraoui. “A price decision approach for multiple multi-energy-supply microgrids considering demand response.” In EnergyCon, 2018 IEEE Cyprus. IEEE, 2018.
- Li Bei, Robin Roche, and Abdellatif Miraoui. “A temporal-spatial natural disaster model for power system resilience improvement using DG and lines hardening.” In PowerTech, 2017 IEEE Manchester, pp. 1-6. IEEE, 2017.
- Li Bei, Robin Roche, and Abdellatif Miraoui. “Sizing of a stand-alone microgrid considering electric power, cooling/heating and hydrogen.” In PowerTech, 2017 IEEE Manchester, pp. 1-6. IEEE, 2017.
- Li Bei, Robin Roche, and Abdellatif Miraoui. “System resilience improvement using multiple energy supply systems under natural disasters.” In Industrial Electronics Society, IECON 2016-42nd Annual Conference of the IEEE, pp. 3912-3917. IEEE, 2016.

Document generated with LaTeX and:
the LaTeX style for PhD Thesis created by S. Galland — http://www.multiagent.fr/ThesisStyle
the tex-upmethodology package suite — http://www.arakhne.org/tex-upmethodology/